DRIFT TYPE PHOTOVOLTAIC PROCESS IN TETRAHEDRALLY-BONDED AMORPHOUS SEMICONDUCTORS

Shuichi NONOMURA

September, 1983

Osaka University
Faculty of Engineering Science
Toyonaka, Osaka

DRIFT TYPE PHOTOVOLTAIC PROCESS IN TETRAHEDRALLY-BONDED AMORPHOUS SEMICONDUCTORS

Shuichi Nonomura

Department of Electrical Engineering
Faculty of Engineering Science
Osaka University, Toyonaka, Osaka

September, 1983

Abstract

Systematic studies on the photovoltaic process in hydrogenated amorphous silicon (a-Si:H) solar cells have been carried out from both view points of theoretical analysis and experimental proof.

The carrier transport across the a-Si:H p-i-n junction has been discussed, and a new model characterized by electric-field-dependent photocarrier generation and recombination is proposed. On the basis of this carrier transport model, carrier collection efficiency and V-I characteristics under the dark and light-illuminated conditions have been calculated. It has been shown that the photovoltaic performances such as short circuit current density J_{sc}, open circuit voltage V_{oc} and fill factor FF are completely represented by five fundamental parameters; built-in potential (V_b), mobility-lifetime products of electrons ($\mu_n\tau_n$) and holes ($\mu_p\tau_p$), and effective surface recombination factors at the interfaces of p/i (S_n) and n/i (S_p). Optimization of the design parameters for the best photovoltaic performance has been also studied. A series of this theoretical analysis relating to the electric-field-

dependent photo-carrier generation and collection is called as "the drift type photovoltaic process theory".

A new characterization method for evaluating the junction built-in field in the a-Si:H solar cells has been developed using the measurement of back-surface-reflected electroabsorption signals. It has been verified from a series of theoretical analyses that the built-in potential in the a-Si:H solar cells can be evaluated from dc bias voltage dependence of electro-optical signal amplitude. A linear relation between the built-in potential V_b and the open circuit voltage V_{oc} has been clarified through measurements of the cells with various combinations of junctions and a-Si:H/metal contacts. An extra-ordinarily large increase of V_b (130 mV) compared with the value for homojunction solar cells has been obtained in heterojunction solar cells having the structure of p-type amorphous silicon carbide/i-type amorphous silicon/n-type microcrystalline silicon.

Through an analysis of collection efficiency spectra under the dc bias voltage, a new method for evaluation of film quality and junction parameters such as mobility-lifetime products of electrons and holes and surface recombination factors at the p/i and n/i interfaces has been developed. Utilizing this method, it has been shown that impurity inclusion in the photovoltaic active region (i-layer) has a strong influence on the mobility-lifetime products. Another important result clarified from this analysis concerns with the origin of the surface recombination. It has also been pointed out that even in a-Si:H solar cells the structural mismatching at the heterojunction interface and the damage during fabrication process are largely responsible for the surface recombination.

The characteristic features of various types of a-Si:H solar cells have been investigated with the analyses of the film quality and the junction parameters, V_b, $\mu_n\tau_n$, $\mu_p\tau_p$, S_n and S_p. From the technological standpoint, a comparison of performance of the a-Si:H solar cell fabricated by separated chamber and single chamber deposition systems has been made. In the separated chamber deposition system, the higher mobility-lifetime products and lower surface recombination cause an improvement of the conversion efficiency. As a result of optimization of fabrication conditions, a conversion efficiency of more than 9 % has been obtained under AM 1 (100 mW/cm^2) illumination.

ACKNOWLEDGEMENT

The author would like to express his sincere thanks to Professor Y. Hamakawa for his kind advice and critical reading of this thesis. The author wishes to make his deep acknowledgement to Professors S. Namba, K. Fujisawa, T. Sueta and S. Yamamoto for their kind guidance in the cource of this study at Osaka University.

This work has been done at the Semiconductor Laboratory, Faculty of Engineering Science, Osaka University, Toyonaka, Osaka, under the direction of Professor Y. Hamakawa, and the author wants to express his greatest gratitude to Professor Y. Hamakawa for his constant advice, suggestion and encouragement throughout the course of this thesis work. Also the author wishes to give his greatest gratitude to Dr. H. Okamoto for his kind encouragement and useful advice in this thesis work. The author wishes to give his highest appreciation to Professors S. Nitta and K. Shimakawa of Gifu University, and Professor A. Hiraki of Osaka University and Professor T. Imura of Hiroshima University for their constant encouragement and useful suggestion.

The author is much indebted to Professor T. Nishino, Drs. M. Okuyama and H. Takakura for their useful advice and discussions throughout the course of this study. Usual and enjoyable discussions with colleagues of the Semiconductor Laboratory, especially, Drs. Y. Yamazoe, H. Nakayama, K. Okamoto, Y. Matsui, Y. Tawada and Messrs. K. Fujimoto, S. Hotta and Y. Fujiwara are much appreciated.

The author wishes to express his gratitude to his co-workers in the Semiconductor Laboratory, Mr. C. Sada for his kind encouragement, useful discussion and significant assistance through this thesis work.

Also Messrs. T. Yamaguchi, M. Kondo, K. Fujii, T. Yamada, H. Kida, K. Fukumoto, Y. Kashima, Y. Takeda, K. Tabuchi and K. Okuda are much appreciated. In particular, the author takes pleasure in acknowledging the important part played by Messrs. H. Kida, K. Fukumoto, Y. Kashima and Y. Takeda.

Finally the author wishes to thank his wife and parents, and also some friends, Messrs. M. Mori, T. Endo, Y. Kitagawa, A. Yamaguchi, Y. Nitta, K. Enomoto, T. Nabeta, N. Nishimoto, K. Nishimura and S. Tamaki for their endless encouragements and supports.

CONTENTS

Chapter I INTRODUCTION 1

1-1. Historical Background 1

1-2. Purpose of the Present Work 4

Chapter II THEORETICAL ANALYSIS OF DRIFT TYPE PHOTOVOLTAIC PROPERTIES IN a-Si:H SOLAR CELLS 10

2-1. Introduction 10

2-2. Carrier Recombination Process in a-Si:H Solar Cells 12

2-3. Representation of Carrier Dynamics 14

2-3-1. Current density representations of excess carriers 14

2-3-2. Photocurrent representations 16

2-3-3. Injection current representations 19

2-3-4. J-V characteristics 21

2-4. Carrier Collection Efficiency 22

2-5. Cell Performances 27

2-6. Summary 31

Chapter III PREPARATION AND CHARACTERIZATION OF TETRAHEDRALLY-BONDED AMORPHOUS SEMICONDUCTORS 35

3-1. Introduction 35

3-2. Preparation of Tetrahedrally-Bonded Amorphous Semiconductors . 37

3-3. Electroreflectance Signal near the Fundamental Edge in a-Si:H 40

3-3-1. Sample fabrication and measurement procedure 41

3-3-2. Effects of RF power 44

3-3-3. Effects of substrate temperature 46

3-3-4. Dependence of modulation electric field 46

3-3-5. Comparison between ER signals and absorption spectra 49

3-4. Summary 52

Chapter IV BUILT-IN POTENTIAL OF HYDROGENATED AMORPHOUS SILICON SOLAR CELLS 55

4-1. Introduction 55

4-2. Electro-Optical Signal in a-Si:H Solar Cells 56

4-2-1. Fundamental representation of reflectance in a-Si:H solar cells 56

4-2-2. Back surface reflected electroabsorption 60

4-3. Built-In Potential in a-Si:H Solar Cells 62

4-3-1. Bias voltage dependence of electro-optical signal 62

4-3-2. Internal electric field in the i-layer 65

4-3-3. P-layer thickness dependence of built-in potential 68

4-3-4. Application to the various types of a-Si:H solar cells .. 73

4-4. Summary 75

Chapter V FILM AND JUNCTION QUALITIES IN AMORPHOUS SILICON SOLAR CELLS 77

5-1. Introduction 77

5-2. Normalized Collection Efficiency Spectra 78

5-3. Evaluation of Mobility-Lifetime Products and Surface Recombination Factors 80

5-3-1. Evaluation method 80

5-3-2. Normalized collection efficiency spectra in practical a-Si:H solar cells 85

5-3-3. I-layer thickness dependence of collection efficiency ... 85

5-3-4. J-V characteristics under illumination 89

5-4. Effects of Preparation Conditions 91

5-4-1. Impurity effects on mobility-lifetime products 91

5-4-2. P-layer thickness dependence on effective surface recombination factors 97

5-5. Effects of Prolonged Light Irradiation 101

5-6. Summary 104

Chapter VI ANALYSIS OF HIGH EFFICIENCY a-Si:H SOLAR CELLS 109

6-1. Introduction 109

6-2. Fabrication of a-Si:H Solar Cells 110

6-3. Physical Parameters in Various Types of a-Si:H Solar Cells . 110

6-4. High Efficiency a-Si:H Solar Cells 114

6-4-1. p-i-n and inverted p-i-n heterojunction solar cells 114

6-4-2. Comparison between single and separated chamber deposition method 116

6-5. Summary 123

Chapter VII CONCLUSIONS 125

VITA

I. INTRODUCTION

1-1. Historical Background

The study of amorphous semiconductors was initiated in the field of chalcogenide semiconductors by Kolomiets at the Leningrad school [1,2]. Though the fundamental concepts of the amorphous semiconductors were accomplished in this area by Ioffe [3], Anderson [4] and Mott [5], there appeared few reseaches orientated to the practical application of amorphous semiconductors. In 1968, Ovshinsky [6] firstly reported high speed reversible electric switching action in chalcogenide amorphous semiconductors containing S, Se and Te. Moreover, several peculiar properties of chalcogenide amorphous semiconductors such as photostructural change and its related phenomena [7,8] have been applied in the field of optical communication or submicron fabrication etc. However nobody in the field of amorphous semiconductors believed the possibility of substitutional doping [9,10] which is one of the most important factors in the development of semiconductor physics and solid state electronic devices of crystalline semiconductors. The difficulty of valency control in the case of amorphous semiconductors was a serious limitation for wide-spread use in the field of solid state electronic devices.

In 1975, Spear's group at Dundee University [11] realized substitutional doping in amorphous silicon produced by a glow discharge technique. This discovery was the first report of structural sensitive amorphous materials and placed large impact on the field of amorphous material science. This event was the prime mile stone in the view of not only breaking up the traditional concept of amorphous materials but also opening the wide variety of application. In the next year, Carlson and Wronski attained the conversion efficiency of 5.5 % in a

Schottky barrier type a-Si:H solar cell [12]. This stimulated the researchers in the field of applied physics of amorphous semiconductors. In 1978, a p-i-n type a-Si:H solar cell with the conversion efficiency of 4.5 % was reported by Hamakawa's group at Osaka University [13]. In the next year, a horizontally multilayered p-i-n unit cell [14] was demonstrated. The study of a-Si:H solar cells has become one of the central themes in the field of amorphous material accompanying with social needs for new energy resources caused by the oil shock since 1974.

The following prime event was an appearance of new amorphous materilas. In 1978, fluorinated amorphous silicon (a-Si:F:H) was announced by Ovshinsky at ECD as a new material which has lower density of states with high doping efficiency and higher stability than those of a-Si:H [15]. This work motivated many researchers to exploit new materials useful for a-Si solar cell. In 1981, a new type of heterojunction solar cell has been developed with utilizing microcrystalline silicon (μc-Si) [16,17] and amorphous silicon carbide (a-SiC:H) [18]. These materials are useful as an electrode layer for constructing the window side junction because of their wide optical gaps. These heterojunction solar cells realized more than 8% conversion efficiency within this year [18,19]. Furthermore, for promoting more efficient utilization of incident light, amorphous silicon germanium was utilized to a stacked cell [20] and more than 8 % conversion efficiency was accomplished in 1982. The study of these new materials containing amorphous silicon nitride (a-SiN:H)[21] and amorphous silicon tin (a-SiSn:H) [22] is now at a starting point.

In the field of device physics, the main difference in design concepts between a-Si:H and crystalline silicon solar cells has been cleared up by Hamakawa's group [23] in 1979. That is, the photovoltaic

process in the a-Si:H solar cells is dominated by drift type carrier transport because the internal electric field within a-Si:H junction exceeds 10^4V/cm. The photogeneration probability of carriers in the presence of such high electric field was discussed by several groups [24,25,26,27]. New knowledge of amorphous material science and device physics has been accumlated day by day.

However, it goes without saying that we have not enough informations for the best utilization of these materials to the practical devices in the present stage. In this sense, the back ground device physics unique to amorphous materials should be developed.

1-2. Purpose of the Present Work

In a view of making a practical active electronic device with amorphous materials, it is necessary to comprehend properties of the junctions consisting of amorphous materials. Moreover, it should be cleared how the preparation and process technologies affect the film quality and the junction properties. The purpose of this thesis work is to develop a characterization method of a-Si:H films and a-Si:H based junctions in terms of experimental and theoretical considerations and to exploit active electronic devices applicable to practical use.

The author has paid his attention on the above points, and carried out systematic investigations of electronic properties of the a-Si:H film by electro-optical effect. On the basis of these results, particularly the electric field dependence of electro-optical signals, a method for evaluating the built-in potential of a-Si:H solar cell has been developed. Furthermore, the junction and film qualities have been characterized in terms of the new model of carrier transport. Utilizing these characterization methods, it has been made clear how the properties of p-i-n amorphous junction are influenced by the preparation conditions and processes. Based upon informations derived from these device physics considerations on cell design and fabrication technologies, an a-Si:H heterojunction solar cell with the conversion efficiency of 9.39 % has been fabricated.

In chapter II, a new carrier transport model explaining the photovoltaic characteristics of a-Si:H p-i-n junction solar cells [28] is described. In this model, the operative i-layer is divided into two regions where either electrons or holes are assumed to act just like the minority carriers controlling the carrier recombination rate. The carrier

collection efficiency spectra and current density-voltage characteristics [29] are understood in terms of several basic parameters such as mobility-lifetime products, effective surface recombination velocities at the p/i and n/i interfaces.

In chapter III, the results of systematic investigation of electroreflectance (ER) [30] is demonstrated with various parametric system of amorphous silicon (a-Si:H) produced by glow discharge decomposition of monosilane (SiH_4). The ER signal changes drastically with the film preparation conditions. High power deposition brings about a distinct change of the ER spectra from a single peak to crystalline-like ER feature. While, the ER spectrum sharpens gradualy with increasing substrate temperature. Based upon these experimental data, the optical transition processes and electronic states near the fundamental edge are described in conjunction with the corresponding change of optical absorption spectra.

In chapter IV, the author also deals with the Electroreflectance (ER) signal as a tool for identifying the built-in field in the practical a-Si:H solar cells [31,32]. It is confirmed, through both the theoretical analysis and experimental verification, that ER signal comes from a field induced intensity change of the light which is reflected at the back surface and hence experiences the internal electric field within the a-Si:H layer. It has been made clear by analyzing the externally applied bias voltage dependence of the ER signal amplitude that the ER signal of actual a-Si:H solar cells is the back-surface-reflected electroabsorption signal, and that the built-in potential V_b can be evaluated from its dc bias dependence. A clear variation of V_b in different heterojunctions utilizing new materials and various substrate materials is demonstrated.

In chapter V, a new characterization method for evaluating some important physical parameters such as mobility-lifetime products and surface recombination velocities in amorphous silicon solar cells [33] is described. This method is based on a new model of carrier transport explaining some characteristic features of the photovoltaic properties in a-Si:H solar cells, where transport of both electrons and holes is taken into consideration. Especially, a new characterization procedure combining with experimental results of collection efficiency and its theoretical calculation is proposed [33]. By applying this procedure to various p-i-n based a-Si:H junctions, several important observations have been made; effects of impurity atoms on mobility-lifetime products, p-layer thickness dependence of effective surface recombination factors, and the change of these parameters under strong light irradiation [33, 34, 35, 36].

In chapter VI, various types of a-Si:H solar cells are analyzed with applying new characterization methods described in previous chapters, and especially a-Si:H solar cells of typical structure with high conversion efficiency are examined in terms of various parameters responsible for the cell performance. The author discusses how to design and fabricate the cells in order to attain higher photovoltaic performances, and demonstrates a-Si:H solar cell having the conversion efficiency of 9.39 % [36].

In the final chapter, some conclusions obtained through this thesis work are summarized.

Reference

[1] N.A. Goryunova and B.T. Kolomiets, J. Tech. Phys. 25 (1955) 984.

[2] B.T. Kolomiets, Phys. Stat. Solidi 7 (1964) 359.

[3] A.F. Ioffe and A.R. Regal, Prog. Semicond. 4 (1960) 239.

[4] P.W. Anderson, Phys. Rev. 109 (1958) 1492.

[5] N.F. Mott and E.A. Davis, "*Electronic Process in Noncrystalline materials*" Second edition (Clarendon Press, Oxford, 1979).

[6] S.R. Ovshinsky, Phys. Rev. Lett. 21 (1968) 1450.

[7] S.A. Keneman, Appl. Phys. Lett. 19 (1971) 205.

[8] I. Shimizu et al., Photog. Sci. Eng. 16 (1972) 291.

[9] A.I. Gubanov, Sov. Phys.-Solid-State 3 (1962) 1694.

[10] N.F. Mott, Phil. Mag. 19 (1969) 835.

[11] W.E. Spear and P.G. LeComber, Sol. Stat. Comm. 17 (1975) 1193.

[12] D.E. Carlson and C.R. Wronski, Appl. Phys. Lett. 28 (1976) 671.

[13] H. Okamoto, Y. Nitta, T. Adachi and Y. Hamakawa, Surf. Sci. 86 (1979) 486.

[14] Y. Hamakawa, H. Okamoto and Y. Nitta, Appl. Phys. Lett. 35 (1979) 187.

[15] A. Madan, S.R. Ovshinsky and E. Benn, Phil. Mag. 40 (1979) 259.

[16] A. Matsuda, M. Matsumura, S. Yamasaki, H. Yamamoto, T. Imura, H. Okushi, S. Iizima and K. Tanaka, Jpn. J. Appl. Phys. 20 (1981) L121.

[17] T. Hamasaki, H. Kurata, M. Hirose and Y. Osaka, Appl. Phys. Lett. 47 (1980) 1084.

[18] Y. Tawada, M. Kondo, H. Okamoto and Y. Hamakawa, Solar Energy Mat. 6 (1982) 299.

[19] H. Haruki, Y. Uchida, H. Sata, M. Nishimura and M. Komiyama, 13th Conf. Solid State Devices, Tokyo, 53 (1981).

[20] G. Nakamura, K. Sata and Y. Yukimoto, Jpn. J. Appl. Phys. 21 (1982) Suppl.21-2, 297.

[21] M. Dohjo, M. Hirose and Y. Osaka, Proc. 1982 Dry Process Symp.(IEEE of Japan, 1982) p.17.

[22] C. Verie, J.F. Rochette and J.P. Rebouillat, J. Phys. 42 (1981) C4-667.

[23] T. Yamaguchi, H. Okamoto, S. Nonomura and Y. Hamakawa, Jpn. J. Appl. Phys. 20 (1981) Suppl.20-2, 195.

[24] H. Okamoto, T. Yamaguchi, S. Nonomura and Y. Hamakawa, J. Phys. 42 (1981) C4-507.

[25] R. Crandall, Appl. Phys. Lett. 36 (1980) 607.

[26] J. Mort, A. Troup, M. Morgan, S. Grammatica, J.C. Knight and R. Lujian, Appl. Phys. Lett. 38 (1981) 277.

[27] R.O. Bell, Appl. Phys. Lett. 37 (1980) 952.

[28] S. Nonomura, H. Okamoto, H. Kida and Y. Hamakawa, Jpn. J. Appl. Phys. 21 (1982) Suppl. 21-2, 279. Proc. 3nd Photovoltaic Sci.&Eng. Conf., Tokyo, 1982.

[29] H. Okamoto, H. Kida, S. Nonomura and Y. Hamakawa, Solar Cells 8 (1983) 317.

[30] S. Nonomura, H. Okamoto, T. Nishino and Y. Hamakawa, J. Phys. 42 (1981) Suppl. 10, C4-761. Proc. 9th Int. Conf. on Amorphous and Liquid Semiconductors, Grenoble, 1981.

[31] S. Nonomura, H. Okamoto and Y. Hamakawa, Jpn. J. Appl. Phys. 21 (1982) L464.

[32] S. Nonomura, H. Okamoto and Y. Hamakawa, Appl. Phys. A 32 (1983) 31.

[33] S. Nonomura, H. Okamoto, H. Kida, K. Fukumoto and Y. Hamakawa, Jpn. J. Appl. Phys. 22 (1982) Suppl. 22-1, 517. Proc. 14th Int. Conf. on Solid State Devices, Tokyo, 1982.

[34] H. Okamoto, H. Kida, S. Nonomura, K. Fukumoto and Y. Hamakawa, J. Appl. Phys. 54 (1983) 3236.

[35] Y. Tawada, K. Nishimura, S. Nonomura, H. Okamoto and Y. Hamakawa, Solar Cells 9 (1983) 53.

[36] S. Nonomura, H. Okamoto, K. Fukumoto, K. Kashima and Y. Hamakawa, Solar Cells (1983) in press.

II. THEORETICAL ANALYSIS OF DRIFT TYPE PHOTOVOLTAIC PROPERTIES IN a-Si:H SOLAR CELLS

2-1. Introduction

There are several unique things on the carrier transport phenomena in amorphous semiconductors, which are mainly due to the existence of localized states distributed in the mobility gap. Such phenomena are classified as the four following processes ; i) dispersive transport [1,2], ii) geminate recombination [3,4], iii) ambipolar carrier transport, iv) drift type photovoltaic effect [5]. Especially in an a-Si:H photovoltaic processes, ambipolar carrier transport and drift type photovoltaic effect give strong influence on the cell performance. On the stand point of these two phenomena, detailed discussion on photovoltaic properties in a-Si:H solar cells are described in this chapter.

There are two important points to which attention must be paid in the course of a study on the photovoltaic properties of a-Si:H solar cells. It is of considerable significance to reveal them before commencing detailed discussions. In the extrinsic crystalline semiconductors which are operative in most electronic devices, the density n_0 (or p_0) of the thermal equilibrium majority carriers is usually much larger than the densities δn and δp of excess carriers and also than the carrier densities n_1 and p_1 which are present in the extended bands when the Fermi level coincides with the recombination level. Under these circumstances, the Shockley-Read carrier recombination rate [6] given by

$$R = \frac{\delta n \delta p + n_0 \delta p + p_0 \delta n}{(\delta n + n_1 + n_0)\tau_p + (\delta p + p_1 + p_0)\tau_n} \qquad (2\text{-}1)$$

can reasonably be reduced to

$$R \tilde{=} \delta p/\tau_p \quad \text{(for n-type material)}$$
$$R \tilde{=} \delta n/\tau_n \quad \text{(for p-type material)} \qquad (2\text{-}2)$$

Here τ_p (τ_n) is the hole (electron) lifetime. Thus the carrier recombination rate is governed by the lifetime and excess density of the minority carriers, which simplifies the mathematical manipulations in analyzing the transport process. However, the situation is completely different in a-Si:H devices because the operative region usually consists of an undoped i-layer where the density δp of the excess carriers far exceeds that of the thermal equilibrium carriers; $\delta p >> p_o, n_o$. Accordingly, the concept of minority carrier transport applicable to crystalline devices no longer holds good in a-Si devices.

It is customary to the representation of the local current density in crystalline solar cells [7] as

$$J(V_a) = J_L - J_o[\exp(\frac{qV_a}{nk_BT}) - 1] \qquad (2\text{-}3)$$

where J_L denotes the photocurrent component and the second term the injection (diode) current component. V_a is the applied voltage and J_o the saturation current density. n is the diode ideality factor, q the elemental charge, k_B Boltzmann's constant and T the absolute temperature. It has often been pointed that the photocurrent density J_L is dependent on the bias voltage in a-Si solar cells [8,9]. However, little attention has so far been paid to the variation of the second term of Eqn.(2-3) under illumination. Even if a separation of the current passing across the cell into the above two components is permitted, there should be an essential connection between the two components in actual a-Si solar cells under illumination.

Recognizing the situation, the author develops the simple but usefull concept of carrier transport for describing photovoltaic properties unique to a-Si solar cells.

2-2. Carrier recombination process in a-Si:H solar cells

In the operative i-layer of a-Si:H solar cells, the condition $\delta p, \delta n >> p_0, n_0, p_1, n_1$ can usually be satisfied as mentioned in Section 2-1. Then the recombination rate R given by eqn.(2-1) can be simplified to

$$R = \frac{\delta n \delta p}{\delta n \tau_p + \delta p \tau_n} \qquad (2\text{-}4)$$

Furthermore, with additional conditions this may be approximated as

$$R \tilde{=} \delta p/\tau_p \quad \text{for} \quad \delta n/\tau_n >> \delta p/\tau_p \qquad (2\text{-}5)$$

$$R \tilde{=} \delta n/\tau_n \quad \text{for} \quad \delta p/\tau_p >> \delta n/\tau_n \qquad (2\text{-}6)$$

These formulae can be interpreted in the following manner by comparison with eqn.(2-2). In the region where $\delta n/\tau_n >> \delta p/\tau_p$, the recombination rate is controlled by the lifetime and excess density of holes. Thus, in the sense used for crystalline semiconductor devices, holes behave just like minority carriers in this region. Similarly, electrons are regarded as the minority carriers in the region where $\delta p/\tau_p >> \delta n/\tau_n$ holds.

Now let us concider a p-i-n junction cell of infinite extent in the y-z plane provided with ohmic contacts at both sides of the junction as shown in Fig.2-1. The operating i-layer streches from x=0 (p/i interface) to x=ℓ (i/n interface). Under steady illumination or forward bias conditions, the distributions of the photogenerated or

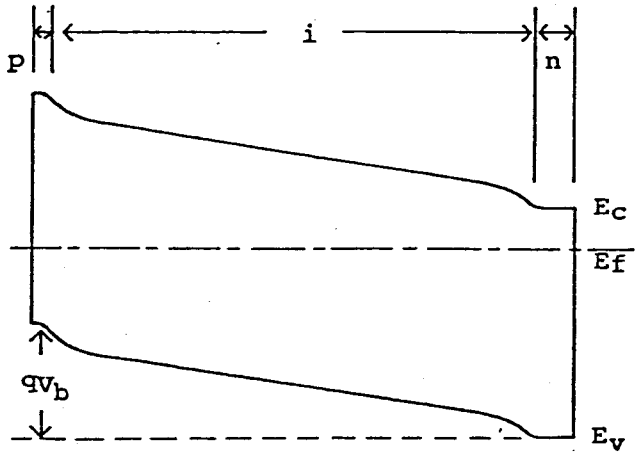

(a) Thermal Equilibrium Condition

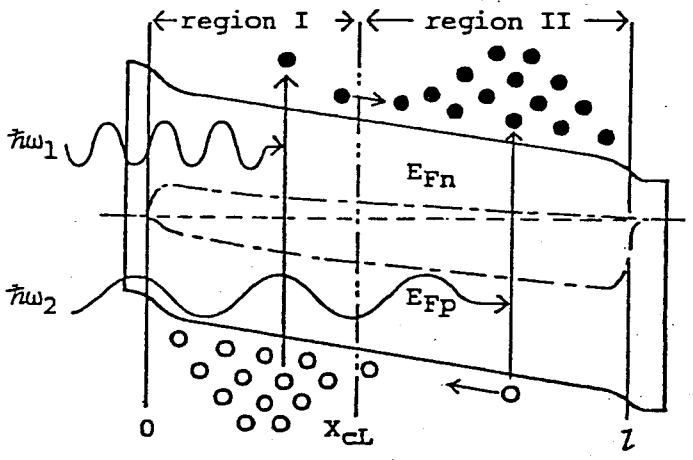

(b) Illuminated (short circuit) Condition

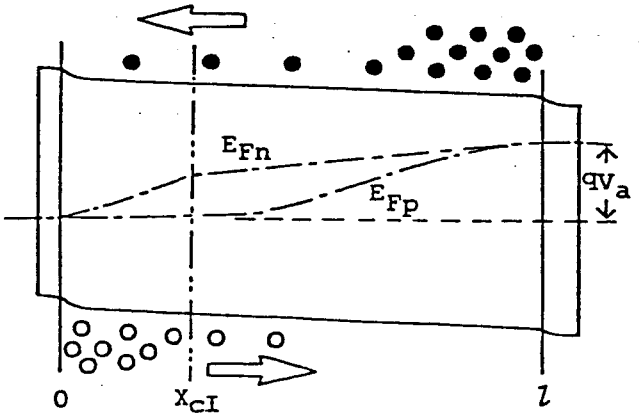

(c) Dark (forward bias) Condition

Fig. 2-1 Schematic band diagrams of a-Si:H p-i-n junction solar cells under thermal eqilibrium (a), illuminated (b) and forward bias conditions (c).

injected holes and electrons would incline toward the p-layer side and the n-layer side respectively. However, it is not always obvious which is the larger, $\delta n/\tau_n$ or $\delta p/\tau_p$. In other words, the situation often occurs that eqn.(2-5) stands as the recombination rate in one part (region II) of the i-layer and eqn.(2-6) holds in the other part (region I). These regions are approximately separated at a characteristic boundary at x_c. The position x_c should be primarily determined not by the distributions of the thermal equilibrium carriers but by those of the excess carriers through

$$\frac{\delta n(x_c)}{\tau_n} = \frac{\delta p(x_c)}{\tau_p} \tag{2-7}$$

and thus the boundary tends to move corresponding to the external perturbation conditions, i.e. the incident light spectra, the bias voltage V_a etc. This leads to the concept of the variable minority carrier transport model as an alternative to the conventional minority carrier transport model familiar in crystalline semiconductor devices.

2-3. Representation of Carrier Dynamics

2-3-1. Current density representations of excess carriers

In this section, theoretical representations for the photocurrent and injection current in the p-i-n junction cell are derived on the basis of the variable minority carrier transport model. First of all, the author introduces the excess carrier propagation functions defined by [10]

$$f_p^{\mp}(x;u) = \exp\{\mp\int_u^x \frac{d\xi}{L_p^{\mp}(\xi)}\} \tag{2-8}$$

for holes and

$$f_n^{\pm}(x;u) = \exp\{\mp\int_u^x \frac{d\xi}{L_n^{\pm}(\xi)}\} \tag{2-9}$$

for electrons. Here

$$L_p(x) = [\{1+\gamma_p^2(x)\}^{1/2} \pm \gamma_p(x)]\, L_p \tag{2-10}$$

with

$$\gamma_p(x) = \frac{qL_pE(x)}{2k_BT}$$

and

$$L_p = (D_p\tau_p)^{1/2}$$

and

$$L_n^{\pm}(x) = [\{1+\gamma_n^2(x)\}^{1/2} \pm \gamma_n(x)]\, L_n \tag{2-11}$$

with

$$\gamma_n(x) = \frac{qL_nE(x)}{2k_BT}$$

and

$$L_n = (D_n\tau_n)^{1/2}$$

where $E(x)$ denotes the internal electric field in the negative x direction as shown in Fig.2-1(b). D_p (D_n) is the diffusion constant for holes (electrons) which is related to the carrier mobility μ_p (μ_n) by the Einstein equation: $D_p = K_BT\mu_p/q$, $D_n = k_BT\mu_n/q$. Equations (2-8) and (2-9) are exact elemental solutions of the

current conservation equation with a uniform generation source located at x=u in the y-z plane when E(x) is constant everywhere [11]; even if this is not so, they give very good approximate solutions as long as $E(x) >> 2k_BT/qL$.

Introducing arbitary functions $C_p^{\pm}$ and $C_n^{\pm}$ of u, we can represent the resulting distribution of the excess carriers at any given position x directly by linear combinations of $f_p^{\pm}(x;u)$ or $f_n^{\pm}(x;u)$;

$$\delta p(x;u) = C_p^-(u)f_p^-(x;u) + C_p^+(u)f_p^+(x;u) \qquad (2\text{-}12)$$

$$\delta n(x;u) = C_n^-(u)f_n^-(x;u) + C_n^+(u)f_n^+(x;u) \qquad (2\text{-}13)$$

Then the corresponding current densities can easily be calculated as

$$J_p(x;u) = qD_p\{\frac{C_p^-(u)f_p^-(x;u)}{L_p^-(x)} - \frac{C_p^+(u)f_p^+(x;u)}{L_p^+(x)}\} \qquad (2\text{-}14)$$

$$J_n(x;u) = qD_n\{\frac{C_n^+(u)f_n^+(u)}{L_n^-(x)} - \frac{C_n^-(u)f_n^-(x;u)}{L_n^+(x)}\} \qquad (2\text{-}15)$$

For convenience, these current densities are described as being in the negative x direction, i.e. along the electric field.

2-3-2. Photocurrent representations

The attention is confined to within region II in Fig.2-1(b) where the lifetime and density of the photogenerated holes control the carrier recombination rate as indicated in eqn.(2-5). Let us consider the case in which photocarrier generation takes place within the region $u \leqq x \leqq u+\Delta u$ at a rate G(x). G(x) can be represented in terms of the photon flux distribution $\Phi(x,\lambda)$ for light of each wavelength λ and the free-carrier generation probability $P_G(x,\lambda)$ as [8]

$$G(x) = \int_0^\infty P_G(x,\lambda) \left\{ \frac{-\partial\Phi(x,\lambda)}{\partial x} \right\} d\lambda \qquad (2\text{-}16)$$

It is best to consider the solution for $\delta p_A(x;u)$ in the subregion $x_c \leqq x \leqq u$ (denoted A) and the solution for $\delta p_B(x;u)$ in the subregion $u \leqq x \leqq \ell$ (denoted B). Using eqn.(2-12), δp_A and δp_B can be rewritten as

$$\delta p_A(x;u) = C_{pA}^-(u) f_p^-(x;u) + C_{pA}^+(u) f_p^+(x;u) \qquad x_c << X << u \qquad (2\text{-}17)$$

$$\delta P_B(x;u) = C_{pB}^-(u) f_p^-(x;u) + C_{pB}^+(u) f_p^+(x;u) \qquad u << x << \ell \qquad (2\text{-}18)$$

The corresponding current densities $J_{pA}(x;u)$ and $J_{pB}(x;u)$ are given by Eqn.(2-14). Now four appropriate conditions are required to fix the arbitrary constants $C_{pA}^{+-}(u)$ and $C_{pB}^{+-}(u)$. The following conditions are imposed here:

$$\delta p_A(u;u) = \delta p_B(u;u) \qquad (2\text{-}19)$$

$$C_{pA}^+(u) = 0 \qquad (2\text{-}20)$$

$$S_{i/n} \delta p_B(\ell;u) = J_{pB}(\ell;u)/q \qquad (2\text{-}21)$$

$$G(u)\Delta u = \frac{J_{pA}(x_c;u)}{q} - \frac{J_{pB}(\ell;u)}{q} + \int_{x_c}^{u} \frac{\delta p_A(\xi;u)}{\tau_p} d\xi + \int_u^{\ell} \frac{\delta p_B(\xi;u)}{\tau_p} d\xi \qquad (2\text{-}22)$$

Equation (2-19) is the carrier continuity condition at x=u, eqn.(2-20) corresponds to the assumption of a non-reflecting boundary at $x=x_{cL}$ [10], eqn.(2-21) represents the boundary condition at $x=\ell$ using an effective surface recombination velocity $S_{i/n}$ and eqn.(2-22) is the overall carrier conservation condition within region II.

Combination of eqns.(2-19)-(2-20) results in the carrier collection probability $P_p(x_c,u)$ that the photogenerated holes can reach the characteristic boundary x_c:

$$P_p(x_c,u) = \frac{J_{pA}(x_c;u)}{qG(u)\Delta u}$$

$$= \frac{L_p^+(x_c)}{L_p^+(x_c)+L_p^-(\ell)} \{1-\Omega_p(\ell)f_p^-(u;\ell)f_p^+(\ell;u)\}f_p^-(x_c;u) \quad (2\text{-}23)$$

Here

$$\Omega_p(\ell) = \frac{S_{i/n} - D_p/L_p^+(\ell)}{S_{i/n} + D_p/L_p^-(\ell)} \quad (2\text{-}24)$$

Equation (2-23) is completely exact only when the internal electric field is constant everywhere: nevertheless it might be applicable to the general case as long as $E(x)>>2k_BT/qL_p$. When the probability $P_p(x_c,u)$ is calculated with eqn.(2-23), the photocurrent $J_{Lp}(x_c)$ in region II can be represented in turn by

$$J_{Lp}(x_c) = q\int_{x_c}^{\ell} P_p(x_c,u)G(u)du \quad (2\text{-}25)$$

Because of the relation

$$\delta p_A(x_c;u) = \frac{L_p^-(x_c)}{qD_p} J_{pA}(x_c;u) \quad (2\text{-}26)$$

the density $\delta p(x_c)$ of the excess holes at $x=x_c$ is given by

$$\delta p(x_c) = \frac{L_p^-(x_c)}{qD_p}\int_{x_c}^{\ell} J_{pA}(x_c;u)du$$

$$\doteq \frac{\tau_p J_{Lp}(x_c)}{qL_p^+(x_c)} \quad (2\text{-}27)$$

Here the relation $L_p^-L_p^+ = L_p^2 = D_p\tau_p$ was used.

In region I, where the lifetime and density of the photogenerated electrons control the carrier recombination rate as given by eqn.(2-6), the procedure mentioned above yields the corresponding results

$$p_n(x_c,u) = \frac{L_n^+(x_c)}{L_n^+(x_c) + L_n^-(0)}\{1-\Omega_n(0)f_n^+(u;0)f_n^-(0;u)\}f_n^+(x_c;u) \quad (2\text{-}28)$$

$$J_{Ln}(x_c) = q\int_0^{x_c} P_n(x_c;u)G(u)du \tag{2-29}$$

$$\delta n(x_c) = \frac{\tau_n J_{Ln}(x_c)}{qL_n^+(x_c)} \tag{2-30}$$

Here $\Omega_n(0)$ is defined in terms of the effective surface recombination velocity $S_{p/i}$ at x=0 as

$$\Omega_n(0) = \frac{S_{p/i}-D_n/L_n^+(0)}{S_{p/i}+D_n/L_n^-(0)} \tag{2-31}$$

Accordingly, the total photocurrent density $J_L(x_c:V_a)$ is given by eqns.(2-25) and (2-29) as

$$J_L(x_c:V_a) = J_{Lp}(x_c) + J_{Ln}(x_c) \tag{2-32}$$

In a situation where excess carriers are yielded only by photogeneration, the condition to be imposed for the determination of x_c can be altered from eqn.(2-7) to

$$\frac{J_{Lp}(x_c)}{L_p^+(x_c)} = \frac{J_{Ln}(x_c)}{L_n^+(x_c)} \tag{2-33}$$

by means of eqns.(2-27) and (2-30).

2-3-3. Injection current representations

In this section, the author calculates the current component in a-Si solar cell that originates in carrier injection from both side of the junction as shown in Fig.2-1(c). The calculation is first carried out within region II as in the previous section. The density $\delta p(x)$ of injected holes and the corresponding current density $J_{Ip}(x)$ in the negative x direction are formulated as

$$\delta p(x) = C_p^+(V_a)f_p^+(x;x_c) + C_p^-(V_a)f_p^-(x;x_c) \tag{2-34}$$

and

$$J_{Ip}(x) = qD_p\{\frac{C_p^-(V_a)f_p^-(x;x_c)}{L_p^-(x)} - \frac{C_p^+(V_a)f_p^+(x;x_c)}{L_p^+(x)}\} \quad (2\text{-}35)$$

Here V_a is the applied bias voltage in the forward bias direction ($V_a >> k_BT/q$). The boundary conditions to be imposed here are written as

$$\delta p(x_c) = P(V_a) \quad (2\text{-}36)$$

$$S_{i/n}\delta p(\ell) = -J_{Ip}(\ell)/q \quad (2\text{-}37)$$

Under these boundary conditions, $J_{Ip}(x_c)$ can easily be solved as

$$J_{Ip}(x_c) = -\frac{qP(V_a)}{\tau_p}\frac{L_p^-(\ell)f_p^-(\ell;x_c) + \Omega_p(\ell)L_p^+(\ell)f_p^+(\ell;x_c)}{f_p^-(\ell;x_c) - \Omega_p(\ell)f_p^+(\ell;x_c)} \quad (2\text{-}38)$$

The same procedure yields the current density $J_{In}(x_c)$ that comes from the injection of electrons into region I:

$$J_{In}(x_c) = -\frac{qN(V_a)}{\tau_n}\frac{L_n^-(0)f_n^+(0;x_c) + \Omega_n(0)L_n^+(0)f_n^-(0;x_c)}{f_n^+(0;x_c) - \Omega_n(0)f_n^-(0;x_c)} \quad (2\text{-}39)$$

Here $N(V_a)$ is defined as $\delta n(x_c)$.

In order to make a reasonable estimate of $P(V_a)$ and $N(V_a)$, the assumption is made that the quasi Fermi level of holes (electrons) is flat everywhere in region I (II), which is equivalent to regarding holes (electrons) as the majority carriers in region I (II). When the electrical potential $\Phi(u;V_a)$ at x=u with respect to $x=x_c$ is introduced, $P(V_a)$ and $N(V_a)$ may be given within the framework of our model as

$$P(V_a) = p_o(0)\exp\{\frac{q\phi(0;V_a)}{k_BT}\} \quad (2\text{-}40)$$

$$N(V_a) = n_o(\ell)\exp\{\frac{-q\phi(\ell;V_a)}{k_BT}\} \qquad (2\text{-}41)$$

where $p_o(0)$ and $n_o(0)$ denote the thermal equilibrium densities of holes and electrons at x=0 and x=ℓ respectively, provided that these densities are almost independent of the applied bias voltage. It is rather convenient for later calculations to rewrite them in terms of the related conductivities $\sigma_p(0)$ and $\sigma_n(\ell)$ as $p_o(0)=\sigma_p(0)/q\mu_p$ and $n_o(\ell)=\sigma_o(\ell)/q\mu_n$.

Now the total injection current density $J_I(X_c:V_a)$ can be represented as

$$J_I(x_c:V_a) = J_{Ip}(x_c) + J_{In}(x_c) \qquad (2\text{-}42)$$

Where as indicated in eqn.(2-7) the position x_c should be determined by solving the next equation;

$$\frac{P(V_a)}{\tau_p} = \frac{N(V_a)}{\tau_n} \qquad (2\text{-}43)$$

in the absence of the photogeneration of carriers.

2-3-4. J-V characteristics

The current passing across the p-i-n junction cell under illumination is formulated as

$$J(x_c:V_a) = J_L(x_c:V_a) + J_I(x_c:V_a) \qquad (2\text{-}44)$$

where $J_L(x_c:V_a)$ and $J_I(x_c:V_a)$ are calculated similarly using eqns.(2-32) and (2-42) respectively. In the present case, however, the position x_c of the characteristic boundary cannot be derived either from eqn.(2-33) or from eqn.(2-43). Instead it must be determined as the solution of

$$\frac{J_{Lp}(x_c)}{L_p^+(x_c)} + \frac{P(V_a)}{\tau_p} = \frac{J_{Ln}(x_c)}{L_n^+(x_c)} + \frac{N(V_a)}{\tau_n} \qquad (2\text{-}45)$$

which is the definite form of the fundamental requirement eqn.(2-7) in the a-Si solar cells under operation. When x_c has thereby been fixed, eqn.(2-44) can easily be used to obtain the corresponding current density as a function of the applied bias voltage V_a for any given incident light.

2-4. Carrier Collection Efficiency

As is now widely known, the distribution of the internal electric field within the operative i-layer of a p-i-n junction solar cell is dominated principally by the density of states in the gap [10,12,13]. It has been concluded from model calculations carried out by assuming simplified but realistic gap state distributions [8,9,10,14] that there exists an almost constant electric field in the i-layer except for in the vicinities of the p/i and i/n boundaries in a p-i-n junction of realistic dimensions made of relatively good quality a-Si films. On the basis of this consideration, a constant internal electric field approximation is adopted in this thesis work, then the internal electric field $E(V_a)$ within the i-layer is represented by the simple form [15].

$$E(V_a) = \frac{\partial \phi(x;V_a)}{\partial x} = \frac{V_b - V_a}{l} \qquad (2\text{-}46)$$

where V_b denotes the built-in voltage defined by $\phi(l;0)-\phi(0;0)$.

This assumption has been verified in various a-Si solar cells with conversion efficiencies of more than 5% by means of back-surface-reflected-electroabsorption measurements [15]. However, the calculation must be adequately modified if we wish to treat a-Si solar cells in which the internal electric field is strongly position dependent. Moreover, for the range of cases considered in this work the internal electric field distribution is assumed not to be violated by the space charge effects due to the photogenerated and/or injected carriers. Thus the analysis in this thesis work is valid only under relatively low injection conditions.

As for the bulk rate G(x) of photogeneration, some detailed discussions have been given in the previous papers [8,9,10]. However, since the present interest is concentrated on the carrier transport, it is taken simply to be

$$G(x) = \int_0^\infty I_o(\lambda)P_G(x,\lambda)\alpha(\lambda)\exp\{-\alpha_p(\lambda)l_p\}\cdot \cdot[\exp\{-\alpha(\lambda)x\}+\rho_b\exp\{\alpha(\lambda)(x-2l)-2\alpha_n(\lambda)l_n\}]d\lambda \quad (2\text{-}47)$$

for the case of light incident on the p-layer. Here $\alpha(\lambda)$, $\alpha_p(\lambda)$ and $\alpha_n(\lambda)$ are the absorption coefficients of the i-, p- and n-layers respectively. ρ_b denotes the fraction of the light internally reflected into the cell at the rear-side boundary ($x=l+l_n$). I_o is the photon flux incident on the a-Si:H layers at $x=-l_p$. In later calculations, the following simplifications are made for convenience: $\alpha(\lambda)=\alpha_p(\lambda)=\alpha_n(\lambda)$ [2] and the free-carrier generation probability $P_G(x,\lambda)$ is fixed at unity for the wavelength region corresponding to photon energies higher than the optical gap energy [8,9,10].

With the simplifications described above, the characteristics of

the a-Si p-i-n junction cell are described by the $\mu\tau$ products for holes and electrons, the surface recombination factor $S_n(S_p)$ which is defined by $S_{p/i}/\mu_n(S_{i/n}/\mu_p)$, the thermal equilibrium conductivity $\sigma_p(0)$ $(\sigma_n(\ell))$ at x=0 (x=ℓ) and other known parameters which must be given: $\alpha(\lambda)$,V_b,V_a, ℓ,ℓ_p and ℓ_n.

A common way of analyzing solar cells is to measure the internal collection efficiency spectra. Model calculations for the internal collection efficiency were carried out with various sets of the above-mentioned parameters by fixing ρ_b=0.8 (a-Si/Al interface), ℓ_p=100Å and ℓ_n=300Å [2]. When $I_o(\lambda)$ in Eqn.(2-47) is set at unity for each wavelength, eqn.(2-32) gives the internal carrier collection efficiency spectra directly. Figure 2-2 shows typical spectra and the position x_c normalized to ℓ as functions of the ratio $\mu_n\tau_n/\mu_p\tau_p$ and $\mu\tau$ products. The other parameters were chosen to have realistic values as denoted in the figure caption. In this figure, the case of light incident on the p-layer is assumed. For generality the spectra are drawn as functions of the absorption coefficient. Roughly speaking, the normalized position x_c is nearly proportional to $\mu_n\tau_n/(1+\alpha\ell)(\mu_n\tau_n+\mu_p\tau_p)$ as shown in the figure. In other words, carriers with larger $\mu\tau$ products can be regarded almost as the limiting carriers for the carrier collection efficiency because the larger the $\mu\tau$ product of a given kind of carrier, the larger the fraction of the photocurrent generation region that would be occupied by the region where carriers of that kind act as the minority carriers. In this situation, to obtain higher carrier collection efficiencies (particularly at shorter wavelengths) it is sufficient to illuminate the cell on the p-layer if $\mu_n\tau_n<\mu_p\tau_p$ and vice versa as shown in Fig.2-2. The effect of the built-in voltage V_b is also presented in the figure. The carrier collection efficiency

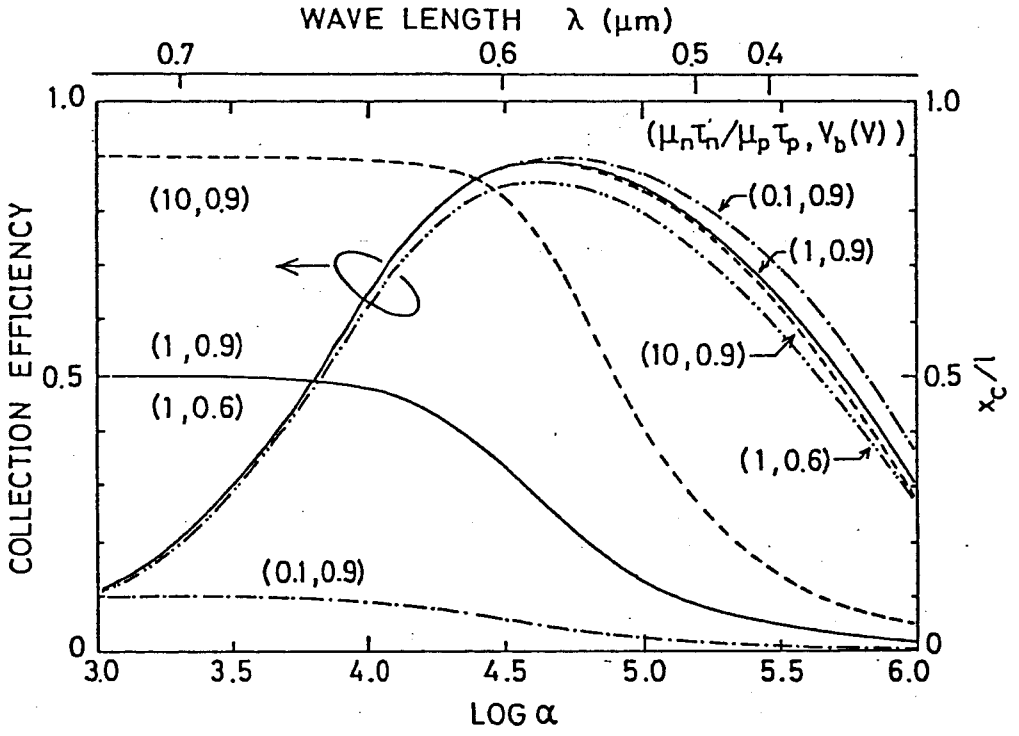

Fig. 2-2 Carrier collection efficiency and normalized characteristic boundary position x_c as functions of the absorption coefficient α for various pairs of parameters $(\mu_n\tau_n/\mu_p\tau_p, V_b)$. Here $\mu_n\tau_n+\mu_p\tau_p=10^{-7}$ cm^2/V, $S_n=S_p=10^4$ V/cm, $l=6000$ Å and V_b is given in volts.

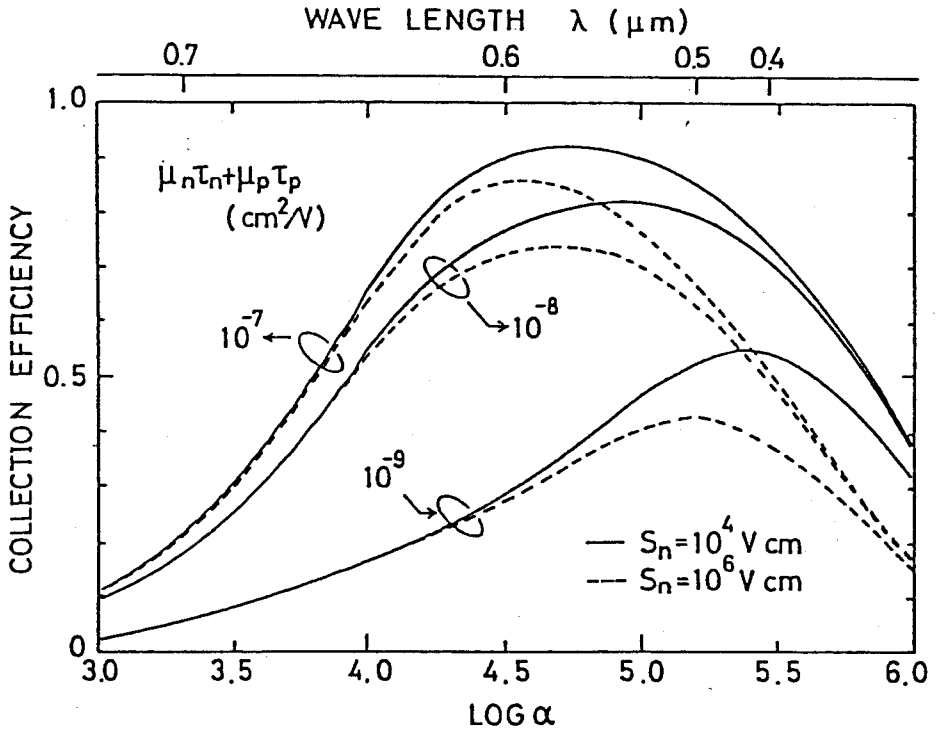

Fig. 2-3 Carrier collection efficiency as a function of absorption coefficient α for various value of $\mu_n\tau_n+\mu_p\tau_p$ (cm^2/V) and the surface recombination factor S_n at the front side interface (p/i interface): ——, $S_n=10^4$ V/cm; ----, $S_n=10^6$ V/cm. Here $\mu_{n_o}\tau_n/\mu_p\tau_p=1$, $S_p=10^4$ V/cm, $V_b=0.9$ V and $\ell=6000$ A.

decreases with decreasing V_b as can easily be imagined.

The carrier collection efficiency is strongly influenced by the sum ($\mu_n\tau_n+\mu_p\tau_p$) of the $\mu\tau$ products as demonstrated in Fig.2-3. A decrease in $\mu_n\tau_n+\mu_p\tau_p$ reduces the carrier collection efficiency markedly and moves the peak of the spectra towards the shorter wavelength region (larger α region). This tendency is essentially attributed to an increase in the distance through which photogenerated holes and electrons must pass as minority carriers when the light penetration depth becomes larger. Moreover, Fig.2-3 indicates the effect of the surface recombination at the front side (p/i interface). An extremely larger reduction in the carrier collection efficiency is observed, especially at shorter wavelengths, when the surface recombination factor S_n is chosen to have a larger value. In contrast, it was confirmed that the surface recombination at the rear side (i/n interface) does not have such a remarkable influence on the collection efficiency spectra.

2-4. Cell Performances

In Fig.2-4, variations in the photovoltaic performance properties with the ratio $\mu_n\tau_n/\mu_p\tau_p$ and the front-side effective surface recombination factor S_n are demonstrated. In the calculations, $\mu_n\tau_n+\mu_p\tau_p$ was fixed at $10^{-7}cm^2V^{-1}$ since typical values of this sum experimentally obtained in a-Si solar cells with efficiencies in the range 6.5%-8.1% are of this order of magnitude as shown in chapter V [16]. As can be seen in the figure, the smaller the ratio $\mu_n\tau_n/\mu_p\tau_p$, the larger the short-circuit current density J_{sc} and curve fill factor FF and the lower the open-circuit voltage V_{oc} are expected to be. In contrast, a reduction in the effective surface recombination factor at the front-side interface

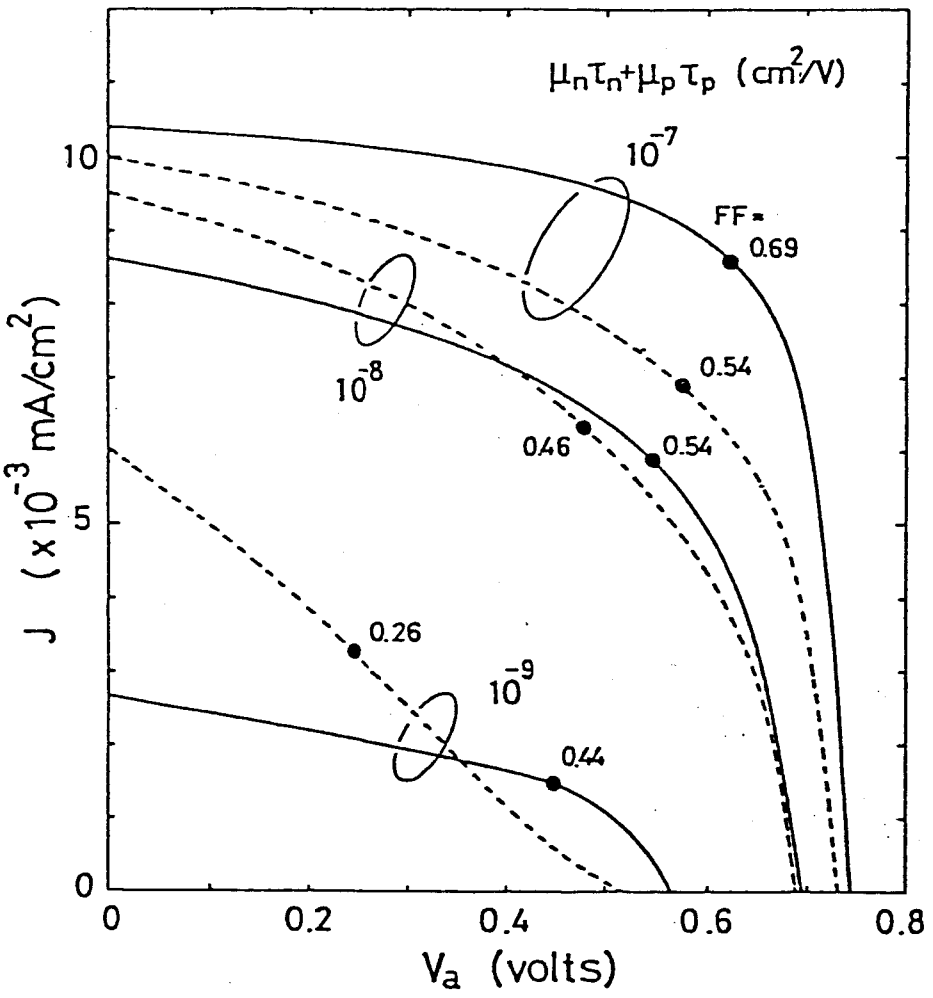

Fig. 2-4 Illuminated J-V characteristics as a function of $\mu_n\tau_n+\mu_p\tau_p$ (cm^2/V) for various absorption coefficients of the incident light; ——, $\alpha=10^4$ cm^{-1};------, $\alpha=10^{5.5}$ cm^{-1}. Here $\mu_n\tau_n/\mu_p\tau_p=1$, $\sigma_n=10^{-5}\Omega^{-1}cm^{-1}$, $\sigma_p=10^{-7}\Omega^{-1}cm^{-1}$, $S_n=S_p=10^4$ V/cm, $V_b=0.9$ V and $\ell=6000$Å. The incident photon flux I_o is fixed at 10^{15}photons $s^{-1}cm^{-2}$.

results in a better photovoltaic performace. This appears that the photovoltaic performance properties are more strongly dominated by the effective surface recombination factor than by the ratio $\mu_n\tau_n/\mu_p\tau_p$. For $S_n=10^2$ Vcm^{-1}, the curve fill factor FF exhibits a non-monotonic change with the absorption coefficient α. Within the range of realistic absorption coefficients of undoped a-Si films available for photocarrier production ($10^4<\alpha<10^{5.5}$) FF rather increases with α, i.e. for shorter wavelengths of the incident light. Therefore, if a-Si solar cells with extremely good interface properties could be fabricated, such a tendency would be observed. The calculated results mentioned above are restricted to the case of light incident on the p-layer. However, the alternative results for n-layer illumination can be obtained by simply exchanging the subscripts n and p. In that case an effective surface recombination factor which was about two orders magnitude smaller ($S_p\sim10^2$ Vcm^{-1}) was found at the i/n interface in the typical p-i-n junction solar cells as shown in later chapter. Hence it is possible to attain better photovoltaic performances when the cells are illuminated on the n-layer regardless of the ratio $\mu_n\tau_n/\mu_p\tau_p$ [17]. In our calculations, however, we ascertained that higher photovoltaic performances are achieved by illumination of the doped layer where the conductivity is lower. Accordingly, the configurational design of a-Si solar cells should be performed by paying attention to those competing factors because the conductivity of the n-layer is generally larger than that of the p-layer and the surface recombination velocity at the i/n interface is usually smaller than that at the p/i interface.

It is interesting to investigate the i-layer thickness dependence of the photovoltaic performance. In Fig.2-5 the short-circuit current

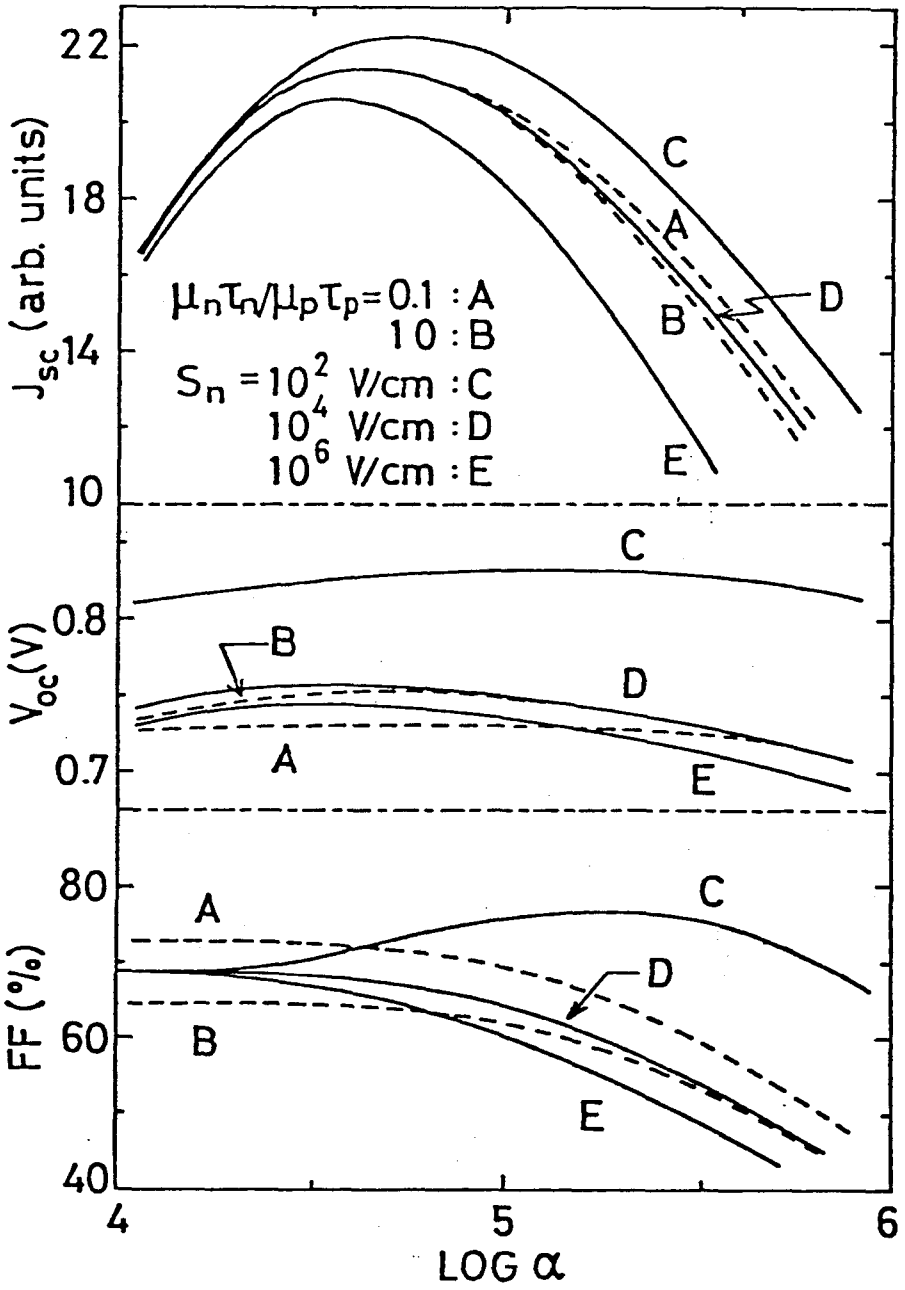

Fig. 2-5 Short-circuit current density J_{sc}, open-circuit voltage V_{oc} and curve fill factor FF as functions of the absorption coefficient α for various values of $\mu_n\tau_n/\mu_p\tau_p$ (curves A, 0.1; curves B, 1.0)(S_n=10^4 V/cm) and S_n (curves C, 10^2V/cm; curves D, 10^4 V/cm; curves E, 10^6 V/cm)($\mu_n\tau_n/\mu_p\tau_p$=1). Here σ_{n_2}=$10^{-5}\Omega^{-1}cm^{-1}$, σ_p=$10^{-7}\Omega^{-1}cm^{-1}$, $\mu_n\tau_{n_o}+\mu_p\tau_p$=$10^{-7}$ cm^2/V, S_p=10^4 V/cm, V_b=0.9 V, λ=6000A and I_o= 10^{15} photons/s·cm^2.

density J_{sc}, the open circuit voltage V_{oc} and the curve fill factor FF are plotted as functions of the i-layer thickness for illumination with two different lights. Some discussion of J_{sc} has already been given in previous section. Here attention is paid to the curve fill factor FF. The curve fill factor FF decreases monotonically with increasing i-layer thickness as shown in the figure regardless of the absorption coefficient for the incident light. Thus the decrease in the curve fill factor FF with increasing i-layer thickness should be attributed essentially to the finite value of the $\mu\tau$ products but not always to series resistance effects. Moreover, although all these calculations were carried out for monochromatic light, they successfully explain the experimental fact that the highest AM 1 conversion efficiency is obtained at an i-layer thickness of around 6000Å [2,3,18].

2-5. Summary

To interprete the characteristic features of a-Si:H p-i-n junction solar cells, a new concept was developed in the carrier transport model, where the operative i-layer is devided into two regions by a variable boundary; in one region, electrons are assumed to behave just like minority carriers and holes are regarded as the minority carriers in the other region. The model in this chapter is considerably simplified; however, some essential physical situations unique to a-Si:H solar cells are successfully taken into account in it. Based on this variable minority carrier transport model, representations were derived to describe the carrier collection efficiency spectra and dark and illuminated J-V characteristics. Several examples of

the calculated results were presented and discussed with the aid of corresponding experimental data.

a-Si p-i-n junction solar cells exhibit various characteristic carrier collection efficiency spectra and dark and illuminated J-V curves with different sets of values of the mobility-lifetime products for electrons ($\mu_n\tau_n$) and holes ($\mu_p\tau_p$), the effective surface recombination velocities $S_{p/i}$ and $S_{i/n}$ and conductivities σ_p and σ_n at the p/i and i/n interfaces, and the built-in voltage V_b. The conditions required for better photovoltaic performances were made clear within the extent of the present study as follows: (i) a large built-in voltage V_b; (ii) large $\mu\tau$ products, i.e. large values of $\mu_n\tau_n+\mu_p\tau_p$; (iii) $\mu_p\tau_p>\mu_n\tau_n$ ($\mu_n\tau_n>\mu_p\tau_p$) for light incident on the p- (n-) layer; (iv) small $S_{p/i}$ and $S_{i/n}$, especially at the front-side interface; (v) $\sigma_n>\sigma_p$ ($\sigma_p>\sigma_n$) for light incident on the p- (n-) layer.

References

[1] M. Silver, L. Cohen and D. Adler, Phys. Rev. B24 (1981) 4855.

[2] J. Orenstein and M. Kastner, Phys. Rev. Lett. 46 (1981) 1421.

[3] D.M. Pai and R.C. Enk, Phys. Rev. 11 (1975) 5163.

[4] R. Crandall, Appl. Phys. Lett. 36 (1980) 607.

[5] Y. Hamakawa: AMORPHOUS SEMICONDUCTOR TECHNOLOGIES & DEVICES, JARECT series, ed. by Y. Hamakawa (OHM Sha& North-Holland, Tokyo, Amsterdam and New York, 1982) Chap.4.

[6] W. Schocklly and W.T. Read, J. Phys. Rev. 87 (1952) 835.

[7] H.J. Hovel, Solar Cells, *"Semiconductors and Semimetals"*, Vol.11, Academic Press, New York, 1975, Chap.3, p.48.

[8] T. Yamaguchi, H. Okamoto, S. Nonomura and Y. Hamakawa, Jpn. J. Appl. Phys., 20 (1981) Suppl.20-2, 195.

[9] H. Okamoto, T. Yamaguchi, S. Nonomura and Y. Hamakawa, J. Phys. 42 (1981) C4-507.

[10] H. Okamoto, T. Yamaguchi and Y, Hamakawa, J. Phys. Soc. Jpn., 49 (1980) Suppl.A, 1213.

[11] J.P. MacKelvey, *"Solid-State and Semiconductor Physics"*, Harper & Row, New York, 1966, p.337.

[12] M. Shur, W. Czubatyj and A. Madan, J. Non-Cryst. Solids 35-36 (1980) 731.

[13] W.E. Spear, P.G. LeComber and A.J. Snell, Phil. Mag. B 38 (1978) 303.

[14] I. Chen and J. Mort, Appl. Phys. Lett. 37 (1980) 952.

[15] S. Nonomura, H. Okamoto and Y. Hamakawa, Jpn. J. Appl. Phys. Lett. 21 (1982) 464.

[16] S. Nonomura, H. Okamoto, H. Kida and Y. Hamakawa, Jpn. J. Appl. Phys. 21 (1982) Suppl.21-2, 279.

[17] Y. Uchida, H. Sakai, M. Fukusho, M. Nishiura and H, Haruki, Proc. 161st Electrochemical Society Meet., Montreal, 1982.

[18] J.J. Hanak, V. Korson and J.P. Pellicane, in R. Van Overstraeten and W. Palz (eds.) Proc. 2nd Eur. Communities Conf. on Photovoltaic Solar Energy, West Berlin, April 1979, Reidel, Boston, 1979, p.270.

III. PREPARATION AND CHARACTERIZATION OF TETRAHEDRALLY-BONDED AMORPHOUS SEMICONDUCTORS

3-1. Introduction

The modulation spectroscopy [1] has been utilized usefully in the study of band structure of crystalline solids. A noticeable advantage of this characterization method is that measurement of differential spectrum yielded by externally applied energy perturbation made it possible to enhance optical structures with high resolution by full use of pase sensitive detection technique. Among various modulation energy parameters in the spectroscopy, electric field modulations; so called "Electroabsorption (EA)" and "Electroreflectance (ER)" are the most advanced one in view of both theoretical background and technological aspects [2].

In the first-derivative modulation spectroscopy where lattice periodicity is retained, momentum is still a good quantum number to within a reciprocal lattice vector, and optical transitions remain vertical in the one-electron band picture although the threshold energy changes with the perturbation. Since the change in threshold energy is generally small in the scale of energy gaps, the perturbation-induced changes in the dielectric function are first order and can be approximated by the first-derivative of dielectric function. On the other hand, in electromodulation the perturbation $e \cdot F \cdot r$ destroys the translational invariance of the Hamiltonian in the field direction in contrast to other first-derivative modulation spectroscopies. The loss of translational invariance under the electric field is the origin of the complexity of electroreflectance [3].

From the analysis of the EA and ER signals with these theoretical backgrounds, much information on the electronic band structures such as, critical points of the joint density of states, effective mass near the band edge, even the type of the band edges has been most precisely obtained [4]. Thus, this type of modulation spectroscopy becomes a useful tool as high resolution characterizations of the electric band structure of crystals, and still spreading into various new mixed compounded semiconductors such as InGaAsP [5], CuInSe [6] etc.

In an amorphous semiconductor field, on the other hand, comparatively small number of works had been done in the decade of 1970. They are, some trials of ER studies on amorphous Selenium by Weiser and Stuke [7], amorphous germanium by several institutes including Seraphin's group [8] and on Hydrogenated amorphous silicon (a-Si:H) by Okamoto et. al. [9]. Freeman et. al. have also reported ER spectra possessing only one distinct peak in sputtered a-Si:H [10]. ER spectra over a wide energy region of plasma deposited a-Si:F:H [11] have been recently demonstrated by Tsu et. al.. Their ER spectra reveal structures around 2 eV which fairly correspond to those reported by Okamoto et. al. and other structures due to higher interband transition in the high energy region.

As is well known in amorphous materials, an exsistence of the internal local electric field due to the disorder inherency in the amorphous structure, no sharp band edge in the density of electronic states has been generally observed. In amorphous materials, there exists no definite band edge energy assignment method so far, except for this electric field modulation spectroscopic identifications. In fact, the optical energy gap reported in the most of amorphous materials has been assigned by an extraporation of $\sqrt{\alpha\hbar\omega}$ vursus $\hbar\omega$

plotts with experienced rule. While, there is no exact theoretical background of this rule so far. On the other hand, a sharp dominant structures both in EA and ER siganls are seen at energies which the critical point occurs in the interband joint density of states function. In other words, ER and EA signals indicate more meaningful band edge assignment on the basis of electronic band structure.

As a first trial of ER study on a-Si:H, the author has conducted a series of systematic measurements of the electroreflectance signals on a-Si:H as functions of various deposition parameters. In this chapter, the author demonstrates the change in the electroreflectance spectra with RF power for decomposition of monosilane (SiH_4) and substrate temperatures, and discusses the electronic structure near the fundamental edge of a-Si:H.

3-2. Preparation of Tetrahedrally-Bonded Amorphous Semiconductors

Hydrogenated amorphous silicon films were deposited by RF plasma decomposition from monosilane (SiH_4) diluted with hydrogen to 10%. A schematic diagram of the deposition system composed of the plasma furnace and the gas introducing system is shown in Fig.3-1. The capacitively coupled closs-field system [12] beeing set outside the quartz reaction chamber with 13.56 MHz oscillator was employed for the decomposition of SiH_4. The distance between the positive column of plasma and the substrate was controlled from 10 cm to 18 cm and the RF power was varied from 35 watt to 140 watt. The rotating stage controlling the substrate temperature is used as substrate susceptor in terms to obtain uniform films. In this chapter, deposition parameters such as RF power and substrate temperature were varied in order to make a-Si:H films with various electronic structures. Amorphous silicon carbide (a-SiC:H) films

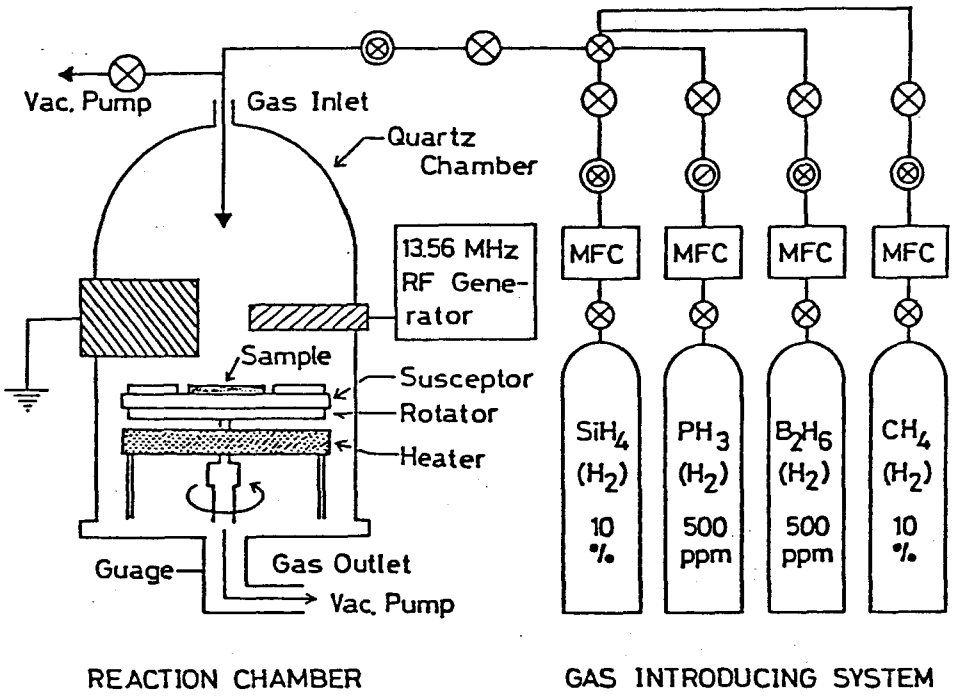

Fig. 3-1 Schematic illustration of the deposition system composed of the plasma furnace and the gas introducing system.

Materials		*Gas Fraction*	E_a	E_g
i-layer	a-Si:H	PH_3/SiH_4 =0.0% B_2H_6/SiH_4=0.0%	0.80 eV	1.8 eV
n-layer	a-Si:H	PH_3/SiH_4 =1.0% B_2H_6/SiH_4=0.0%	0.20 eV	1.8 eV
	μc-Si	PH_3/SiH_4 =1.0% B_2H_6/SiH_4=0.0%	0.02 eV	1.9 eV
p-layer	a-Si:H	PH_3/SiH_4 =0.0% B_2H_6/SiH_4=0.3%	0.40 eV	1.8 eV
	a-SiC:H	$CH_4/(SiH_4+CH_4)$=70% PH_3/SiH_4 =0.0% B_2H_6/SiH_4=0.3%	0.48 eV	2.0 eV

Table 3-1 Gas fraction, activation energy and optical gap of i-, n- and p-layer used for the a-Si:H solar cells.

were prepared by decomposition of monosilane (SiH_4) and mathen (CH_4) gas. And also doped a-Si:H and a-SiC:H films were grown with containing a desired amount of phosphine (PH_3) and diborane (B_2H_6) for n-type and p-type respectively. The gas fraction, activation energy (determined from temperature dependence of DC dark conductivity) and optical gap energy (from $\sqrt{\alpha\hbar\omega}$ vursus $\hbar\omega$ plotts) of the films used for this thesis work are summarized in Table 3-1. These conditions are also employed for the a-Si solar cells dealt with latter chapter.

3-3. Electroreflectance Signal near the Fundamental Edge in a-Si:H

The introduction of hydrogen into tetrahedrally-bonded amorphous semiconductor has an effect of reducing the density of mid gap states by several order of magnitude. This effect is called as the dangling bond passivation or termination, and firstly investigated systematically by Spear and LeComber [14]. Freeman and Paul [10] have recently studied the effect of hydrogenation on the optical properties of a-Si:H, and suggested that the dangling bond passivation effect makes the optical band edge steeper and shift it to higher energy side. Experimental verifications on this effect have also been done by several workers on various materials [15]. With the progress of film quality improvement after 1980, much more clear ER signals have been observed on both a-Si:H and microcrystalline silicon (μc-Si) [9,10,11,16]. In the electrolyte electroreflectance data taken by Tsu et. al. on a-Si:F:H based material, not only the signal based upon the fundamental edge but also those of higher interband transitions were observed. However, the feature of the $\Delta R/R$ spectrum was completely broadened as compared with those obtained from single crystalline silicon [17], and much more similar to that of

a-Si:H [10]. The clearness of its line shape of the electro-optical spectra also shows film quality of a-Si:H which is dependent upon the grade of hydrogen passivation effect to the electronic activity of the dangling bonds in the amorphous network. The author demonstrates and discusses a systematic investigations on the relation between ER signal and deposition conditions.

3-3-1. Sample fabrication and measurement procedure

Electroreflectance measurements have been carried out by using field modulation both in the Schottky barrier Au(~50Å/a-Si:H/n-type c-Si (0.1 Ωcm)). It has been pointed out by Broadsky et. al. that ER signal often involves a considerable thermoreflectance components [18] due to the Joul's heat by the modulation field applied. To eliminate this thermal dark current, the sample is formed to have a good blocking barrier such as n-i-p or Schottky junction for the longitudinal mode field modulation. Moreover, it has been checked that the thermo-reflectance signal amplitude obtained in the forward bias voltage conditions is much smaller than that in the case of reverse bias voltage. ER measurements in this thesis work were carried out in the double lock-in technique as shown in Fig.3-2. The detected ER signal of a-Si film is usually accompanied with many interference fringes as shown in Fig.3-3. To minimize such interference fringes the author has used very thin a-Si:H films with the thicknesses of about less than 1500Å [19]. By checking the invariance of the ER lineshape with the angle of light incidence to the film surface, the author has confirmed that the ER signal are almost free from the influence of interference fringes.

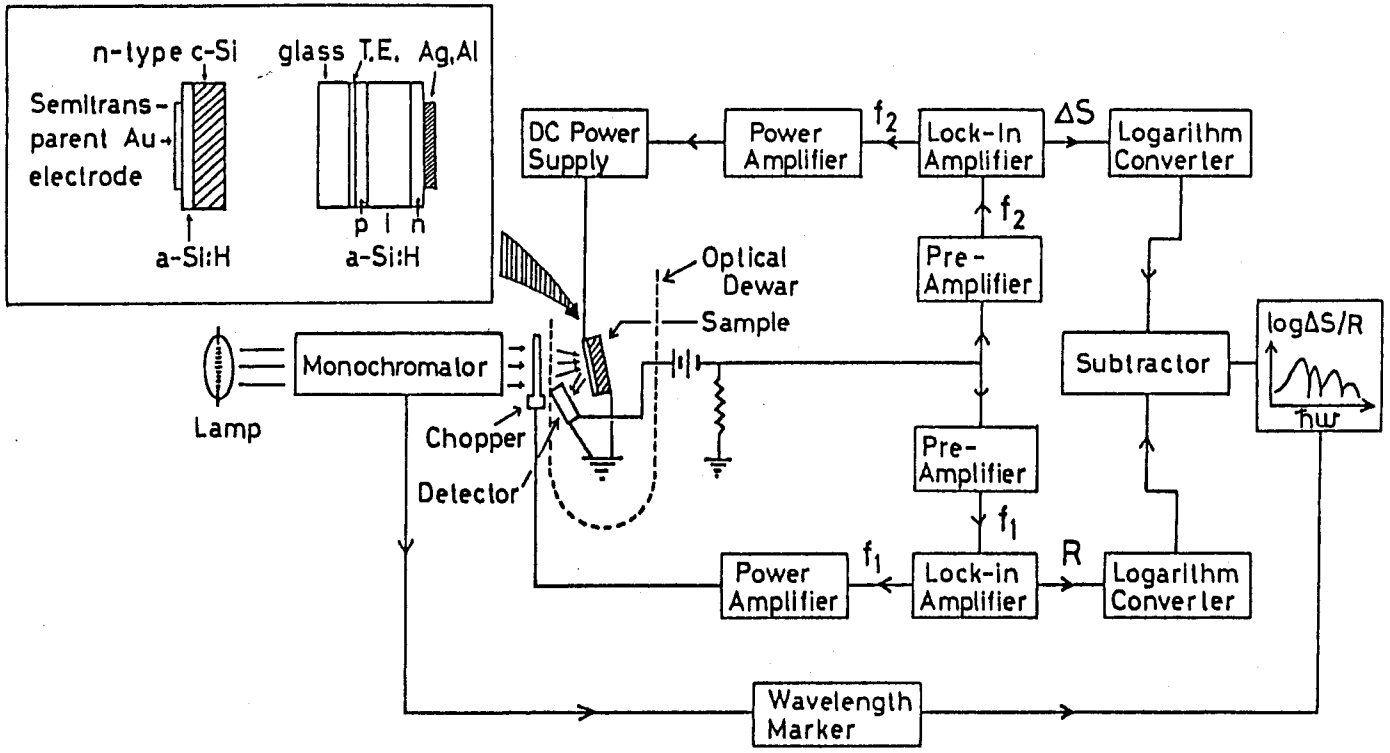

Fig. 3-2. Schematic illustration of the electroreflectance (ER) measurement system and its light path configuration in the sample. This system is coincide with that of back-surface-reflected-electroabsorption method explained in the chapter IV.

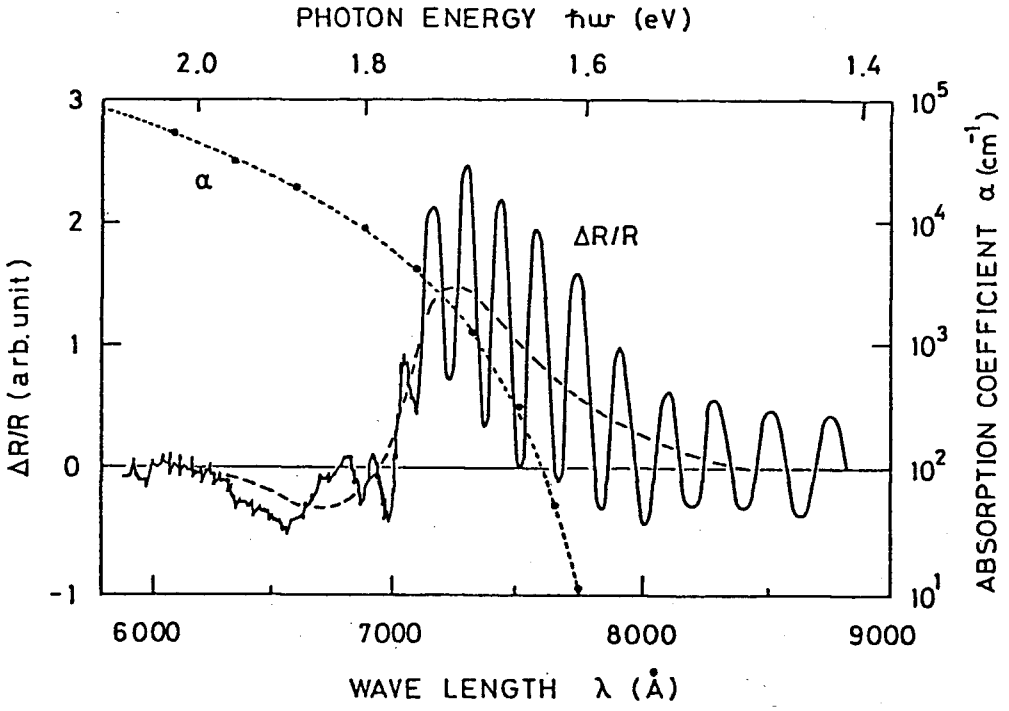

Fig. 3-3 Electroreflectance spectra near the optical energy gap in a-Si:H with the Schottky barrier electro-modulation at room temperature.

3-3-2. Effects of RF power

Effects of RF power during the plasma deposition of a-Si:H films have been investigated in ER spectra near the optical gap [19]. Figure 3-4 shows a set of experimental data for RF powers of P_{rf}=35, 100 and 140 W, respectively. ER measurements were carried out at room temperature with a constant modulation voltage of 3 V in the schottky-barrier geometry. As seen in the figure, the ER spectrum of P_{rf}=35 W has a broad single peak and resembles ER spectra obtained with sputtered a-Si:H films [10]. Increasing RF power, the spectrum comes to exhibit similar features to those seen near an M_0 critical point in crystalline semiconductors. It would be considered that optical transitions between extended states in the completely disordered system would hardly be altered by the presence of the external modulation electric field because the lifetime of an electron in the hypothetical Bloch states is so short. That is, the lifetime broadening prevails the influence of external electric field to diminish the modulated reflectance signal associated with transitions between the extended states. This is the case seen in a-Si:H prepared with low RF power or usual sputtering method, where the field induced change in the dielectric constant might be dominated by that of transition between diffused tail states and extended states as suggested by Jalali and Weiser [20]. On the other hand, ER spectra in plasma deposited a-Si:H with higher RF power exhibit broad but distinct structure originated from the field induced change in optical transitions between parabolic extended bands. This implies that the higher power deposition promotes structural orderness and thus weakens the lifetime broadening.

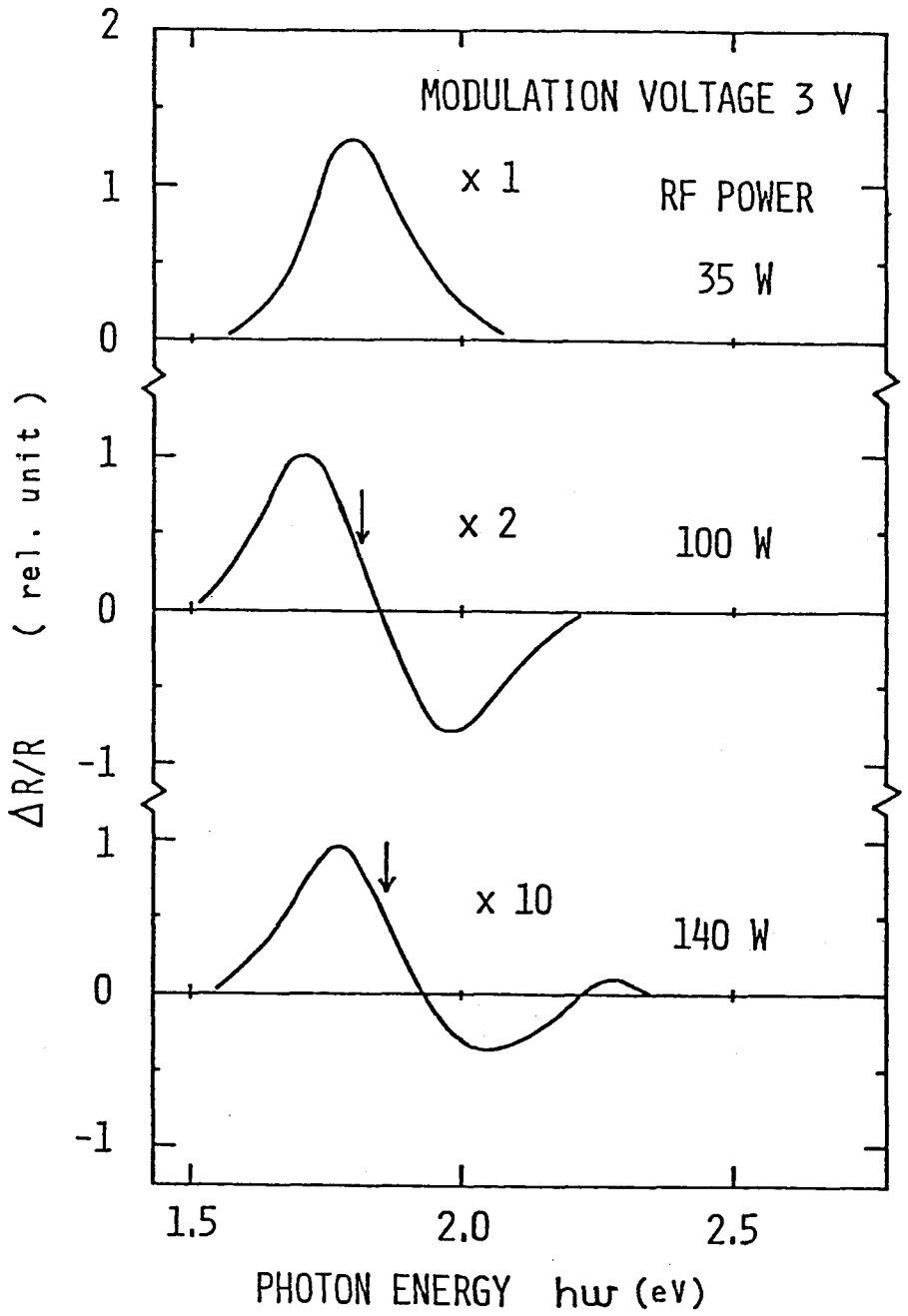

Fig. 3-4 Change in the electroreflectance signal ΔR/R with the rf power. The arrow in the figure indicates the optical energy gap identified by $\sqrt{\alpha\hbar\omega}$ vs $\hbar\omega$ plotts of absorption spectra.

3-3-3. Effects of substrate temperatures

Effects of substrate temperatures during the plasma deposition of a-Si:H films have been studied in ER spectra near the optical gap. Figure 3-5 shows the substrate temperatures dependence of ER spectra in a-Si:H films prepared with representative RF power for photovoltaic device application [21]. The arrows in the figure indicate the positions of the optical gap $E_{g(opt)}$ determined from $\sqrt{\alpha\hbar\omega}$ vursus $\hbar\omega$ plotts. It is noticeable that the increase of substrate temperature shifts the ER peak toward lower energy side according to the change in the optical gap $E_{g(opt)}$, and also decreases the half width of ER spectra. The narrowing of the half widthes might indicate a shrinking of diffused tail states with increasing the substrate temperature. This fact implies that local disorder in the amorphous net work might be smeared out with increasing the substrate temperature as has been suggested by Freeman and Paul [15].

3-3-4. Dependence of modulation electric field

Applied modulation voltage ΔV_{pp} dependence of $\Delta R/R$ peak heights are plotted in Fig.3-6. The modulation voltages ΔV_{pp} are applied at the flat band position. The slopes in log $\Delta R/R$ vursus log ΔV_{pp} are very close to 2 in all of the peaks in ER spectra. The electric field would be applied almost uniformly over the a-Si:H layer when the film thickness is very thin of 2000Å[22] in contrast to the case of crystalline bulk semiconductors in which the applied electric field extends only in the surface barrier region. These results indicate the square dependence of $\Delta R/R$ on the modulation electric field. Moreover, we confirmed the lineshape invariance of ER

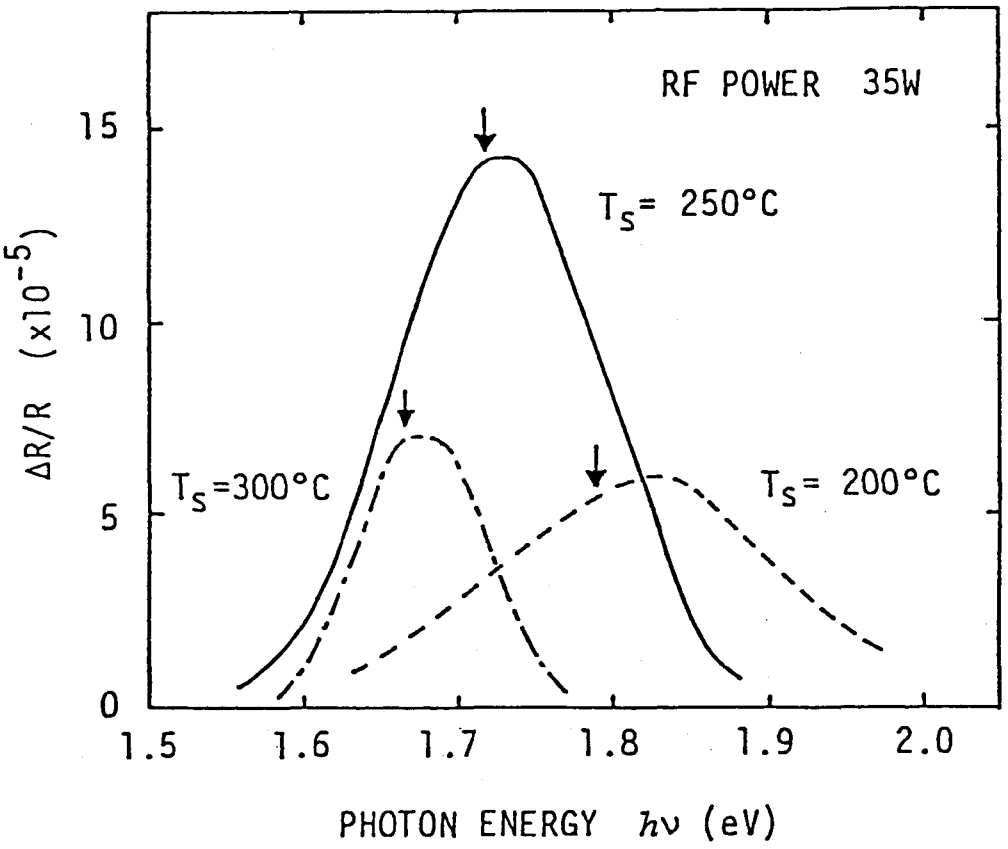

Fig. 3-5 Change in the ER signal line shape with the substrate temperature at constant rf power in the fabrication condition.

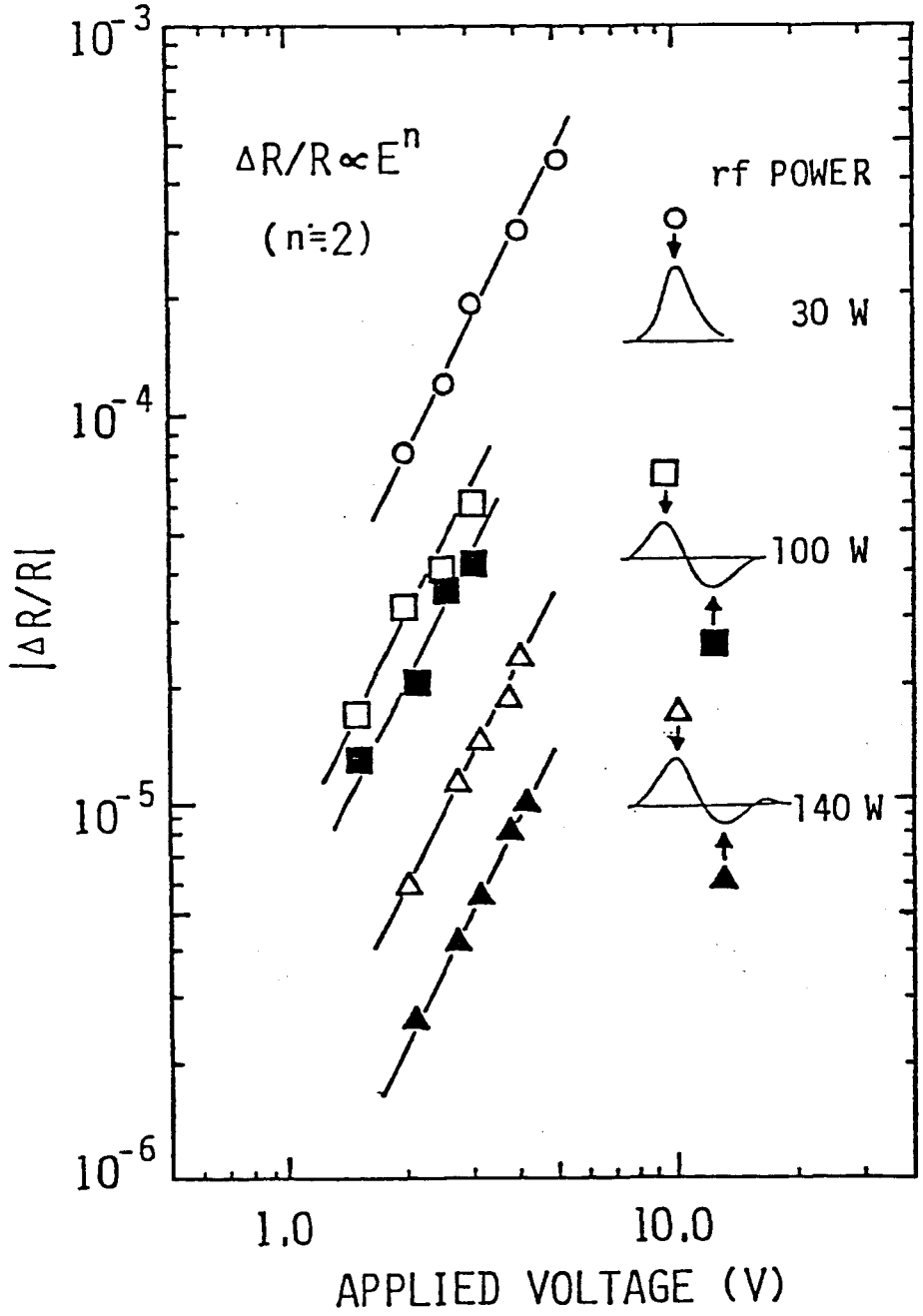

Fig. 3-6 Applied modulation voltage V_{app} dependence of ΔR/R peak hights in a-Si:H as the parameters of rf power.

spectra with respect to the modulation electric field. Thus, it is easily supposed that the ER theory in the low field regime developed by Aspnes for crystalline solids [3] holds good to a cirtain extent in the case of the a-Si:H deposited by higher RF power. Furthermore, it is possible to determine the position of the energy gap, that is the fundamental edge, by the three point adjusting method [3] which is indicated by arrows in Fig.3-4. This is a convenient method for determining the optical gap for μc-Si films because of no applicable of $\sqrt{\alpha\hbar\omega}$ vursus $\hbar\omega$ plotts as has been used for amorphous materials. While, for the lower power deposited a-Si:H, the electric field dependence of ER spectra is in coincidence with that theoretically verified by Esser in the electro-optical signal associated with local states [23].

3-3-5. Comparison between ER signal and absorption spectra

The absorption coefficient spectra near the fundamental edge of the films used for ER measurements are shown in Fig.3-7. As can be seen from the figure, change in the substrate temperatures makes a Parallel shift of the absorption spectra and also a variation in the slope of log α versus $\hbar\omega$ plots in lower photon energy regions. The former corresponds to the change in the optical energy gap with hydrogen content in the a-Si network, and the latter fact tells the spreadings of the localized diffused tail states with decreasing substrate temperatures. While, the higher deposition power gives rise to a drastical change in absorption spectra as found in ER spectra shown in Fig.3-4. Probably due to the structural orderness brought about in the a-Si:H network, the absorption coefficient in higher power deposited a-Si:H can be no longer fitted the $\sqrt{\alpha\hbar\omega}$

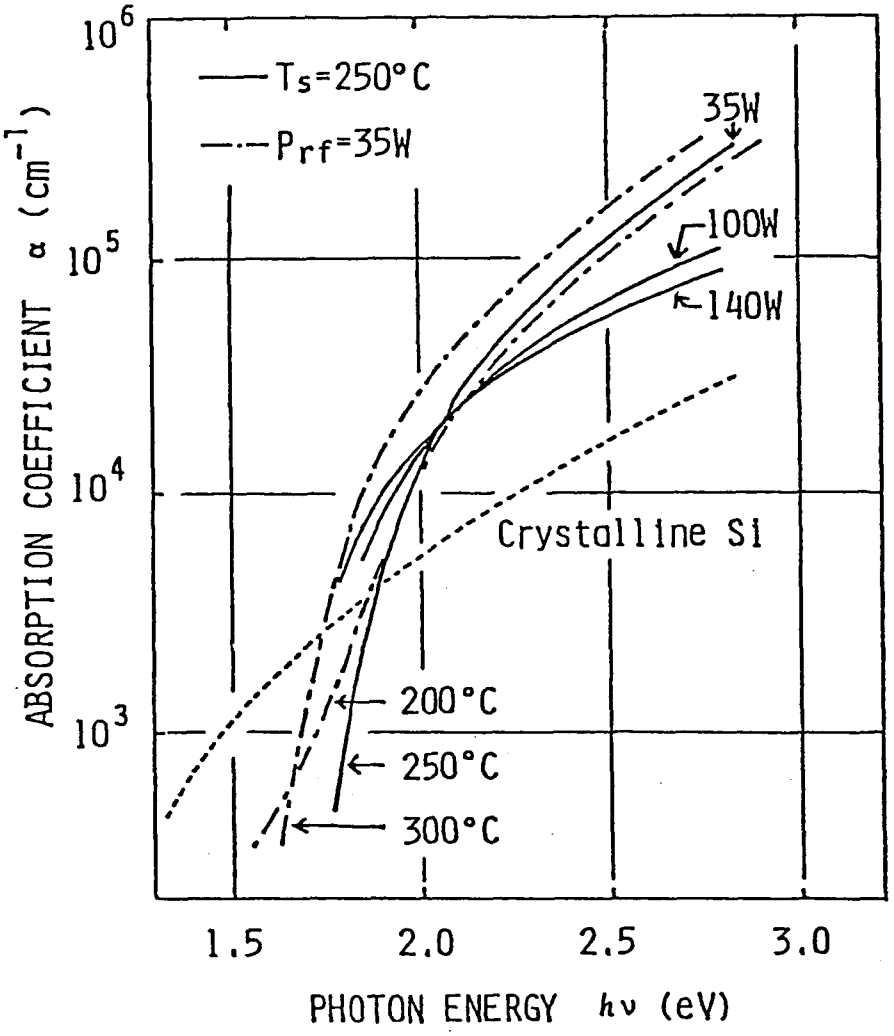

Fig. 3-7 Energy spectra of the absorption coefficient $\alpha(\hbar\omega)$ near the optical band edge on a-Si:H and μc-Si:H films prepared by various plasma reaction rf powers. The dashed line shows $\alpha(\hbar\omega)$ of crystalline Si.

versus $\hbar\omega$ plotts which is characteristic of the non-direct optical transition unique to disordered system. These observations also support the interpretation of the RF power or substrate temperature dependence of ER spectra.

a-Si:H is considered to consist of very small pure silicon islands surrounded by the Si-H rich regions [24]. These pure silicon island could be regarded as silicon crystallites put under a strong strain field caused by the surrounding hydrogen rich region. Accordingly, the overall electronic properties of a-Si:H closely correlate with the crystallite size and also the strength of the strain field. The higher deposition power might enhance the size and concentration of pure silicon islands, which recover the wave vector coherence or in other words the lifetime of an electron in this region and thus lead to crystalline-like ER spectra. However, within the extent of the deposition conditions, the crystallite size is still so samll to be directly detected by x-ray analysis. With the aid of high density of hydrogen radicals, the crystallite size sufficienctly large to the regime of microcrystalline could be grown up. As was presented by Tsu et al. this microcrystalline Si (μc-Si) [16] exhibits a similar ER feature to higher power deposited Si:H near the fundamental edge region, and some structures are found in the higher energy regions. This fact can be understood by assuming a further recovery of wave vector coherence which brings about ER signal associated with the interband transition. On the other hand, the random strain field originated in the structural mismatching at the crystallite/a-Si:H interface would be weakened by moderately high substrate temperature. This results in the decrease of diffused tail states and the shrinking of ER spectra. The characteristic feature

of ER spectra in a-Si:H prepared with various different conditions could be interpreted on the basis of the simple structural models on a-Si:H. So, ER method can be utilized as a good tool for the local structural orderness and the spreading of the diffused tail states in a-Si:H.

3-4. Summary

Results of electroreflectance studies revealed that ER signal depends critically on the film preparation conditions, RF power and substrate temperature. With increasing RF power, the feature of ER signal varies from a single broad peak to a structural signal similar to that seen in crystalline semiconductors near the M_0 critical point. This trend might reflect the change of the local structural orderness in a-Si:H network. While, the higher substrate temperature sharpens the ER peaks, which indicates a decrease of the localized tail states diffusing from the the extended bands. The ER measurement coupled with conventional electronic and structural studies would give a detailed information on the structure of a-Si:H and its electronic states relating to the optical transitions.

References

[1] M. Caldona, *Modulation Spectroscopy* (Academic Press, New York & London, 1969).

[2] D.E. Aspnes and N. Bottka, *Modulation Techniques*, ed. by P.K. Willirdson and A.C. Beer (Semiconductor and Semimetals vol.9, Academic Press, New York & London, 1972) Chap.6.

[3] D.E. Aspnes, Surface Sci. 37 (1973) 418.

[4] Y. Hamakawa and T. Nishino, *Optical Properties of Solids, new developments* ed. by B.O. Seraphine (North-holland/American Elsevier, Amsterdam, Oxford & New York, 1976) Chap.6.

[5] for example, Y. Yamazoe, T. Nishino and Y. Hamakawa, IEEE J. QE-17 (1981) 139.

[6] for example, J.L. Shay, Proc. of 11th Int. Conf. on Phys. of Semiconductors, Warszwa (1972) 787.

[7] G. Weiser and J. Stuke, Phys. Stat. Solid 35 (1969) 747.

[8] H. Piller, B.O. Seraphin, M. Markel and J.E. Fischer, Phys. Rev. Lett. 23 (1969) 775.

[9] H. Okamoto, Y. Nitta, T. Adachi and Y. Hamakawa, Surface Sci. 86 (1979) 486.

[10] E.C. Freeman, D.A. Anderson and W. Paul, Bull Amer. Phys. Soc. 24 (1979) 330.

[11] M. Brodsky and P. Leady, J. Non-cryst. Solids 35&36 (1980) 487.

[12] Y. Hamakawa, *Amorphous Semiconductor Technologies & Devices*, ed. by Y. Hamakawa (Japan Reviews in Electronics, Computers & Telecommunications, Ohm/North-Holland, Tokyo, Amsterdom & New York, 1982) Chap.4.

[13] Y. Tawada, M. Kondo, H. Okamoto and Y. Hamakawa, Sol. Energy Mat. 6 (1982) 299.

[14] W.E. Spear and P.G. LeComber, Phil. Mag. 33 (1976) 935.

[15] E.C. Freeman and W. Paul, Phys. Rev. B20 (1979) 716.

[16] R. Tsu, M. Izu, V. Cannela and S.R. Ovshinsky, J. Phys. Soc. Japan 44 (1980) Suppl.A, 1249.

[17] A. Frova, P. Handler, F.A. Germano and D.E. Aspnes, Phys. Rev. 145 (1967) 575.

[18] M. Brodski and P. Leady, J. Non-cryst. Solids, 35&36 (1980) 487.

[19] S. Nonomura, H. Okamoto, T. Nishino and Y. Hamakawa, J. Phys. 42 (1981) C4-761.

[20] S. Jalali and G. Weiser, J. Non-cryst. Solids 41 (1980) 1.

[21] Y. Tawada, T. Yamaguchi, S. Nonomura, S. Hotta, H. Okamoto and Y. Hamakawa, Jpn. J. Appl. Phys., 20 (1981) Suppl.20-2, 219.

[22] H. Okamoto, T. Yamaguchi, S. Nonomura and Y. Hamakawa, J. Phys., 42 (1981) C4-507.

[23] B. Esser, Phys. Stat. Sol. 51(b) (1972) 735.

[24] J. Knights, Jpn. J. Appl. Phys. 18 (1979) 101.

IV. BUILT-IN POTENTIAL OF HYDROGENATED AMORPHOUS SILICON SOLAR CELLS

4-1. Introduction

In order to achieve a higher conversion efficiency, it is necessary to obtain more detailed informations about physical quantites influencing the cell performance. As has been remarked in the chapter II, the main transport mechanism of photogenerated carriers in an a-Si:H solar cell is the drift of carriers [1]. Under such a circumstance, the magnitude of the internal electric field in the active i-layer has a direct effect upon the carrier collection. In this sense, it is worthy to know the value of the built-in potential V_b in actual a-Si:H solar cells. In crystalline semiconductor devices, the built-in potential can be easily determined by capacitance-voltage or conductance-voltage characteristics. However, these conventional methods are not useful in a p-i-n junction cell of practical quality and dimention because the space charge region would spread throughout the i-layer [2].

In this chapter, it is shown that the electro-optical (electroreflectance ER) signal [3] in the p-i-n a-Si:H solar cell configuration is really an electroabsorption (EA) signal [3] in the course of study on the optical confinement effect near the band edge photons of a-Si:H, and that the ER method is a useful tool for evaluating V_b in practical a-Si:H solar cells. Furthermore, consideration of internal electric field distribution in a-Si:H solar cells is also presented. Utilizing this method, it is demonstrated that the largeness of V_b is how influenced by employing new materials such as p-type a-SiC:H and n-type μc-Si as for the doped layer.

4-2. Electro-Optical Signal in a-Si:H Solar Cells

4-2-1. Fundamental representation of reflectance in a-Si:H solar cells

A typical ER spectrum observed in an a-Si:H p-i-n type solar cell configuration and the absorption coefficienct α of the i-layer used for the cell are shown in Fig.4-1(a). From this figure, it is seen that the ER signal appears at the low absorption region in the vicinity of the optical absorption edge defined from $\sqrt{\alpha\hbar\omega}$ versus $\hbar\omega$ plotts [4]. In actual a-Si solar cells, the total thickness of a-Si:H layers is around 6000Å [5] and the light penetration depth ($\sim 1/\alpha$) at the wavelength where ER signal appears is almost the same or larger than the total thickness. Figure 4-1(b) shows the results of computer calculations [2] on the light penetration into a-Si:H p-i-n junction. The most of photons having the energy 1.8 eV which is corresponding to just above the band edge are reflected from the back surface and come out again through the i-layer of a-Si:H. In such a situation, it is rather reasonable to consider that the observed ER signal does not come only from the field modulated component of the light reflected at the front surface (SnO_2/a-Si:H) but also from that reflected at the back surface (a-Si:H/metal) can also contribute to the signal.

Now consider an a-Si:H p-i-n junction ($-d_p<x<l+d_n$) of infinite extent in the y-z plane sandwiched between a transparent electrode layer ($x<-d_p$) and a metal contact electrode ($x>l+d_n$) as shown in Fig. 4-2. In this geometrical arrangement, the ER measurement is carried out by directing a light of wavelength λ in the positive direction of x and detecting the change of the reflectance induced by the applied voltage V_a.
The reflectance R (under the applied voltage V_a) is described by taking into account the multiple reflection effect within the a-Si:H

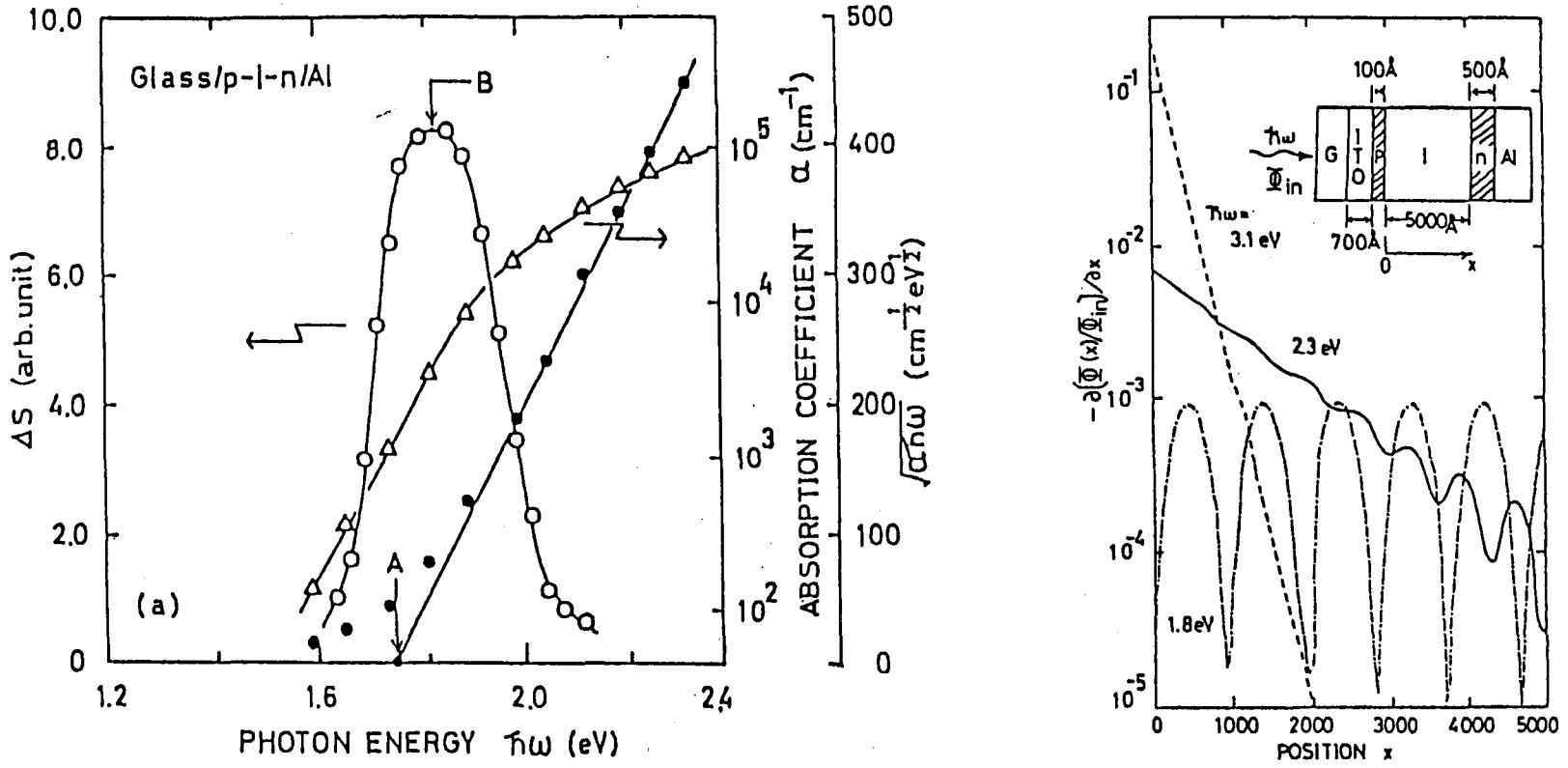

Fig. 4-1 Typical BASREA signal $\Delta S(\hbar\omega)$ and absorption coefficient spectra near the optical band edge of a-Si:H (a). Results of computer calculations on the light penetration into a-Si:H p-i-n junction (b). The most of photons having the energy 1.8 eV which is corresponding to just above the band edge, are reflected from the back surface and come out again through the i-layer of a-Si:H.

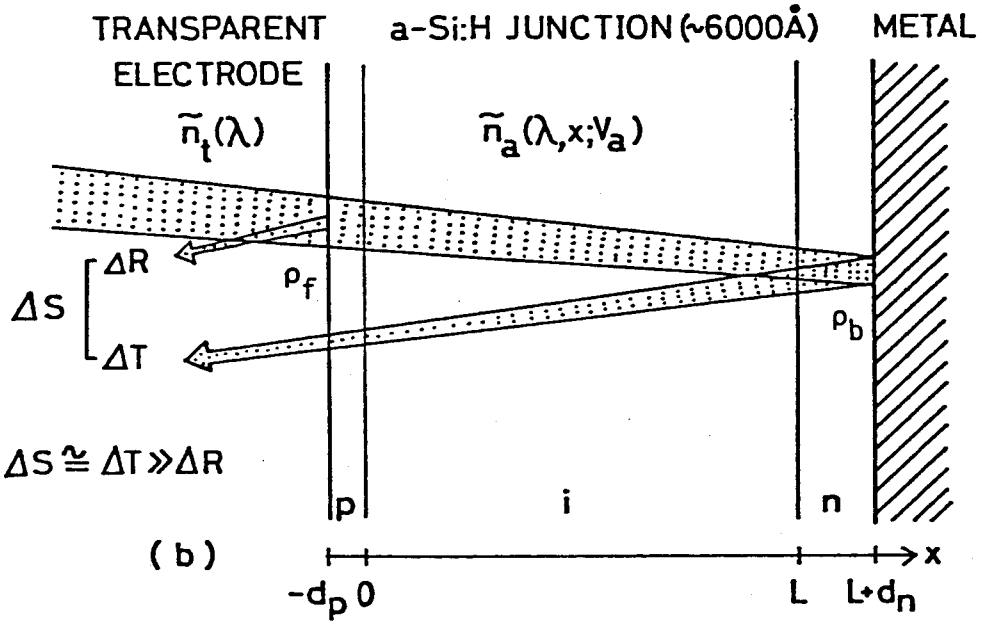

Fig. 4-2 Optical configuration of a-Si:H solar cell. The p-i-n junction of a-Si:H is sandwiched between a transparent electrode (left hand side) and a metal electrode (right hand side).

layer as

$$R = |\hat{\rho}|^2, \tag{4-1}$$

here, $$\hat{\rho} = \frac{\rho_f + \rho_b \gamma^2}{1 + \gamma^2 \rho_f \rho_b} \quad . \tag{4-2}$$

ρ_f and ρ_b are reflection coefficients at the front surface (transparent electrode/a-Si:H) and back surface (a-Si:H/metal) interfaces, respectively. ρ_f and γ can be described by utilizing the complex refractive indexes of the transparent layer $\tilde{n}_t(\lambda)$ and the a-Si:H layer $\tilde{n}_a(\lambda,x;V_a)$ which has a position dependence as reflecting the internal electric field distribution $E(x;V_a)$:

$$\rho_f(\lambda;V_a) = \frac{\tilde{n}_t(\lambda) - \tilde{n}_a(\lambda,0;V_a)}{\tilde{n}_t(\lambda) + \tilde{n}_a(\lambda,0;V_a)} \quad , \tag{4-3}$$

and $$\gamma(\lambda;V_a) = \exp\{ i\frac{2\pi}{\lambda} \int_{-d_p}^{\ell+d_n} \tilde{n}_a(\lambda,x;V_a)dx \} \quad . \tag{4-4}$$

Here, ℓ, d_n and d_p are i-, n- and p-layer thicknesses of a-Si:H layers, and i denotes the imaginary number. We assume ρ_b to be independent of the applied voltage V_a because the n-type a-Si:H/Al possesses a good ohmic property and the electric field in the vicinity of the back surface is always negligible.

The complex refractive index of a-Si:H layer is described as

$$\tilde{n}_a(\lambda,x;V_a) = n_a(\lambda,x;V_a) + i\frac{\lambda}{4\pi}\alpha_a(\lambda,x;V_a). \tag{4-5}$$

The position dependence of the real part of the refractive index $n_a(\lambda,x;V_a)$ and the absorption coefficient $\alpha_a(\lambda,x;V_a)$ in Eq.(4-5) mainly results from the spatial distribution of the internal electric field within the i-layer.

4-2-2. Back surface reflected electroabsorption

The electric field dependence of the optical constants in amorphous semiconductors has been discussed by several researchers from both the experimental and theoretical standpoints. According to them, optical constants, n_a and α_a are simply written as

$$n_a(\lambda,x;V_a) = n_{ao}(\lambda) + B(\lambda)E^2(x;V_a) \ , \tag{4-6}$$

$$\alpha_a(\lambda,x;V_a) = \alpha_{ao}(\lambda) + C(\lambda)E^2(x;V_a) \ . \tag{4-7}$$

$n_{ao}(\lambda)$ and $\alpha_{ao}(\lambda)$ are refractive index and absorption coefficient in the absence of an electric field. $B(\lambda)$ and $C(\lambda)$ are wavelength dependent quantities determining the line shape of ER spectrum. These representations are identical with those for the electric field dependent constants in crystalline semiconductors under the weak-field limit [6]. However, we have no detailed informations related to broadening factors in amorphous materials. So, we limit this treatment within the condition of ER spectrum line shape invariances. From Eqs.(4-6) and (4-7), we can write the change of the complex refractive index of a-Si:H i-layer caused by the modulation voltage ΔV_{pp} with the DC bias voltage V_{dc},

$$\Delta\tilde{n}_a(\lambda,x;V_{dc},\Delta V_{pp}) = \tilde{n}_a(\lambda,x;V_{dc}+\Delta V_{pp}/2) - \tilde{n}_a(\lambda,x;V_{dc}-\Delta V_{pp}/2) \tag{4-8}$$

$$= \{B(\lambda) + i\frac{\lambda}{4\pi}C(\lambda)\}\Delta E^2(x;V_{dc},\Delta V_{pp}) \ . \tag{4-9}$$

Then, corresponding change of $\hat{\rho}$ is derived from Eq.(4-2) as

$$\Delta\hat{\rho}(\lambda,x;V_{dc},\Delta V_{pp}) = [(1-\gamma^4\rho_b^2)\Delta\rho_f + \rho_b(1-\rho_f^2)\Delta(\gamma^2)](1+\gamma^2\rho_f\rho_b)^{-2} . \tag{4-10}$$

From Eqs.(4-1) and (4-10), ER signal ΔR is described as

$$\Delta R(\lambda,x;V_{dc},\Delta V_{pp}) = 2Re[\hat{\rho}(\lambda,x;V_{dc},\Delta V_{pp})\Delta\hat{\rho}(\lambda,x;V_{dc},\Delta V_{pp})]$$
$$= 2Re[\frac{(1-\gamma^4\rho_b^2)\hat{\rho}}{(1+\gamma^2\rho_f\rho_b)^2}\Delta\rho_f + \frac{(1-\rho_f^2)\rho_b\hat{\rho}}{(1+\gamma^2\rho_f\rho_b)^2}\Delta(\gamma^2)]. \quad (4\text{-}11)$$

Here, utilizing Eqs.(3) and (4), we can derive the field induced change of $\rho_f(\lambda;V_a)$ and $\gamma^2(\lambda;V_a)$, that is $\Delta\rho_f(\lambda;V_{dc},\Delta V_{pp})$ and $\Delta\{\gamma^2(\lambda;V_{dc},\Delta V_{pp})\}$, as

$$\Delta\rho_f(\lambda;V_{dc},\Delta V_{pp}) = \frac{-2\tilde{n}_t(\lambda)}{\{\tilde{n}_t(\lambda) + \tilde{n}_a(\lambda,0;V_{dc},\Delta V_{pp})\}^2}\Delta\tilde{n}_a(\lambda,0;V_{dc},\Delta V_{pp}), \quad (4\text{-}12)$$

$$\Delta\{\gamma^2(\lambda,V_{dc},\Delta V_{pp})\} \cong i\frac{4\pi}{\lambda}\gamma^2(\lambda;0)\int_0^l \Delta\tilde{n}_a(\lambda,x;V_{dc},\Delta V_{pp})dx. \quad (4\text{-}13)$$

Here, the potential drop within the p- and n-layer is considered to be negligibly small because the density of states around the Fermi level in p- and n-layer are generally two or three orders of magnitude larger than that in i-layer. Therefore, the integration in Eq.(4-13) is performed within the i-layer.

Here, it is noted that Eq.(4-10) is constructed by two terms. The first term is the component of field induced change of the light reflected at the front side interface (transparent electrode/a-Si:H), that is the ER component. The second term is the component of field induced change of the light reflected at the back side interface (a-Si:H/metal), that is the EA component. In order to compare the magnitudes of these two terms in Eq.(4-10), let's set ρ_b=0, which anihilates the second term and simplifies Eq.(4-10) to ER component. This condition is approximately satisfied in the sample structure of SnO_2/p-i-n(a-Si:H)/ITO. In this sample structure, it was experimentally checked that the detected signal amplitude of ΔR was about two orders of magnitude smaller compared with

that of the actual solar cell structure [SnO_2/p-i-n(a-Si:H)/Al] under the same modulation conditions. Therefore, we can assume that $\Delta R(\lambda,x;V_{dc},\Delta V_{pp})$ of the actual a-Si:H solar cells is mainly caused by the component of field induced change of the light reflected at the back side interface (a-Si:H/metal). In other words, the detected signal on actual a-Si:H solar cells results essentially from the EA effect. In this sense, the ER method applied to thin a-Si:H solar cells is refered as back surface reflected electroabsorption (BASREA) method. Thereby, we exchange the notation of $\Delta R(\lambda,x;V_{dc},\Delta V_{pp})$ by $\Delta S(\lambda,x;V_{dc},\Delta V_{pp})$ to avoid a probable confusion. From above discussion and Eqs.(4-9),(4-11) and (4-13), $\Delta S(\lambda;V_{dc},\Delta V_{pp})$ is written as

$$\Delta S(\lambda;V_{dc},\Delta V_{pp}) = D(\lambda)\int_0^l \Delta E^2(x;V_{dc},\Delta V_{pp})dx, \qquad (4\text{-}14)$$

$$\text{here, } D(\lambda) = 2Re\left[\frac{(1-\rho_f^2)\rho_b\gamma^2(\lambda;0)}{(1+\gamma^2\rho_f\rho_b)^2}\ \{C(\lambda) - i\frac{4\pi}{\lambda}B(\lambda)\}\right]. \qquad (4\text{-}15)$$

It is worthy to note that the signal detected by BASREA method is described by a combination of two separated functions, one of which is dependent only on the light wavelength and the other is dependent only on the electric field.

4-3. Built-In Potential in a-Si:H Solar Cells

4-3-1. Bias voltage dependence of electro-optical signal

Figure 4-3(a) shows the intensity of BASREA signal ΔS plotted as a function of the DC bias voltage V_{dc} with various AC modulation voltages ΔV_{pp}. The result in Fig.4-3(a) is for a SnO_2/p-i(a-Si:H)-n(μc-Si)/Al type solar cell. The light wavelength used for the measurement was

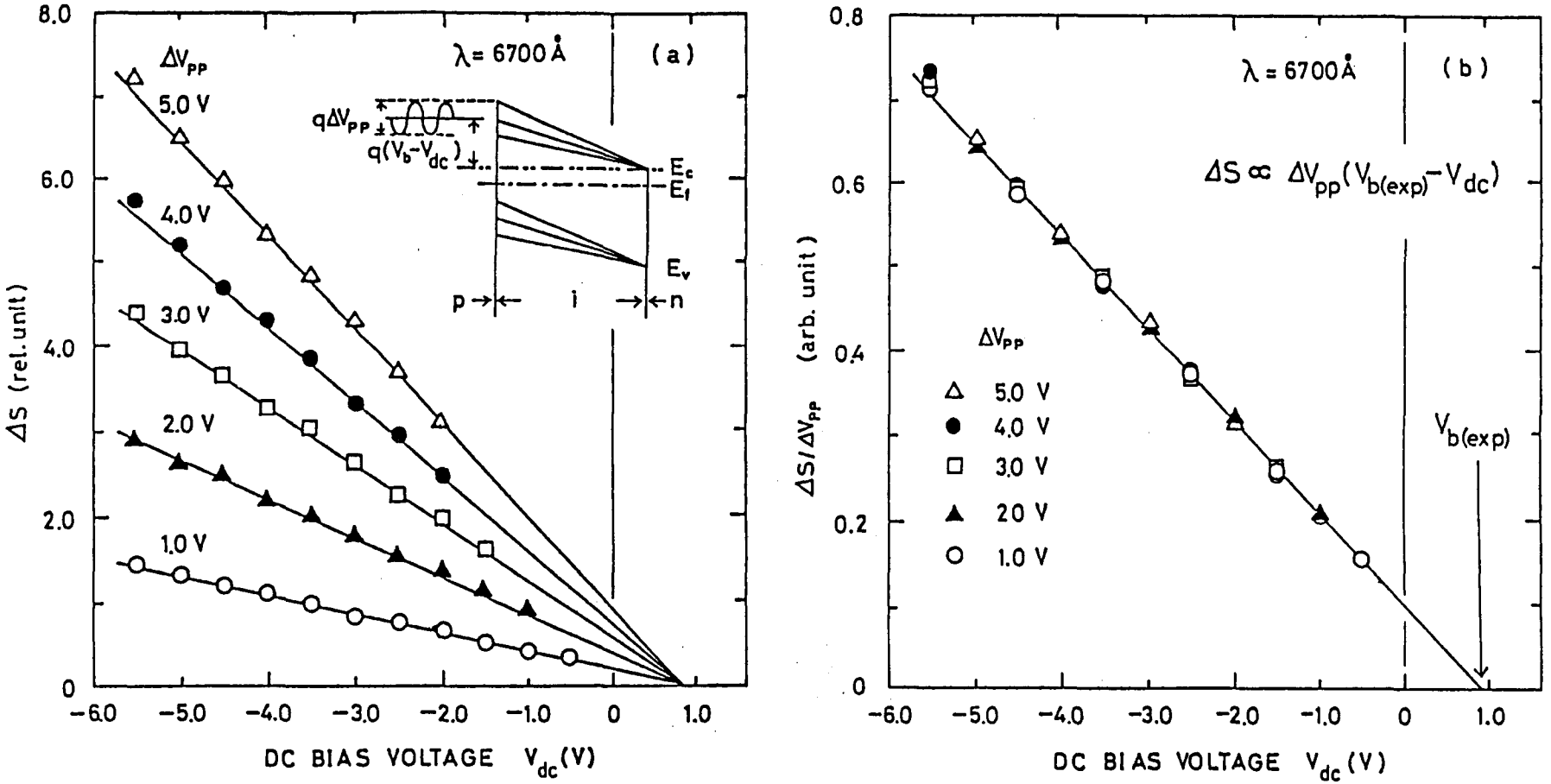

Fig. 4-3 BASREA signal intensity ΔS as a function of the applied DC bias voltage V_{dc} for various modulation voltages ΔV_{pp}. The modulation frequency is 1 kHz and the measurement temperature is 25°C (a). Normalized BASREA signal intensity ΔS as a function of the applied dc bias voltage V_{dc} for various AC modulation bias voltages ΔV_{pp} (b).

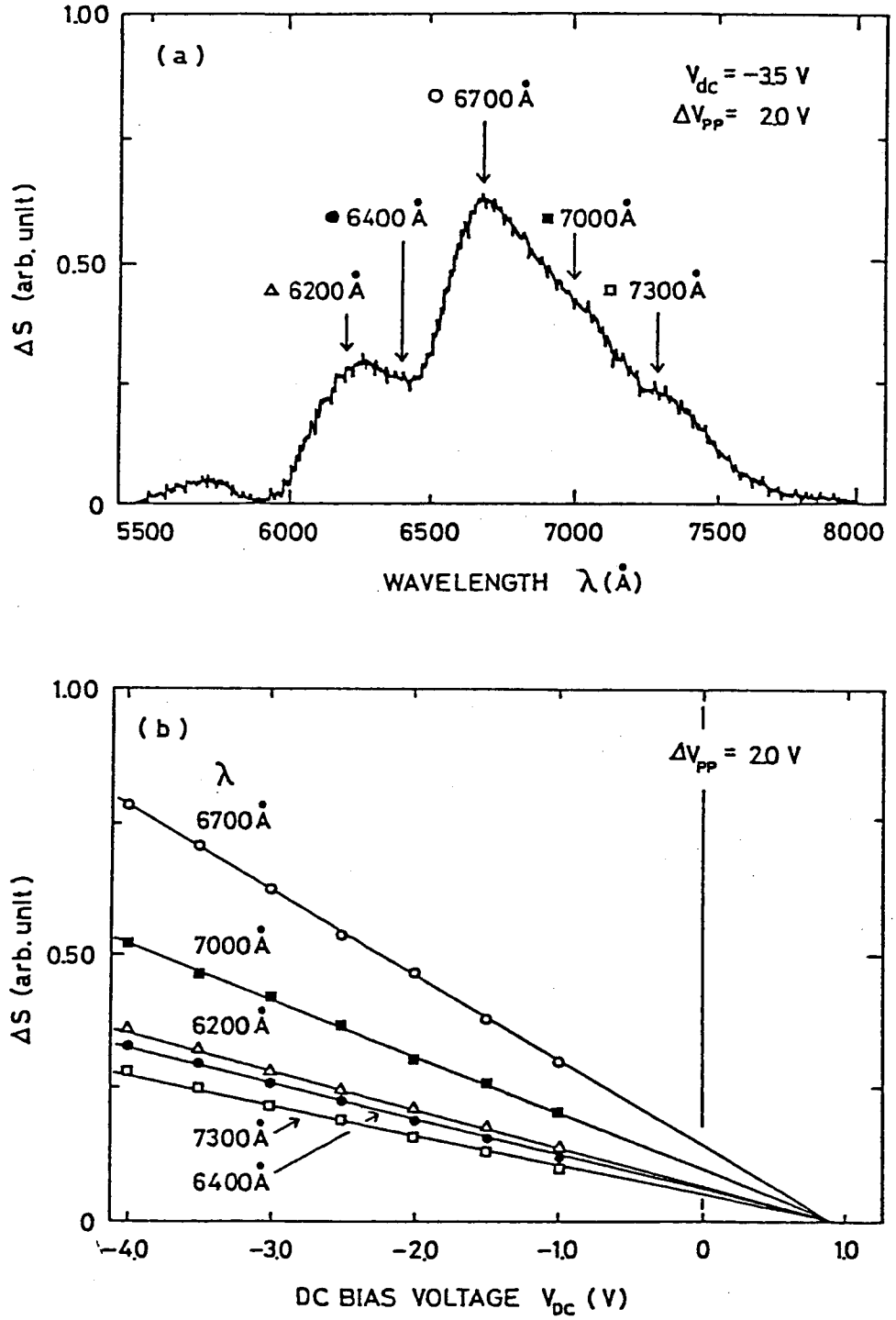

Fig. 4-4 Detected BASREA spectra in actual a-Si solar cell with DC bias voltages. Extremes of spectra come from the interference effect. (a). BASREA signal intensity ΔS as a function of the applied DC bias voltage V_{dc} for various measurement wavelengthes (b).

6700Å. It can be seen that ΔS has a linear dependence on V_{dc} and all the extrapolated straight lines for various ΔV_{pp} intercept the DC bias voltage axis at the same point. Figure 4-3(b) demonstrates the DC bias dependence of ΔS normalized by ΔV_{pp}. It is noted that all the data points can be placed on a single straight line. From this tendency, DC and AC bias dependence on ΔS is written empirically by

$$\Delta S(\lambda;V_{dc},\Delta V_{pp}) \propto \Delta V_{pp}[V_{dc}-V_{b(exp)}], \tag{4-16}$$

where the crossing point on the DC bias voltage axis is denoted as $V_{b(exp)}$.

Figure 4-4(a) shows the detected BASREA spectrum in actual a-Si solar cell [SnO_2/p-i(a-Si:H)-n(μc-Si)/Al]. It is seen that there are several extremes in BASREA spectrum. The peaks are originated from interference effects. Usually, the light wavelength which gives the extremes of BASREA spectrum shifts with varying the total thickness and optical constants of a-Si:H layers constructing the junction. Figure 4-4(a) shows the DC bias voltage dependence of ΔS with various light wavelengthes shown by arrows in Fig.4-4(a). It can be seen that ΔS has a linear dependence on V_{dc} and all the extrapolated straight lines with various light wavelengthes intercept the DC bias voltage axis at the same point as shown in Fig. 4-4(b). This experimental result verifies that V_b has no wavelength dependence as predicted by Eq.(4-14) and allows us to use the light wavelength which possesses the maximum intensity of BASREA signal for all the cells.

4-3-2. Internal electric field in the i-layer

The characteristic relation as shown in section 4-3-1 can be easily obtained in two simple cases by utilizing Eq.(4-14): uniform and

exponential-like distributions of the internal electric field $E_i(x;V_a)$ in the i-layer. In the case of a uniform field distribution, the internal electric field with externally applied voltage V_a is described as $E_i(x;V_a)=(V_b-V_a)/\ell$, where we defined V_b as the electric potential within the i-layer of a-Si:H solar cell in the case of no applied bias voltage;

$$V_b = \int_0^{\ell} E_i(x;0)dx \ . \qquad (4\text{-}17)$$

Then, it is easily proven through Eq.(4-14) that $V_{b(exp)}$ is just V_b. The other choice is an exponential-like field distribution. In this case, $V_{b(exp)}$ is described by

$$V_{b(exp)} = (\Delta\mu_p+\Delta\mu_n) + (\Delta\Psi_n/\cosh\frac{d_n}{\Delta_n} - \Delta\Psi_p/\cosh\frac{d_p}{\Delta_p}). \qquad (4\text{-}18)$$

Here, $\Delta\mu_p$ is the Fermi level difference of bulk p- and i-layer and $\Delta\mu_n$ is that of n- and i-layer. Δ_p and Δ_n are quantities related to gap states density around Fermi level position and defined as $\Delta=\sqrt{\varepsilon\varepsilon_o/q^2D_F}$ where ε_o and q are free space permitivity and electron charge. ε and D_F are dielectric constant and density of states around the Fermi level for p- and n-layer, respectively. $\Delta\psi_p$, $\Delta\psi_n$ and the derivation related to Eq.(4-18) are shown in the appendix A. This exponential-like field distribution is essentially originated in the energetically uniform density of states in the gap. It is also verified that $V_{b(exp)}$ in Eq.(4-18) is coincident with the electrical potential within the i-layer in the case of no applied voltage, that is the built-in potential V_b by our definition. Therefore, we can determine the built-in potential in a-Si:H solar cells experimentally from the crossing point $V_{(exp)}$ on the DC bias axis despite of any detailed information about internal potential distribution.

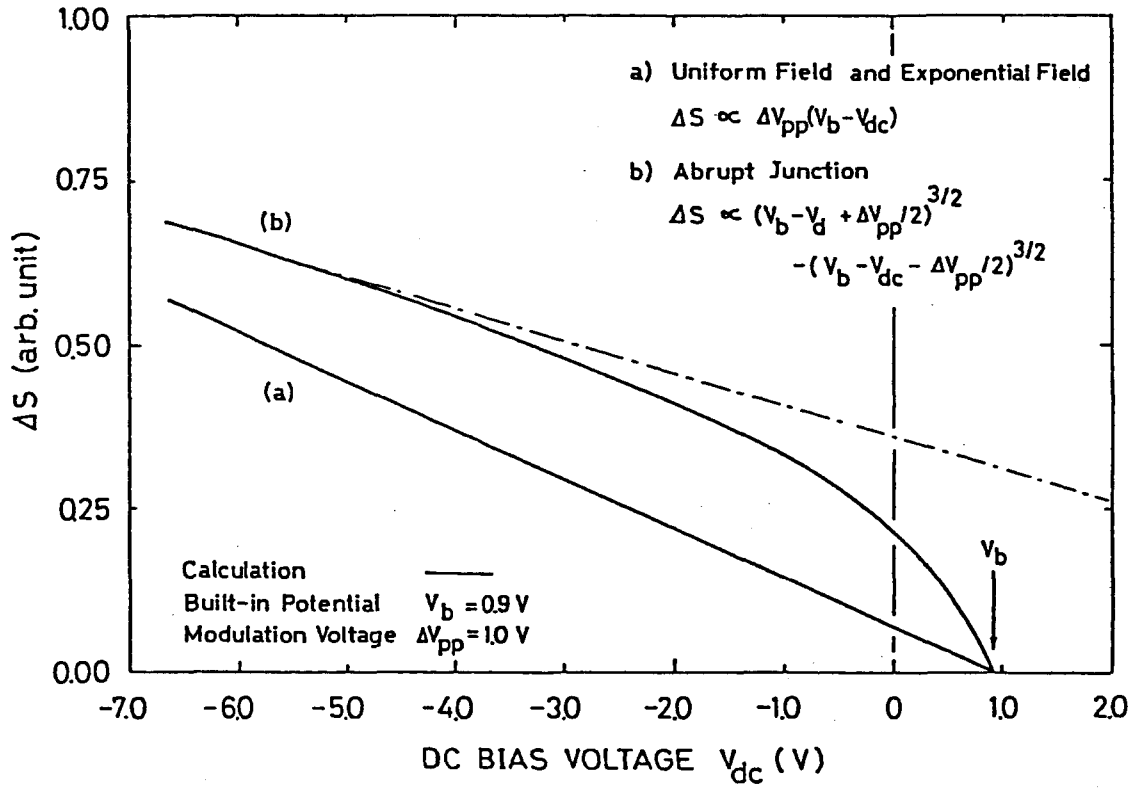

Fig. 4-5 Calculated results of DC bias dependence of BASREA signal for various internal electric field distribution of a-Si solar cells.

Figure 4-5 shows the calculated results of the V_{dc} dependence of ΔR assuming the uniform and exponential-like and the field distribution of abrupt junction in the case of crystalline junction. So, within the limits of a-Si solar cells processing the conversion efficiency more than 5∿6%, the distribution of internal electric field of a-Si p-i-n junction solar cells are supposed to be uniform or almost uniform even in the case of exponential-like field distribution.

It must be noted that Eq.(4-18) holds only when the relaxation time of the space charge distribution with applied AC modulation voltage is much smaller than the inverse of the modulation frequency. Therefore, the modulation frequency of AC bias voltage applied to the sample should be severely checked. In the higher frequency range ($\geqq$10 kHz), the ΔS had no linear dependence on DC applied voltages V_{dc}. As for the sample employed in the present work, the linear dependence on V_{dc} and the coincident value of V_b were obtained within the modulation frequency range from 50Hz to 10kHz as shown in Fig.4-6. No linear dependence on V_{dc} is not found in the frequency more than 100 kHz [7]. In such a high frequency region, modulation voltage might not be applied to whole the i-layer as in the case of low modulation frequency but to regions near the p/i and i/n interfaces. In this circumstance, no linear dependence on V_{dc} is obtained as shown in Fig.4-5.

4-3-3. P-layer thickness dependence of built-in potential

Figure 4-7 shows variations of the V_b with the doped layer thickness at the front side. Three types of a-Si:H solar cells having different structures were employed; (a) SnO_2/p-i(a-Si:H)-n(μc-Si)/Al, (b) SnO_2/ p(a-SiC:H)i(a-Si:H)-n(μc-Si)/Al, (c) ITO/n(μc-Si)-i(a-Si:H)-p(a-SiC:H)/ stainless Steel. The thickness of the back side doped layers was

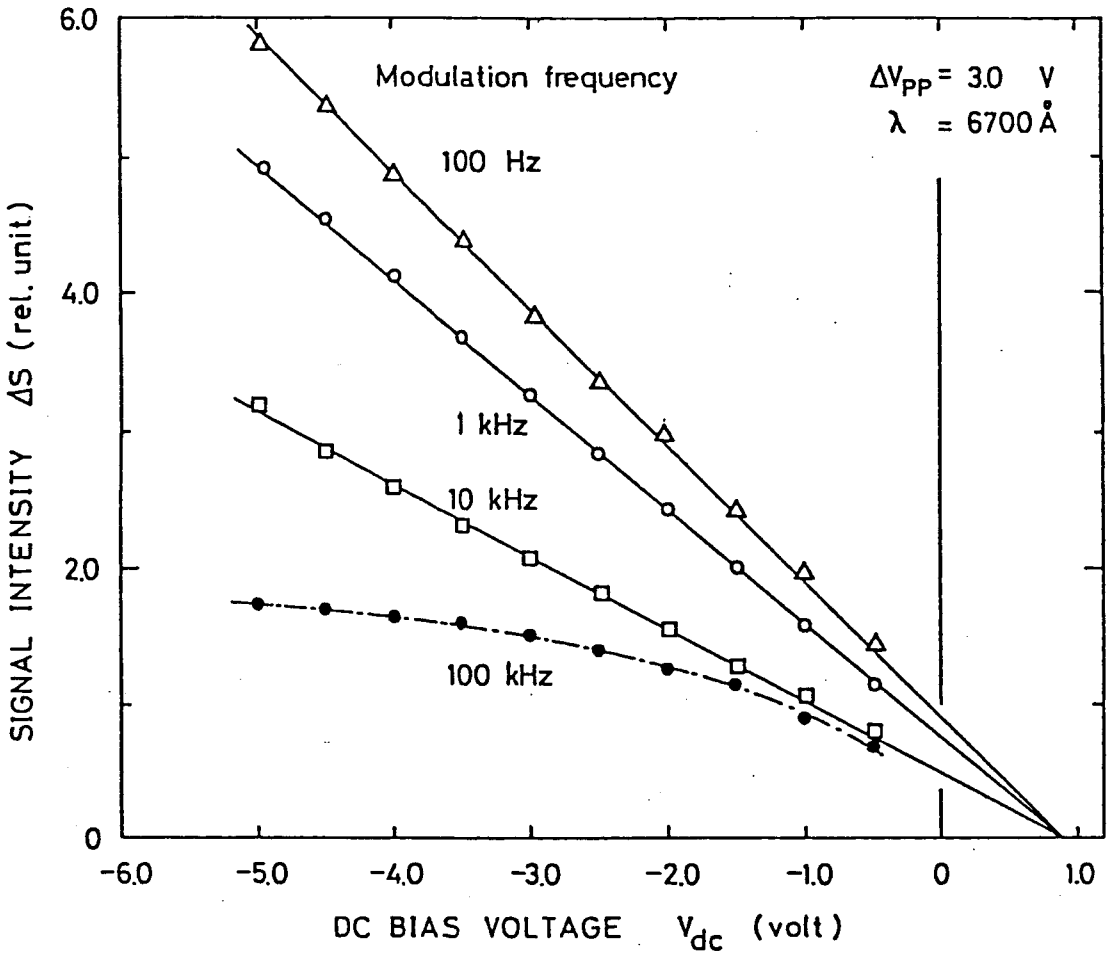

Fig. 4-6 DC bias dependence of BASREA signal intensity ΔS with a parameter of modulation frequency.

fixed at 500Å. There is found the same tendency for each type of cells, that is, the V_b becomes gradually larger with increasing the thickness of the front side doped layer and saturates in the thicker layer region ($\geq$150Å). The saturation value of V_b in type (a) cell is 0.93V. In the case of type (b) cell where p-type a-SiC:H is employed instead of p-type a-Si:H, the saturation value of V_b increases by about 80mV from that of type (a). While, the largest saturated value of V_b is seen in the cell type (c) and is about 1.2V.

The experimentally obtained tendency of V_b described above can be explained by Eq.(4-18). The solid lines in Fig. 4-7 are calculated through Eq.(4-18) with appropriately chosen fitting parameters, Δ_p and $\Delta\Psi_p$ (or Δ_n and $\Delta\Psi_n$), as inserted in this figure. The value of Δ_p and Δ_n is related to the density of localized states D_F around the Fermi level as mentioned in the previous section. D_F evaluated for p-type a-Si:H, p-type a-SiC:H and n-type μc-Si are $1.7\times10^{19}cm^{-3}/eV$, $4.6\times10^{19}cm^{-3}/eV$ and $8.5\times10^{18}cm^{-3}/eV$, respectively. Because the localized gap states density may make a large influence on the recombination rate of the photogenerated carriers, it could be considered that the interface recombination velocity of the cell type (b) is largest among the three types of cells concerned here. This discussion is fully supported by more direct experimental results deduced by means of both the photovoltaic analysis [8] and the transient grating technique [9].

According to eq.(4-18), the saturated value of V_b corresponds to $\Delta\mu_n+\Delta\mu_p$. When the doped layers in the p-i-n junction cells are sufficiently thick, $\Delta\mu_n+\Delta\mu_p$ might be related to the Fermi level positions ΔE_n and ΔE_p which are measured from the conduction and valence band edges in n- and p-type materials used for the cell.

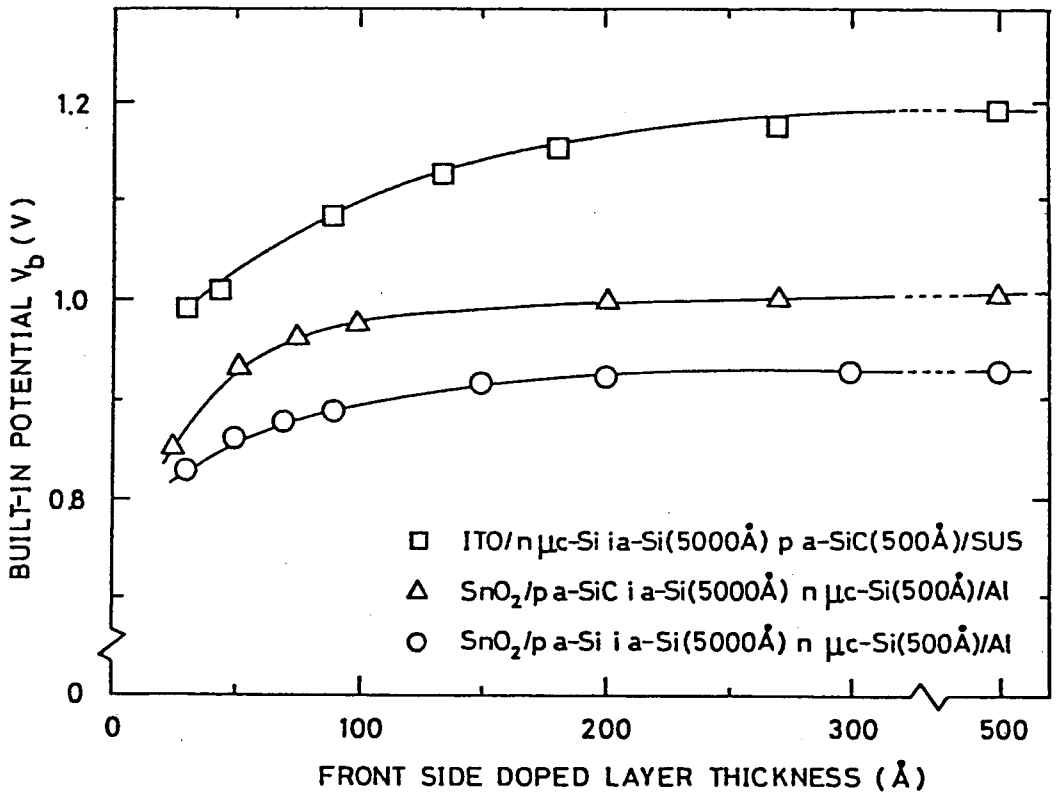

Fig. 4-7 Variation of the built-in potential V_b for various types of a-Si solar cells as a function of the front side doped layer thickness. These values are measured at 25°C.

$$\Delta\mu_n + \Delta\mu_p = E_g - \Delta E_n - \Delta E_p + \delta_p + \delta_n, \qquad (4\text{-}19)$$

here, E_g is the optical gap of the undoped a-Si:H layer ($\sim$1.8eV). δ_p and δ_n are the energy discontinuity at the p/i and i/n interfaces which are related to the difference of the band gap and the work functions between doped (p- and n-type) and undoped (intrinsic) layer. It should be noted here that this equation would hold only in the ideal case where the electric parameters (ΔE_n, ΔE_p, E_g etc.) of layers composing the cell are not influenced by the cell fabrication process. Because such influence has often been observed, we will only give a qualitative discussion on $\Delta\mu_n+\Delta\mu_p$ by means of eq.(4-19). ΔE_p and ΔE_n for p-type a-Si:H and a-SiC:H are shown in Table 3-1. These values are estimated from the activation energy of the temperature dependence on the dark conductivity. Equation (4-19) tells us that the saturation values of V_b, that is $\Delta\mu_n+\Delta\mu_p$, may be enhanced by the presence of the energy discontinuity δ_p and δ_n. This phenomenon can be indeed assured when the values of $\Delta\mu_n+\Delta\mu_p$ are compared in homojunction cell (a) and heterojunction cell (b). Namely, in spite of smaller ΔE_p in type (b) compared with that of type (a), the $\Delta\mu_n+\Delta\mu_p$ in cell type (b) is larger than that of type (a).

In addition, it is worth to note that the saturation values of V_b in the inverted type cell (c) is about 200mV larger than that of type (b) despite that these two types of cells are made of the p-, i- and n-layers of the same thicknesses and qualities. A probable reason for this discrepancy may be the difference of the substrates on which cells are fabricated. In the cell type (b) which is constructed on the glass coated with SnO_2 (or ITO/SnO_2), the transparent electrode layer could be reduced by hydrogen plasma and elements such as Sn and O (or In) could diffuse into the p-layer [10], which results in a Fermi level shift in

the p-layer toward mid gap and thereby lowers the built-in potentials. It is of a great significance to improve the transparent electrode chemically strong against the hydrogen plasma in order to get higher efficiency in type (b) cell.

4-3-4. Application to the various types of a-Si:H solar cells

Figure 4-8 shows the correlation between V_b determined from BSREA and the open circuit voltage V_{oc} under AM 1 ($100mW/cm^2$) illumination in various types of a-Si:H solar cells. In a Schottky barrier cell utilizing a gold (Au) contact, the V_b is about 0.7V and V_{oc} is 0.55V. Whereas V_b of inverted type cell [ITO/n(μc-Si)-i(a-Si:H)-p(a-SiC:H)/Stainless Steel] is about 1.2V and V_{oc} is 0.88V. V_b of the p-i-n type homojunction cell constructed on the transparent electrode is around 0.84V, V_{oc} is about 0.79V. It is found that the value of V_b is enhanced by about 50mV by employing n-type μc-Si instead of n-type a-Si:H. In addition, about 80mV increase of V_b was also found in the case of p-type a-SiC:H. It is seen that V_{oc} becomes larger with increasing V_b.

This tendency can be interpreted utilizing the general relation:

$$V_{oc} = \int_0^l E_i(x;0)\left[\frac{\Delta\sigma(x)}{\sigma_o(x)+\Delta\sigma(x)}\right]dx. \qquad (4\text{-}20)$$

$\sigma_o(x)$ and $\Delta\sigma(x)$ are dark and photo-induced change of conductivity, respectively. Under the constant intensity of light illumination ($100mW/cm^2$), the term in the square bracket of Eq.(4-20) is considered to be constant. So, V_{oc} is linearly dependent on V_b because of the integration of internal electric field within the i-layer being V_b as mentioned in the previous section. The V_b of the inverted type cell is 0.88V in spite of largest built-in potential. This lower V_{oc} as

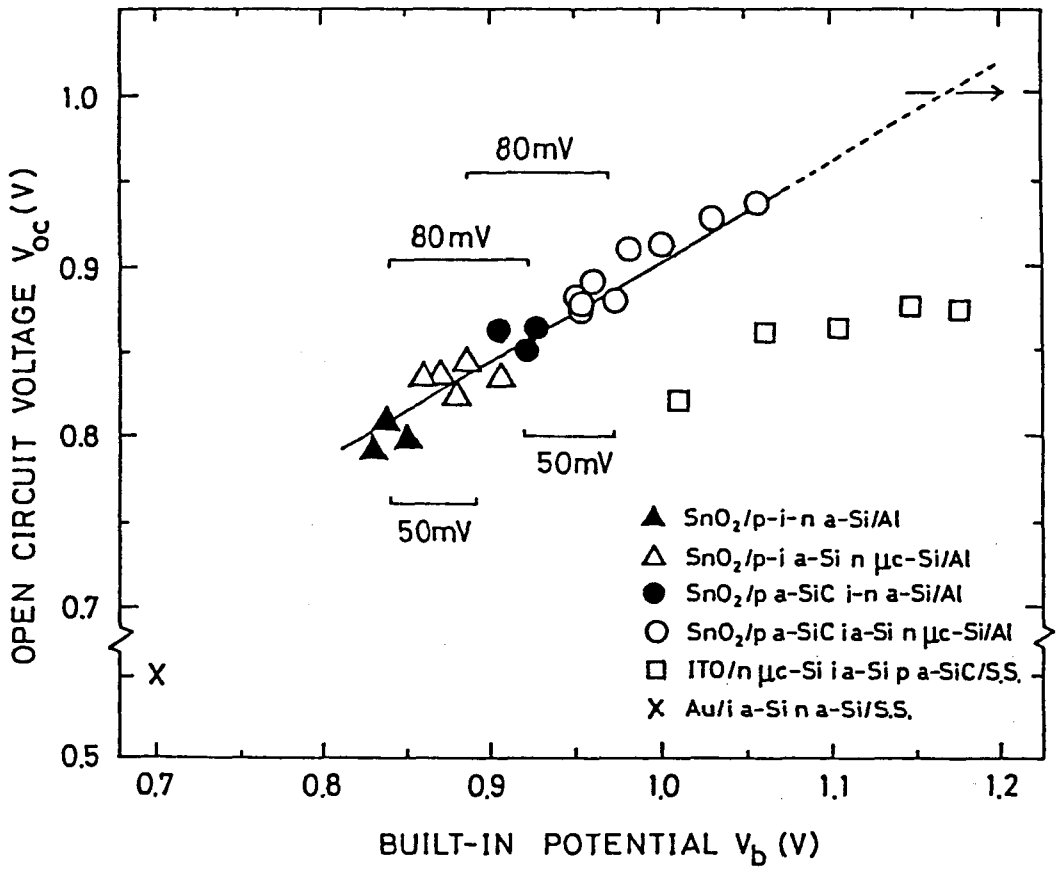

Fig. 4-8 Comparison between the built-in potential V_b and open circuit voltage V_{oc} under AM 1 (100 mW/cm^2) illumination for various types of a-Si solar cells measured at 25°C.

compared with cells constructed on the transparent electrode might result from the space charge distortion caused by photogenerated carriers, which could shield the original internal electric field. The same results are predicted from the stand point of computer analysis by Hack and Shur, and they interprete this trend of V_b by bulk recombination of photogenerated carrier [11]. In the present stage, the maximum V_{oc} achieved so far is 936.6mV in SnO_2/p(a-SiC:H)-i(a-Si:H)-n(μc-Si)/Al type cell. The V_b of this cell is 1.06V. If the built-in potential would increase up to 1.2V by improving the transparent electrode, the V_{oc} close to 1.0V will be obtained as expected from the extrapolated solid line in Fig. 4-8.

4-4. Summary

The Back Surface Reflected Electroabsorption (BASREA) method was proposed as a powerful tool for determining the built-in potential of a-Si:H solar cell. It was cleared up that the BASREA signal ΔS in actual a-Si:H solar cells was mainly originated from Electroabsorption component in spite of using the measurement system of Electroreflectance, and that the built-in potential of a-Si:H solar cells is determined by utilizing DC and AC external bias voltage dependence of ΔS. The V_b were shown in various types of a-Si:H solar cells by employing this method. Furtheremore, as for the heterojunction solar cells constructed on the transparent electrode, increases of V_b were found by utilizing the p-type a-SiC:H and n-type μc-Si).

References

[1] H. Okamoto, T. Yamaguchi, S. Nonomura and Y. Hamakawa, J. Phys. 42 (1981) C4-507.

[2] T. Yamaguchi, H. Okamoto, S. Nonomura and Y. Hamakawa, Jpn. J. Appl. Phys. 20 (1981) Suppl.20-2, 195.

[3] S. Nonomura, H. Okamoto and Y. Hamakawa, Jpn. J. Appl. Phys. 21 (1982) L464, S. Nonomura, H. Okamoto and Y. Hamakawa, Appl. Phys. A 32 (1983) 31.

[4] J. Tauc, *Amorphous and liquid Semiconductors* (Plenum Press, London and New York, 1974).

[5] H. Okamoto, Y. Nitta, T. Adachi and Y. Hamakawa, Surface Sci. 86 (1979) 486.

[6] D.E. Aspnes and J.E. Rowe, Phys. Rev. B5 (1972) 4022.

[7] S. Nonomura, K. Fukumoto, H. Okamoto and Y. Hamakawa, 10th Int. Conf. on Amorphous & Liquid Semiconductor, Tokyo, (1983) to be published.

[8] S. Nonomura, H. Okamoto, H. Kida and Y. Hamakawa, Jpn. J. Appl. Phys. 21 (1982) Suppl.21-2, 279.

[9] S. Komuro, Y. Aoyagi, Y. Segawa, S. Namba, A. Masuyama, H. Okamoto and Y. Hamakawa, Appl. Phys. Lett. to be published.

[10] N. Fukada, T. Imura, A. Hiraki, Y. Tawada, K. Tsuge, H. Okamoto and Y. Hamakawa, Jpn. J. Appl. Phys. 21 (1982) 271.

[11] M. Hack, M. Shur, W. Czubatyj, J. Yang, J. McGill, J. Non-Cryst. Solid (1983) to be published. 10th Int. Conf. on Amorphous & Liquid Semiconductors, Tokyo (1983).

V. FILM AND JUNCTION QUALITIES IN AMORPHOUS SILICON SOLAR CELLS

5-1. Introduction

In amorphous silicon solar cells, the carrier collection efficiency varies with applied bias voltage V_a. Such kind of field-dependent carrier collection efficiency results from, in a part, the field-dependent photocarrier generation[1] and, in other part, the field-dependent photocarrier collection[2]. However, the quantum efficiency of photocarrier generation was estimated almost at unity in a good quality hydrogenated amorphous silicon (a-Si:H) film so far as the excitation photon energy exceeds the optical gap energy and the internal electric field is higher than about 10^4 V/cm [3,4]. Hence, when the above conditions are satisfied in the practical experiments, the field-dependent carrier collection efficiency could be ascribed to the field dependent photocarrier collection. While, this field-dependent photocarrier collection is originated in both the finite magnitude of the mobility-lifetime products and the interface property [5]. Accordingly, through a careful examination on the variation of the carrier collection efficiency spectrum with the applied bias voltage V_a, the mobility-lifetime products and the interface property can be characterized in actual a-Si:H solar cells [6,7].

Based upon these considerations, we developed a method for evaluating the mobility-lifetime products of electrons ($\mu_n\tau_n$) and holes ($\mu_p\tau_p$) and the effective surface recombination factors at the p/i(S_n) and i/n(S_p) interfaces through the theoretical analysis of the carrier collection efficiency under the external bias voltage in p-i-n basis a-Si:H solar cells [7]. This characterization method has been applied to clarify the variations of the mobility-lifetime products with impurity

doping, temperature, and prolonged light exposure.

5-2. Normalized Collection Efficiency Spectra

The spectral dependence of the photocurrent $J_L(\lambda,V_a)$ was measured under various applied bias voltages V_a using the standard lock-in technique and optical system. The p-i-n junction cells were illuminated on the p-layer with monochromatic light, in the wavelength λ region from 0.4 to 0.7 μm, which was chopped at a frequency of 43 Hz. The monochromatic light flux incident on the cells was in the range $10^{14} \sim 10^{15}$ photons/$s \cdot cm^2$ [1], where the photocurrent depends linealy on the incident photon flux. Analysis of the carrier collection efficiency was carried out on the normalized carrier collection efficiency $\eta(\lambda,V_a)/\eta(\lambda,0)$, Which is readily calculated by $J_L(\lambda,V_a)/J_L(\lambda,0)$ as shown in Fig.5-1. This normalization procedure can successfully cancel out the spectral dependences of the optical system including monochromator and light source. Examples of $\eta(\lambda,V_a)/\eta(\lambda,0)$ are shown in Fig. 5-1 (c). For the sake of generality, the spectra are given as a function of the absorption coefficient α of a-Si:H. Consequently, the spectral dependence of $\eta(\alpha,V_a)/\eta(\alpha,0)$, that is $J_L(\alpha,V_a)J_L(\alpha,0)$, is described in terms of five fundamental parameters: the built-in potential V_b, the mobility-lifetime products of electrons ($\mu_n\tau_n$) and holes ($\mu_p\tau_p$) in the active i-layer and the effective surface recombination factors at p/i (S_n) and i/n (S_p) interfaces, which are defined by the effective surface recombination velocities ($S_{p/i}$, $S_{i/n}$) divided by the relevant carrier mobilities (μ_n, μ_p).

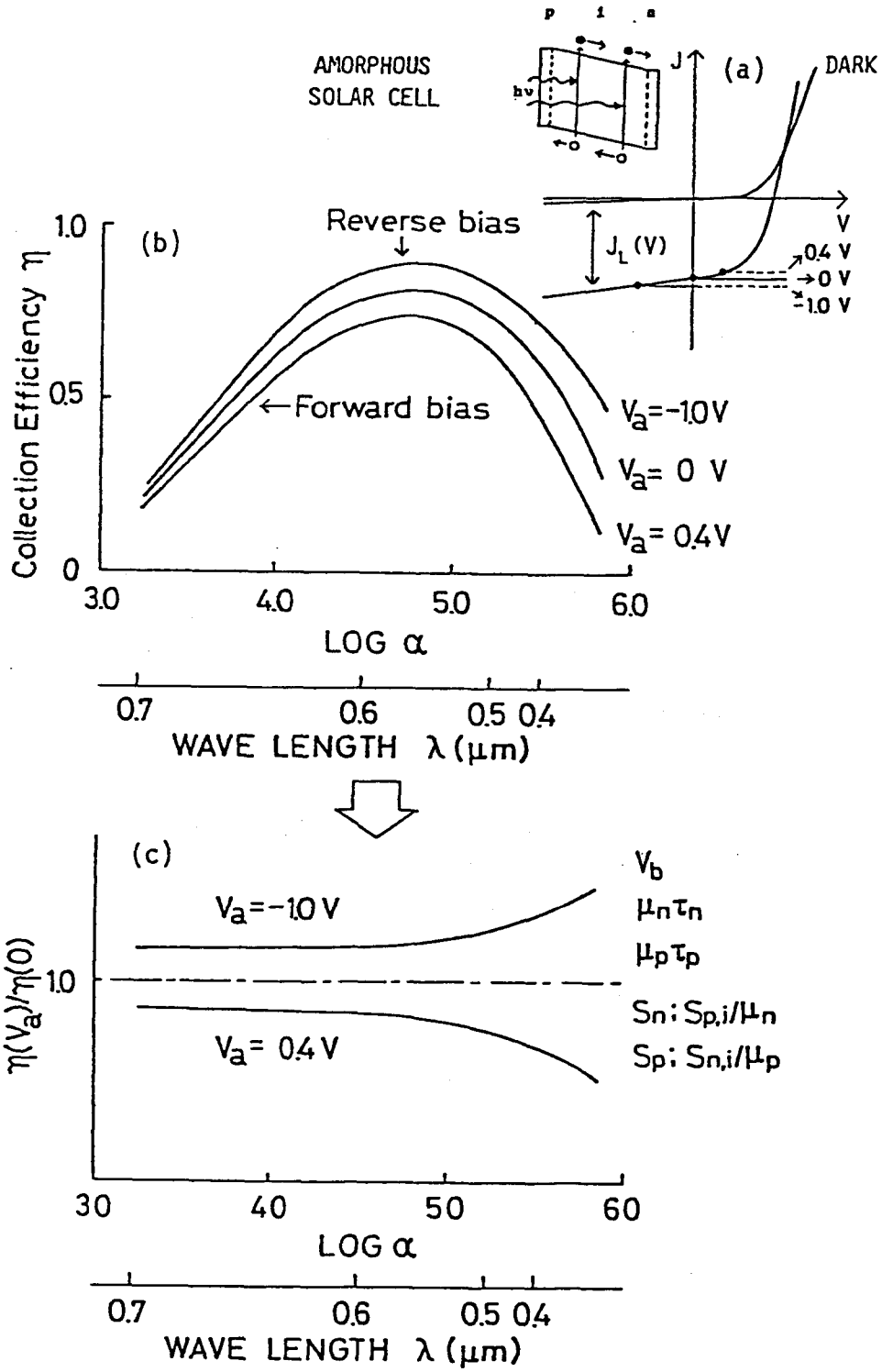

Fig. 5-1 Typical J-V characteristic of a-Si solar cell (a) and its collection efficiency spectra with the conditions applied the forward, zero and reverse bias voltages (b). Normalized collection efficiency spectra derived from collection efficiency spectra of (b) (c).

5-3. Eavaluation of Mobility-Lifetime Products and Surface Recombination Factors

5-3-1. Evaluation Method

Figure 5-2 and 5-3 show calculated results on the collection efficiency spectra $\eta(V_a)$ under the bias voltage of V_a, normalized by the collection efficiency under the short circuit condition $\eta(0)$, that is, $\eta(V_a)/\eta(0)$. For the generality, $\eta(V_a)/\eta(0)$ spectra drawn as a function of the absorption coefficient α of undoped a-Si. These results correspond to the case of light incident on the p-layer. One can obtain the similar results, if one wishes, for the n-side illumination only by exchanging the subscripts n and p. Understandings of $\eta(V_a)/\eta(0)$ spectra are of great importance because they are directly related with the curve fill factor (FF) of actual cells. Figure 5-2 demonstrate $\eta(V_a)/\eta(0)$ as a parameter of $\mu_n\tau_n+\mu_p\tau_p$ with the condition, $\mu_n\tau_n/\mu_p\tau_p=1$. Other parameters are fixed as inserted in the figure. One can observe a drastic change of $\eta(V_a)/\eta(0)$ with $\mu_n\tau_n+\mu_p\tau_p$. However, it should be noted here that $\eta(V_a)/\eta(0)$ rather weakly depends on $\mu_n\tau_n+\mu_p\tau_p$ at the shorter wavelength region ($\log\alpha=5.0\sim6.0$). While, Figure 5-3 displays the change of $\eta(V_a)/\eta(0)$ with varying the ratio of $\mu_n\tau_n$ and $\mu_p\tau_p$ from 0.1 to 1.0 for a fixed value of $\mu_n\tau_n+\mu_p\tau_p=1\times10^{-7}cm^2/V$. It is also noticeable that $\eta(V_a)/\eta(0)$ varies with $\mu_n\tau_n/\mu_p\tau_p$ only at the shorter wavelength region ($\log\alpha \leq 4.5$) but almost insensitive to it at the longer wavelength region. The similar examinations have been made on the dependence of $\eta(V_a)/\eta(0)$ on S_n and S_p, which reveals that the front side and back side surface recombination have a significant influence on $\eta(V_a)/\eta(0)$, particularly at the shorter and longer wavelength region, respectively.

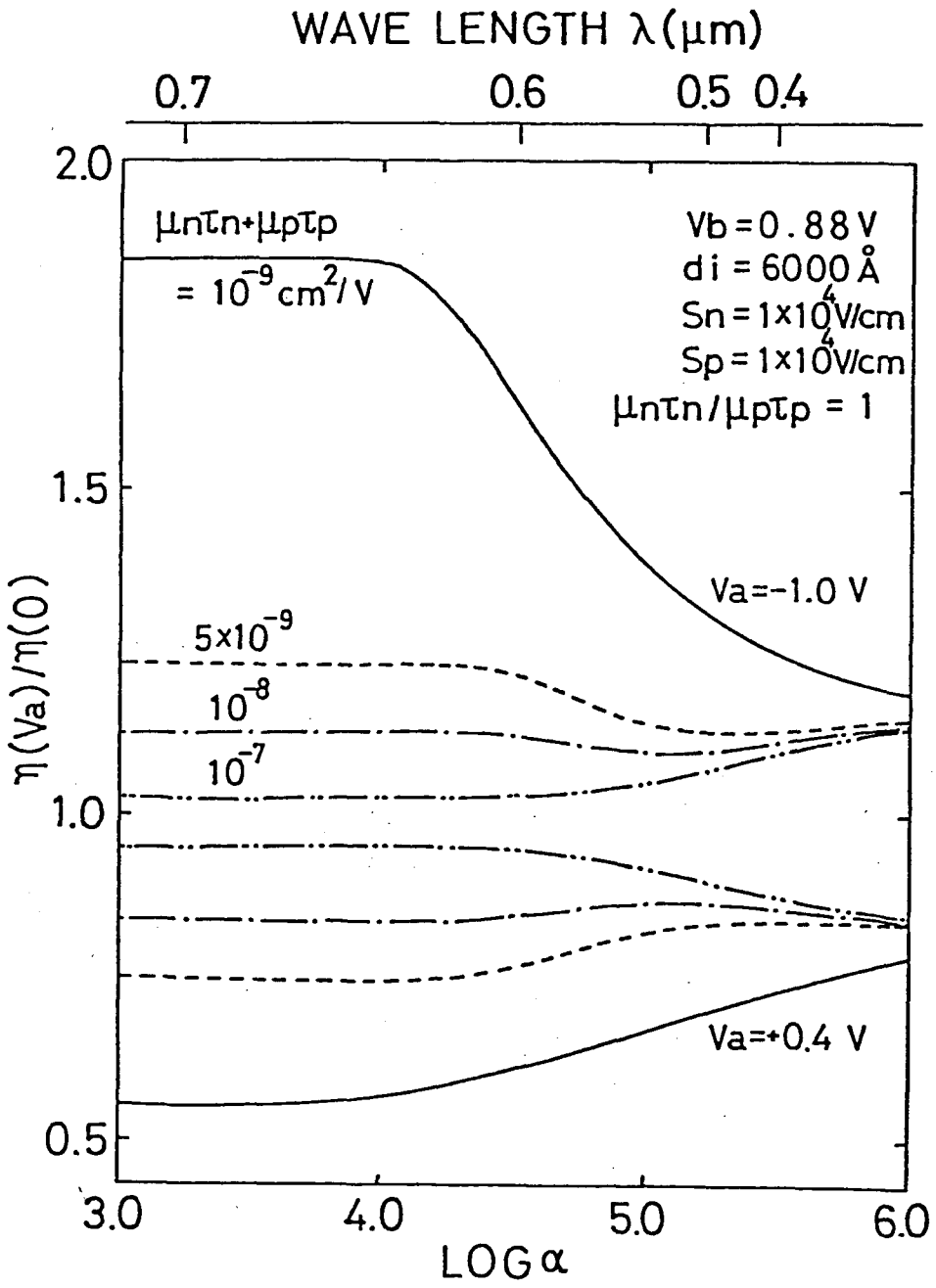

Fig. 5-2 Calculated result on normalized collection efficiency spectra $\eta(V_a)/\eta(0)$ as a parameter of $\mu_n\tau_n+\mu_p\tau_p$.

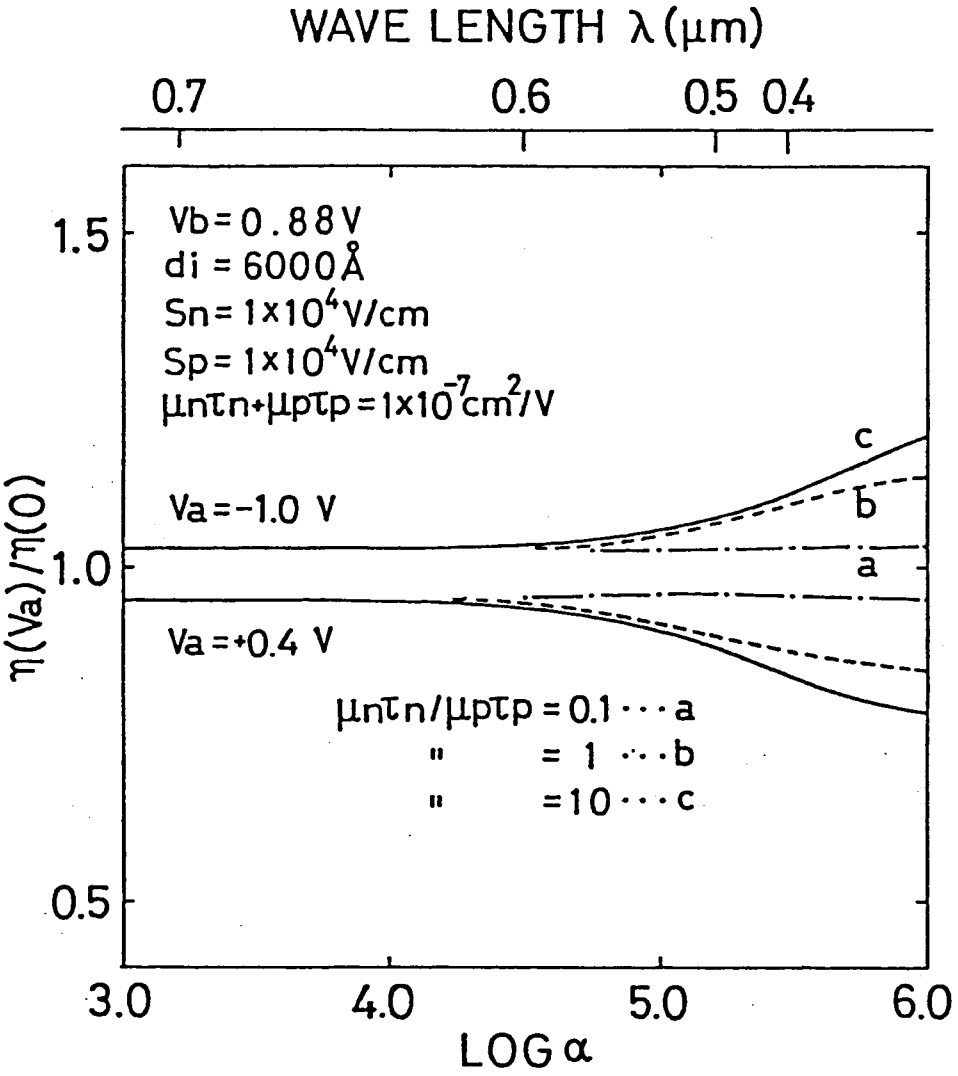

Fig. 5-3 Calculated result on normalized collection efficiency spectra $\eta(V_a)/\eta(0)$ as a parameter of $\mu_n\tau_n/\mu_p\tau_p$.

These features are interesting and important because one can estimate $\mu_n\tau_n+\mu_p\tau_p$ and S_n from the magnitude of $\eta(V_a)/\eta(0)$ at the longer wavelength region, and those of $\mu_n\tau_n/\mu_p\tau_p$ and S_p with $\eta(V_a)/\eta(0)$ at the shorter wavelength region. Of course, at least more than two data of $\eta(V_a)/\eta(0)$ for different values of V_a are required in each wavelength region to determine four physical parameters. Detailed examination of $\eta(\alpha,V_a)/\eta(\alpha,0)$ spectra has shown that they are mainly dominated by the magnitude of $\mu_n\tau_n+\mu_p\tau_p$ and $S_n xS_p$ at the lower absorption region and by $\mu_n\tau_n/\mu_p\tau_p$ and the front side effective surface recombination parameter at the higher absorption region, respectively[5,8]. Making use of this trend, when experimental data of $\eta(\alpha,V_a)/\eta(\alpha,0)$ at least for two different applied voltages V_a in both lower and higher absorption regions are given, $\mu_n\tau_n$, $\mu_p\tau_p$, S_n and S_p can be separately evaluated. An example of this procedure is demonstrated in Fig.5-4(a) and (b). These diagrams correspond to the case of light incident on the p-layer, and here the auther assumes V_b=0.9V and adopt V_a=-1.0 and 0.4V. Similar plots for the case of light incident on the n-layer can be easily obtained only by exchanging the subscripts n and p in Fig. 5-4(b). Firstly, as can be seen in Fig.5-4(a) , utilizing experimental values $\eta(\alpha,V_a)/\eta(\alpha,0)$ at the lower absorption region (here α=1.0x10^4 cm^{-1}), both $\mu_n\tau_n+\mu_p\tau_p$ and $S_p xS_n$ are determined. Then, as indicated in Figure 5-4(a), values of $\mu_n\tau_n+\mu_p\tau_p$ and S_n are evaluated by comparing experimental data of $\eta(\alpha,V_a)/\eta(\alpha,0)$ at the higher absorption region (here α=1.74x10^{5}cm^{-1}) with those theoretically calculated under the condition already settled on $\mu_n\tau_n+\mu_p\tau_p$ and $S_n xS_p$. Consequently , a coupling of ($\mu_n\tau_n+\mu_p\tau_p$, $S_n xS_p$) and ($\mu_n\tau_n/\mu_p\tau_p$, S_n) determined in Fig. 5-4(a), (b), respectively, gives separated values of $\mu_n\tau_n$, $\mu_p\tau_p$, S_n and S_p. Once these parameters are determined in amorphous solar

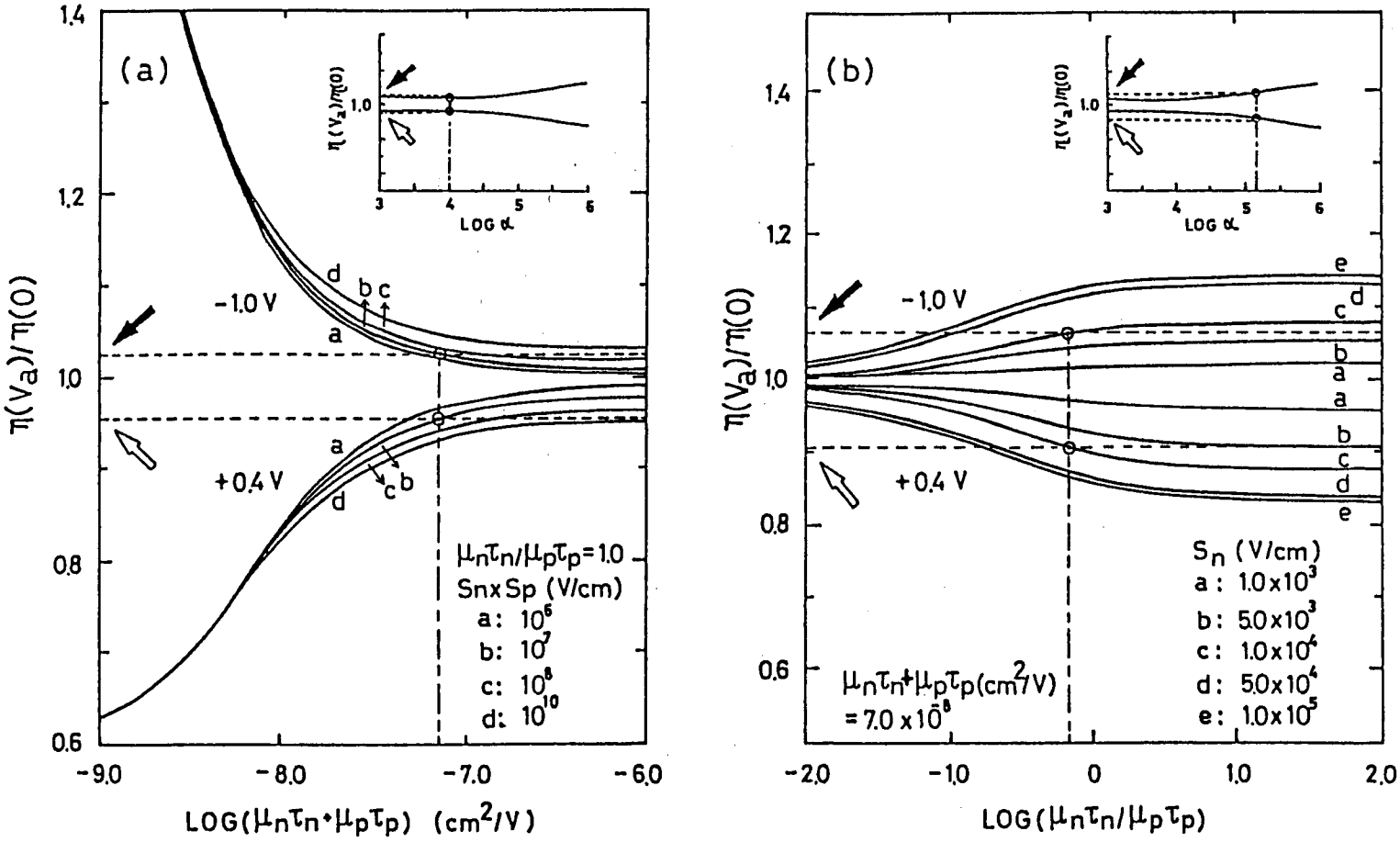

Fig. 5-4 Diagrams for evaluating physical parameters from experimentally obtained $\eta(\alpha,V_a)/\eta(\alpha,0)$ spectra. $\eta(\alpha,V_a)/\eta(\alpha,0)$ in the lower absorption region (a) and in the higher absorption region (b).

cells, $\eta(\alpha,V_a)/\eta(\alpha,0)$ spectra can be easily calculated and compared with their experimental counterparts.

5-3-2. Normalized collection efficiency spectra in practical a-Si:H solar cells

It will be demonstrated that examples of $\eta(V_a)/\eta(0)$ spectra in actual a-Si solar cells and their theoretical curves obtained by parameter fitting demonstrated by the previous section. In figure 5-5, $\eta(V_a)/\eta(0)$ spectra of a SnO_2/p-i-n/Al type solar cell exhibiting an efficiency of 6.5% under AM 1 illumination is plotted by open circles. The best fitting between the experimental data and theoretical curve is obtained with physical parameters inserted in the figure. The magnitude of $\mu\tau$ products of both carriers are found on the order of $10^{-8}cm^2/V$. The effective surface recombination velocities at p/i and n/i interfaces; $S_{p/i}$ and $S_{n/i}$, are estimated at around 10^4cm/sec and 1 cm/sec if we assume μ_n and μ_p to be 1 and 0.01 cm^2/Vsec. While, as shown in Fig 5-6. in the cell structure of ITO/n-i(B:$\sim 5\times10^{18}cm^{-3}$)-p/SUS 304, the $\mu\tau$ product, especially $\mu_p\tau_p$, is very small compared with that of the previous cell. Moreover, $S_{n/i}$ increases up to about $10^{2.5}$cm/sec. Corresponding to these degradiation of the physical parameters, this cell exhibits a conversion efficiency of only 2.3%. The above differences of the physical parameters in the two cells are not solely originated in the present conditions of the a-Si layer but also attributed to uncontrollable contamination, thermal histrical and ion or electron damages during whole the cell fabrication processes.

5-3-3. i-layer thickness dependence of collection efficiency

It is one of the most important problems how the collection

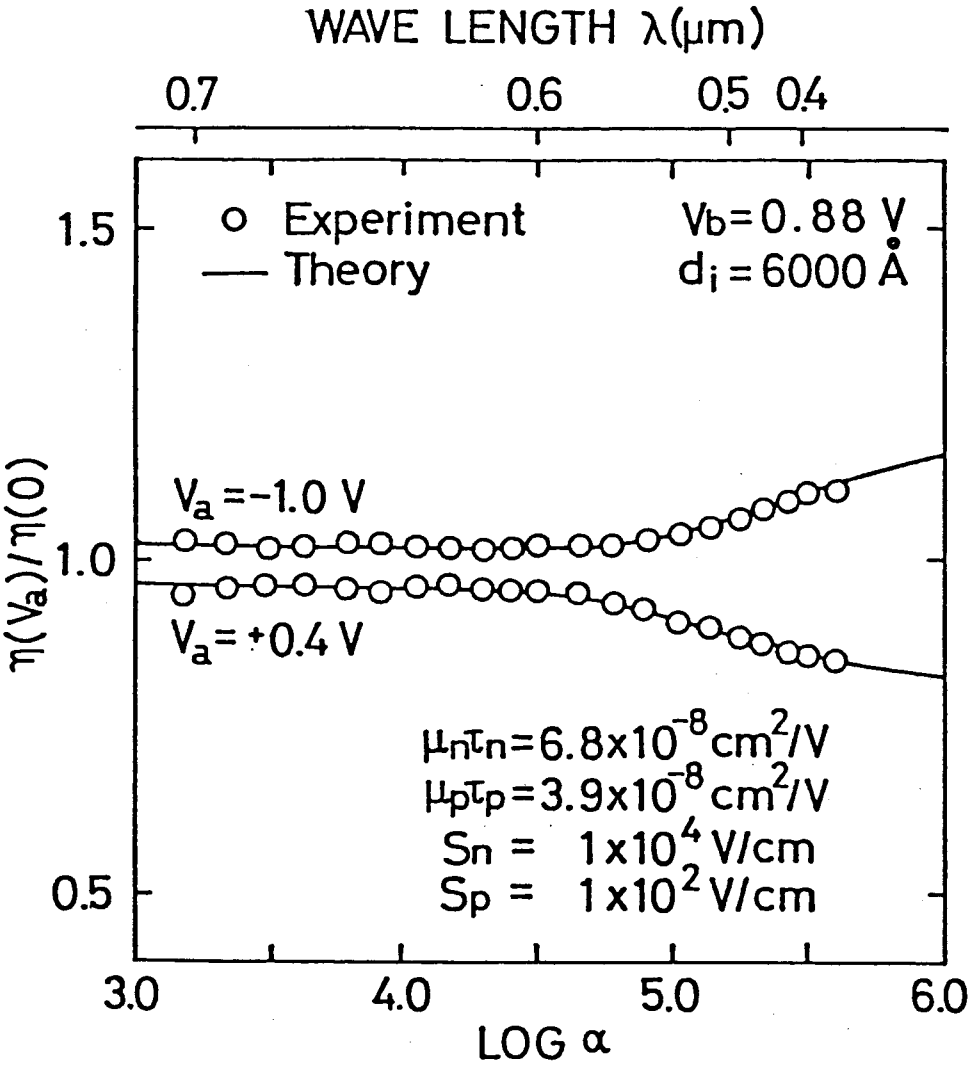

Fig. 5-5 Plots of normalized collection efficiency spectra $\eta(V_a)/\eta(0)$ for a SnO_2/p-i-n/Al type solar cell (open circles) and theoretical curves fitted to them.

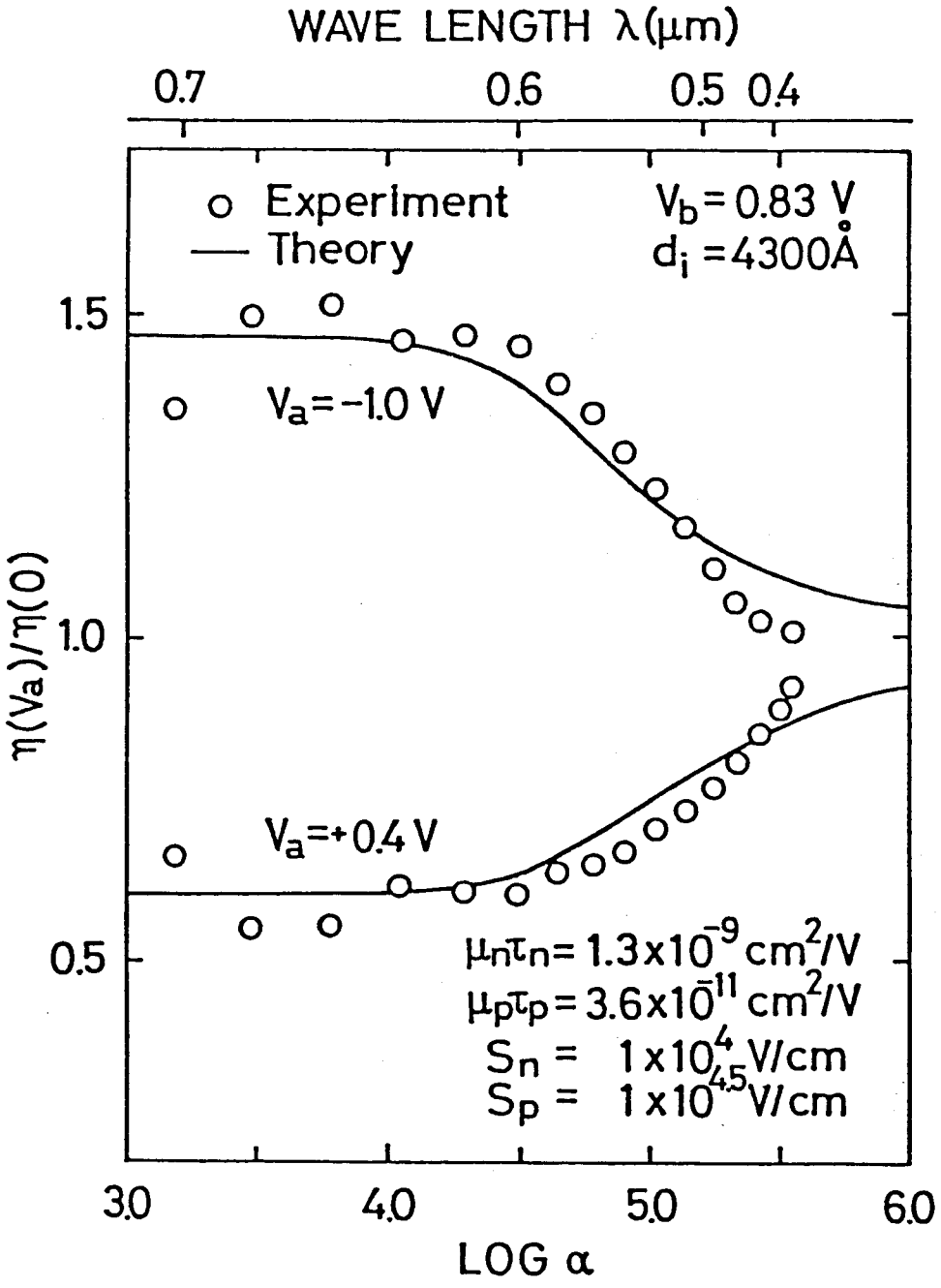

Fig. 5-6 Plots of normalized collection efficiency spectra $\eta(V_a)/\eta(0)$ for ITO/n-i(B)-p/SUS 304 type solar cell (open circles) and theoretical curves fitted to them.

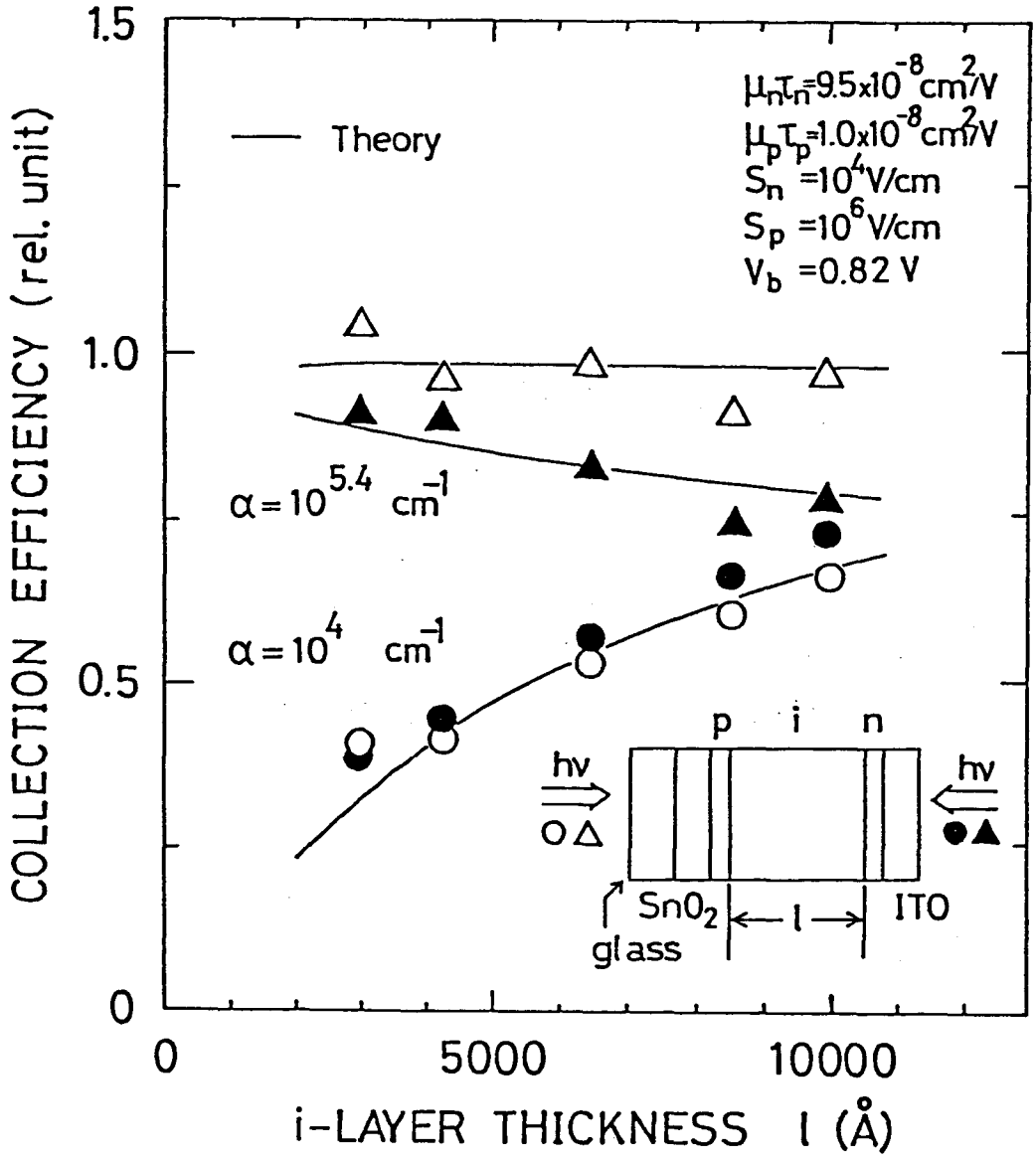

Fig. 5-7 Experimentally obtained collection efficiency as a function of i-layer thickness and theoretical curves for them.

efficiency depends on the active i-layer thickness d_i in the case of p-side and n-side illuminations. In order to check this dependence, we have prepared Glass/SnO_2/p-i-n/ITO type solar cells with various i-layer thicknesses on glass substrates coated with SnO_2 films. Figure 5-7 shows the results for the monochromatic light wavelength of which is 4500Å and 6500Å. As can be seen in the figure, the trend is almost the same both in p- and n-side illuminations for λ=6500Å. For λ=4500Å, on the other hand, the collection efficiency is almost independent of the i-layer thickness ℓ in the case of light incident on the p-layer, but it falls down generally with increasing ℓ when the cells are irradiated on the n-layer.
One can simulate these tendencies with theoretical calculations using physical parameters determined for this cell through the same analysis as presented in the previous section. Calculated results are drawn by solid lines in the figure. A considerable good coincidence found between experimental plots and theoretical curve proves a validity of the variable minority carrier transport model proposed in chapter II. Several researchers so far tried to interprete the difference of i-layer thickness dependence of the collection efficiency lying between p-side and n-side illuminations only by that between $\mu_n\tau_n$ and $\mu_p\tau_p$ [9,10]. However, we can mention here that this difference is rather due to the surface recombination effects which is very sensitive to the cell fabrication process.

5-3-4. J-V characteristics under illumination

The auther demonstrates an example of the comparison of the experimental and theoretical results. In Fig.5-8, dark and illuminated J-V characteristics of the SnO_2/(p-i-n)/Al solar cell mentioned in

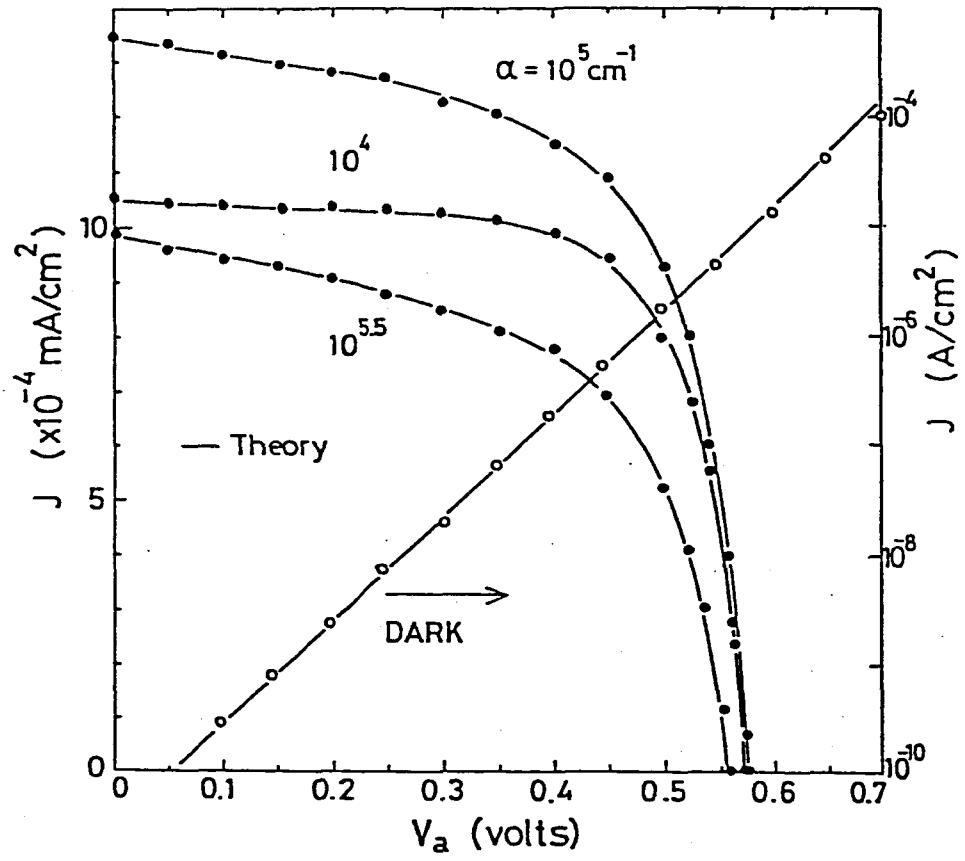

Fig. 5-8 Dark (o) and illuminated (•) J-V characteristics obtained experimentally in the SnO_2/(p-i-n)/Al solar cell and the theoretical curves (——) fitted to them. $\mu_n\tau_n$, $\mu_p\tau_p$, S_n and S_p are the same as indicated in the caption of Fig.5-5. The incident photon flux is 10^{14} photons $s^{-1}cm^{-2}$ for each wavelength of the incident light.

section 5-3-1 are plotted as open and full circles respectively. The illuminated J-V characteristics were measured under monochromatic light of three different wavelengths, the corresponding absorption coefficients of which were 10^4, 10^5 and $10^{5.5}cm^{-1}$. The incident photon flux was fixed at 10^{14} photons/scm^2 for each case. Employing the basic parameters $\mu_n\tau_n$, $\mu_p\tau_p$, S_n and S_p given in the caption of Fig.5-5 and choosing σ_n and σ_p to be $1.3x10^{-3}\Omega^{-1}cm^{-1}$ and $3.3x10^{-7}\Omega^{-1}cm^{-1}$ respectively, the best fit between the experimental plot and the theoretical curve for the dark J-V characteristics [8] is obtained. Once these six parameters are fixed, the experimental plots of the illuminated J-V characteristics are automatically reproduced by the theoretical calculations as shown in the figure. The excellent agreement between the experimental and theoretical plots indicates the plausibility of the basic model for analyzing a-Si solar cells.

5-4. Effect of Preparation Conditions

5-4-1. Impurity effect on mobility-lifetime products

In amorphous semiconductors, there would exist more than one set of carrier recombination channels associated with localized states in the gap. The carrier lifetimes τ_n and τ_p involved in Eq.(2-4) are not determined by the density and capture cross sections of a single recombination center, but are controlled by the energetic distribution and occupation of the gap states which act as recombination centers. Thereby, they essentially depend on the Fermi level position, deposition temperature and light intensity.

In this section, effects of impurity inclusion on the mobility-lifetime products is demonstrated. The built-in potential

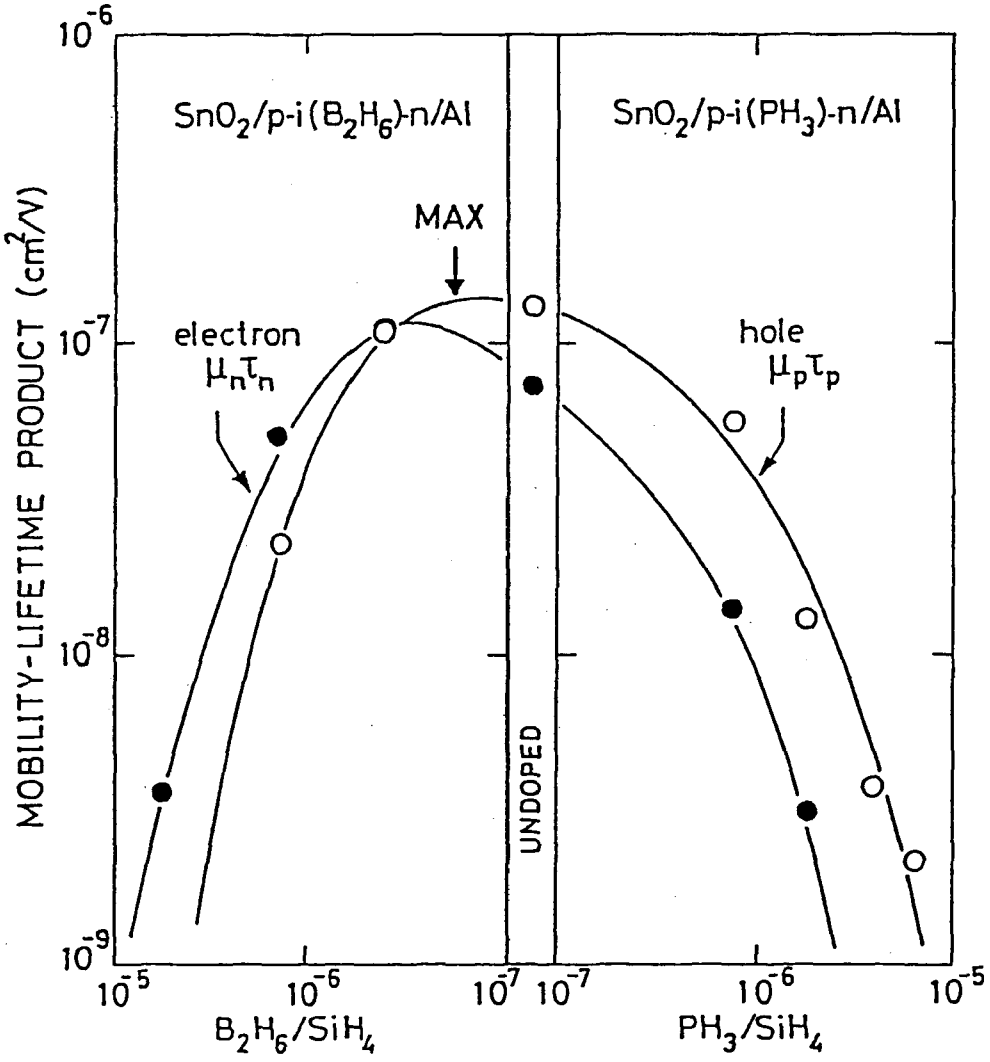

Fig. 5-9 Mobility-lifetime products of electrons ($\mu_n\tau_n$) and holes ($\mu_p\tau_p$) at 20°C as a function of gaseous composition during plasma deposition of the i-layer.

were almost the same at 0.9V for all the cells employed in this experiment. Figure 5-9 shows the $\mu_n\tau_n$ and $\mu_p\tau_p$ as a function of the gaseous compositions B_2H_6/SiH_4 and PH_3/SiH_4 during the deposition of the i-layer in the SnO_2/p-i a-Si:H/n μc-Si:H/Al solar cells. As can be seen in this figure, both $\mu_n\tau_n$ and $\mu_p\tau_p$ have the maximum values when the a-Si:H includes a small amount of boron atoms (B_2H_6/SiH_4=0.1∿1 vppm), which roughly corresponds to B/Si in a-Si:H of around 0.2∿2 vppm). The maximum mobility-lifetime products of electrons and holes are on the order of $10^{-7}cm^2/V$, which corresponds to the carrier diffusion length in excess of 5000Å.

In the process of cell fabrication, the amorphous layers were deposited successively as p and i layers in a single chamber. Therefore, as was reported by the Sanyo group [11] the i-layer inevitably contains boron atoms of several tens of parts per million even without intentional doping. Namely, the boron content which gives the maximum mobility-lifetime products is considered to be several tens of parts per million. With just this amount of boron atoms, the conductivity of a-Si:H becomes the lowest and the intrinsic conduction occurs [12], in other word, the Fermi level lies at the mid of the gap. This behavior of the mobility-lifetime products resembles that of the minority carrier lifetime with the Fermi level shift in crystalline semiconductors [13]. While, the magnitude of the mobility-lifetime product, especially the summation $\mu_n\tau_n+\mu_p\tau_p$, is a most significant parameter for the photovoltaic performance [5,6]. Therefore, it is easily understood that the photovoltaic performance is maximized in both p-i-n and inverted p-i-n junction solar cells when the i-layer includes boron atoms of several tens of parts per million [14].

Also, as shown in Fig. 5-9, $\mu_p\tau_p$ is larger than $\mu_n\tau_n$ when the Fermi level lies at the upper half of the gap, and the inverse situation takes place when the Fermi level moves towards the valence band edge. As we demonstrated in chapter II, the higher performance is expected with $\mu_n\tau_n>\mu_p\tau_p$ ($\mu_p\tau_p>\mu_n\tau_n$) for the n-(p-) side illumination if the interface properties at the p/i and i/n are equivalent. Indeed, the TIT group found in the ITO/p-i-n/ITO structure that the higher photovoltaic performance is obtained in the case of n- (p-) side illumination when the i-layer includes a small amount of boron (phosphorus) atoms [15]. Consequently, they achieved the higher performance in an ITO/n-i(B)-p/ITO solar cell with n-side illumination [15]. This experimental result is perfectly consistent with our experimental and theoretical considerations.

Temperature dependences of the mobility-lifetime products have been investigated in an a-SiC:H/a-Si:H heterojunction cell. The built-in potential V_b varied in the range 0.98∿0.70V for temperatures of 20∿120°C. Figure 5-10 shows the result together with the temperature dependence of the normalized photoconductivity $(\mu\tau)_{pc}$ of an undoped a-Si:H films, where the quantum efficiency of photocarrier generation is assumed at unity. As can be seen in this figure, the mobility-lifetime products increase with temperature. This result partially accounts for the increase of the short circuit current density with increasing cell temperature [16]. While, $\mu_n\tau_n$ and $\mu_p\tau_p$ have the activation energies of 0.23 and 0.09eV, respectively. The activation energy of $(\mu\tau)_{pc}$ is the same as that of $\mu_p\tau_p$. This implies that τ_{pc} has the same physical meanings as the hole lifetime τ_p provided that the carrier mobility is weakly dependent on temperature in the range 20∿120°C [17,18].

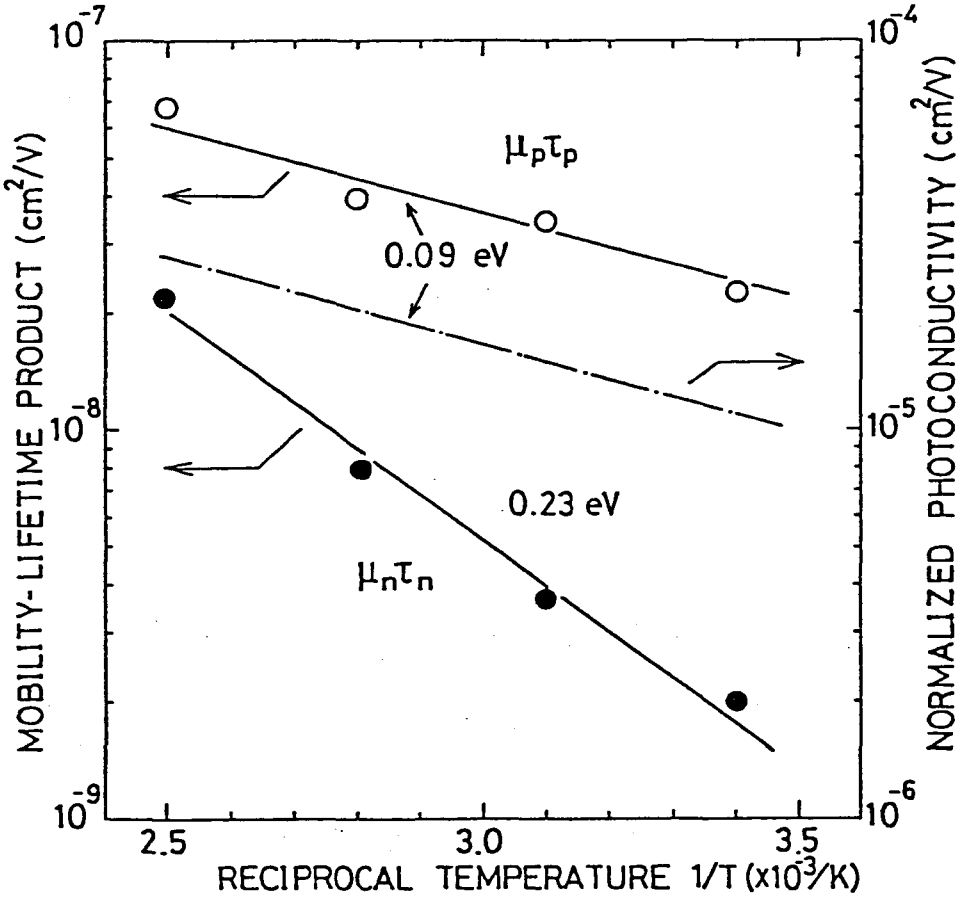

Fig. 5-10 Temperature dependence of the mobility-lifetime products $\mu_n\tau_n$ and $\mu_p\tau_p$, and the normalized photoconductivity of an undoped a-Si:H film.

Here, the author gives a brief discussion on the photoconductivity: mobility-lifetime products $(\mu\tau)_{pc}$. If $\delta n=\delta p$ is assumed, eqn.(2-4) readily leads to a representation of $(\mu\tau)_{pc}$ as

$$(\mu\tau)_{pc} \sim (\mu_n + \mu_p)(\tau_n + \tau_p). \qquad (5\text{-}1)$$

Then, recalling the experimental result $\mu_p\tau_p>\mu_n\tau_n$ for undoped a-Si:H, a relation $\tau_p>\tau_n$ may be accepted unless $\mu_p>\mu_n$. Therefore, $(\mu\tau)_{pc}$ is characterized by $(\mu_n+\mu_p)\tau_p$ in the present case. Namely, this simple consideration supports the above speculation that τ_{pc} is identical with the hole-lifetime τ_p in undoped a-Si:H where the Fermi level locates some what above the middle of the gap.

While, in Boron doped a-Si:H where the Fermi level lies below the intrinsic Fermi level, the situation $\tau_n>\tau_p$ would take place as understood from Fig.5-9. In this case, $(\mu\tau)_{pc}$ may be written by $(\mu_n+\mu_p)\tau_n$. Then the activation energy of $(\mu\tau)_{pc}$ is expected to be identical with that of $\mu_n\tau_n$, that is , 0.23 eV. This variation of the activation energy of $(\mu\tau)_{pc}$ from $\sim$0.09 to $\sim$ 0.23 eV with boron doping is really observed by many researchers [19,20,21]. A larger discrepancy between $(\mu\tau)_{pc}$ and $\mu_p\tau_p$, $\mu_n\tau_n$ seen in Fig. 5-10 is now open question. One way to explain it may be to assume $\mu_n>>\mu_p$, which yields $(\mu\tau)_{pc}=\mu_n\tau_p >>\mu_p\tau_p>\mu_n\tau_n$ in undoped a-Si:H. However, the above assumption is not necessarily varid because the Hall mobilities of electrons and holes are almost on the same order [17,18]. Then, a detailed examination is needed on the carrier recombination kinetics and conduction mechanism to fairly interpret this discrepancy.

5-4-2. P-layer thickness dependence on effective surface recombination factors

The interface property in a-Si:H solar cell is characterized by the effective surface recombination velocity which defines the recombination velocity "seen" by carriers in the i-layer. This physical parameter at the front side interface is predominately responsible for the photoresponce in the blue portion of the spectrum. In our analysis, we can evaluate the effective surface recombination factor, which is defined as the effective surface recombination velocity divided by the relevant carrier mobility [5,6,7]. For example, the effective surface recombination factor S_n at the p/i interface is represented by

$$S_n = S_r + \frac{\exp[-\Delta\epsilon/k_BT]}{\gamma^2-\Omega_o} \times [(k_BT/qL_{np})(\gamma-1)(\gamma-\Omega_o) + S_{no}\gamma(1-\Omega_o)], \qquad (5\text{-}1)$$

where $\gamma=\exp[d_p/L_{np}]$, $\Omega_o=(S_{no}-k_BT/qL_{np})/(S_{no}+k_BT/qL_{np})$ and $L_{np}=\sqrt{k_BT(\mu_n\tau_n)_p/q}$. A derivation of Eqn.(5-1) and notations used are described in the Appendix B. Figure 5-11 shows the variation of the effective surface recombination factor S_n at the p/i interface in SnO_2/p-i a-Si:H/n μc-Si solar cells with p-layer thickness. The built-in potential V_b was in the range 0.40∿0.92 V, corresponding to the p-layer thickness d_p of 0∿300Å. As can be seen in this figure, S_n gradually increases with d_p and saturates at d_p of 250∿300Å. The magnitude of S_n has a great influence on the photovoltaic performance particularly in the case of the p-layer illumination. Hence, the increase of S_n with d_p might be one limiting factor for the p-layer thickness. A typical value of S_n for the practical p-layer thickness 50∿100Å [22] is $2\sim3\times10^4$ V/cm.

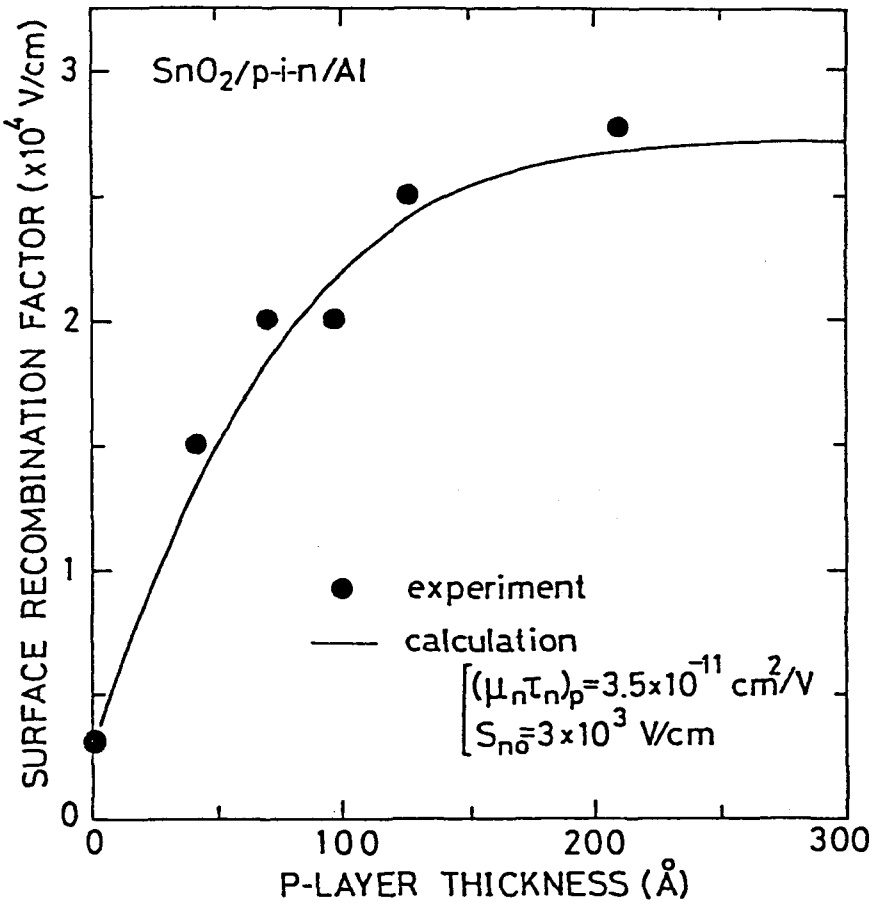

Fig. 5-11 Effective surface recombination factor S_n at the p/i interface as a function of the p-layer measured at 20°C. The curve is that calculated with the $\mu\tau$ product of electrons in the p-layer and the surface recombination factor S_{no} at the SnO_2/p a-Si:H interface indicated in the figure.

If the electron mobility as assumed at 0.1 cm^2/Vs this corresponds to the effective surface recombination velocity of $2\sim3x10^3$ cm/s.

In the case of homojunction, S_r and $\Delta\varepsilon$ in eqn.(5-1) could be neglected. Then we can estimate the surface recombination factor S_{no} at the SnO_2/p a-Si:H interface and the mobility-lifetime product of electrons $(\mu_n\tau_n)_p$ in the p-layer through the best procedure on the thickness dependence of S_n utilizing eqn. (5-1). The result is also shown in Fig.5-11 by a solid line. $(\mu_n\tau_n)_p$ and S_{no} are evaluated at $3.5x10^{-11}$and $3x10^3$ V/cm, respectively. A considerably small value of $(\mu_n\tau_n)_p$ is easily understood by recalling the experimental results in Fig.5-9. While, the surface recombination velocity (S_{no}/μ_n) at the SnO_2/a-Si:H interface is estimated at $3x10^2$ cm/s with an assumption of electron mobility at 0.1 cm^2/Vs [22], and is by two orders magnitudes larger than that at the free surface of a-Si:H film ($\sim$1 cm/s) deduced by the delayed-collection-field method [23]. This discrepancy might be attributed to the effect of oxygen and reduced tin diffused near around the SnO_2/a-Si:H interface [24].

It is interesting to investigate the interface properties at the p a-SiC:H/i a-Si:H [25,26] and i a-Si:H/n μc-Si:H [27] since solar cells exhibiting the highest performance are constructed by utilizing these heterojunction. Next, the auther deals with the surface recombination factors at the SnO_2/p a-SiC:H and i a-Si:H/n μc-Si:H/Al interfaces measured in the SnO_2/a-SiC:H/i a-Si:H/n μc-Si:H/Al type solar cells having the conversion efficiencies more than 8% under AM 1 illumination. The layer thickness are about 120, 5000 and 300Å for p, i and n layers, repectively. The results are summalized by vertical bars in Fig. 5-12 together with the effective surface recombination factors in

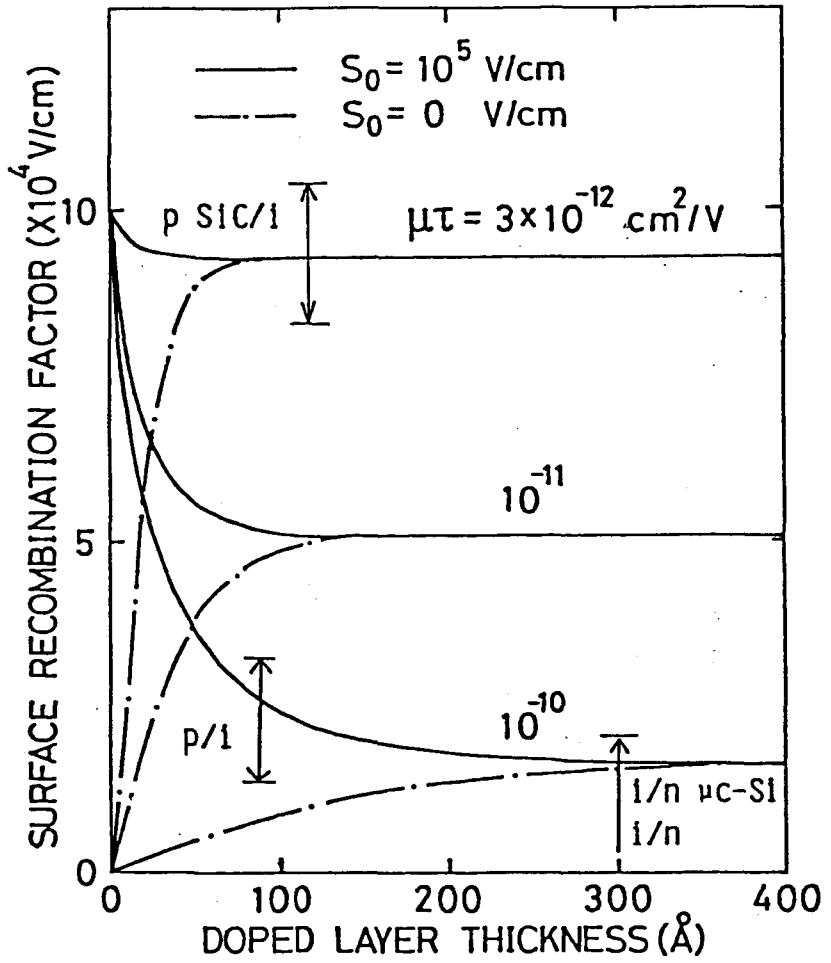

Fig. 5-12 Relation between the effective surface recombination factor and the doped layer thickness at 20°C. The curves are calculated for different surface recombination factors S_0 at the electrode/doped layer interface and mobility-lifetime products $\mu\tau$ in the doped layer. Some experimental results are also shown with vertical bars for various interfaces.

homojunction case.

In this case, the relation between the effective surface recombination factor and doped layer thickness calculated by eqn.(5-1) with $\Delta\varepsilon=0$ and S_r is also illustrated. Detailes are described in the figure caption. As can be seen in this figure, the effective surface recombination factor S_n at the SnO_2/p a-SiC:H/i a-Si:H is in the range $8\times10^4 \sim 10^5$ V/cm. A roughly estimated value of the mobility-lifetime product of electrons in the p a-SiC:H $(\mu_n\tau_n)_p$ is about $10^{-12}cm^2/V$. This small value gives an answer to the equation why the optimum thickness of the p a-SiC:H in this type of heterojunction solar cells is in the range 100~150Å [28] in spite of its excellent optical transparency [25]. Therefore, the further improvement of the photovoltaic performance must be essentially accompanied by that of the photoelectric property in doped a-SiC:H films.

On the other hand, the effective surface recombination factor S_p at the i a-Si:H/n μc-Si or a-Si:H/Al is less than 2×10^4 V/cm. The mobility lifetime product of holes in these phosphorus doped n-layers $(\mu_p\tau_p)_n$ would exceed about 10^{-10} cm^2/V. In this sense, there remains a possibility to get photovoltaic performance compatible with the a-SiC:H/a-Si:H heterojunction solar cells in the inverted solar cells like a n μc-Si:H/ p-i a-Si:H structure if the front side transparent electrode layer (ITO) can be deposited onto silicon layers without any harmful influences.

5-5. Effects of Prolonged Light Irradiation

Many articles have been reported concerning with the photoinduced degradation of a-Si:H solar cells [29,30]. In the present work, we have investigated changes of the mobility lifetime products and effective

surface recombination factors caused by prolonged light exposure and subsequent annealing heat treatment in a SnO_2/p-i a-Si:H/n μc-Si:H/Al solar cell. The as deposited cell (state A) were subjected the light irradiation ($\sim 1.4 \times 10^{17}$ photons/s·cm^2) at a wavelength 6328 Å (He-Ne laser). This light wavelength was chosen so as to promote the photoinduced change within the entire region of the cell of ~5000Å. The photoresponse dropped upon light exposure almost uniformly in its spectrum. After a 4-h light exposure (state B), the cell were annealed at 120°C for 90 min (state C).

Figure 5-13 summalizes the result. The mobility-lifetime products of electrons ($\mu_n\tau_n$) and holes ($\mu_p\tau_p$) decrease with a four hours light exposure down to about one-fouth of their original values. The increase of the effective surface recombination factor S_n and also observed. These degradiations are recovered by subsequent annealing heat treatment as seen in the figure. The photovoltaic performances, particularly, the short circuit current density and curve fill factor, behaved in the manner as can be expected from the above physical parameters [16].

The change observed in the mobility-lifetime products with light exposure and subsequent annealing heat treatment is thought to be based upon the same physical process as that in the stabler-Wronski effect [31]. Indeed, a similar degree of photoinduced change was observed in the photoconductivity of a-Si:H used for this thesis work under the same amount of light exposure.

Concerning the effective surface recombination factors S_n and S_p, these parameters refers, by definition, to both the mobility-lifetime products in the doped layers and the surface recombination factors at the SnO_2/p a-Si:H (S_{no}) and n μc-Si:H/Al (S_{po}) interfaces. Staebler et al.

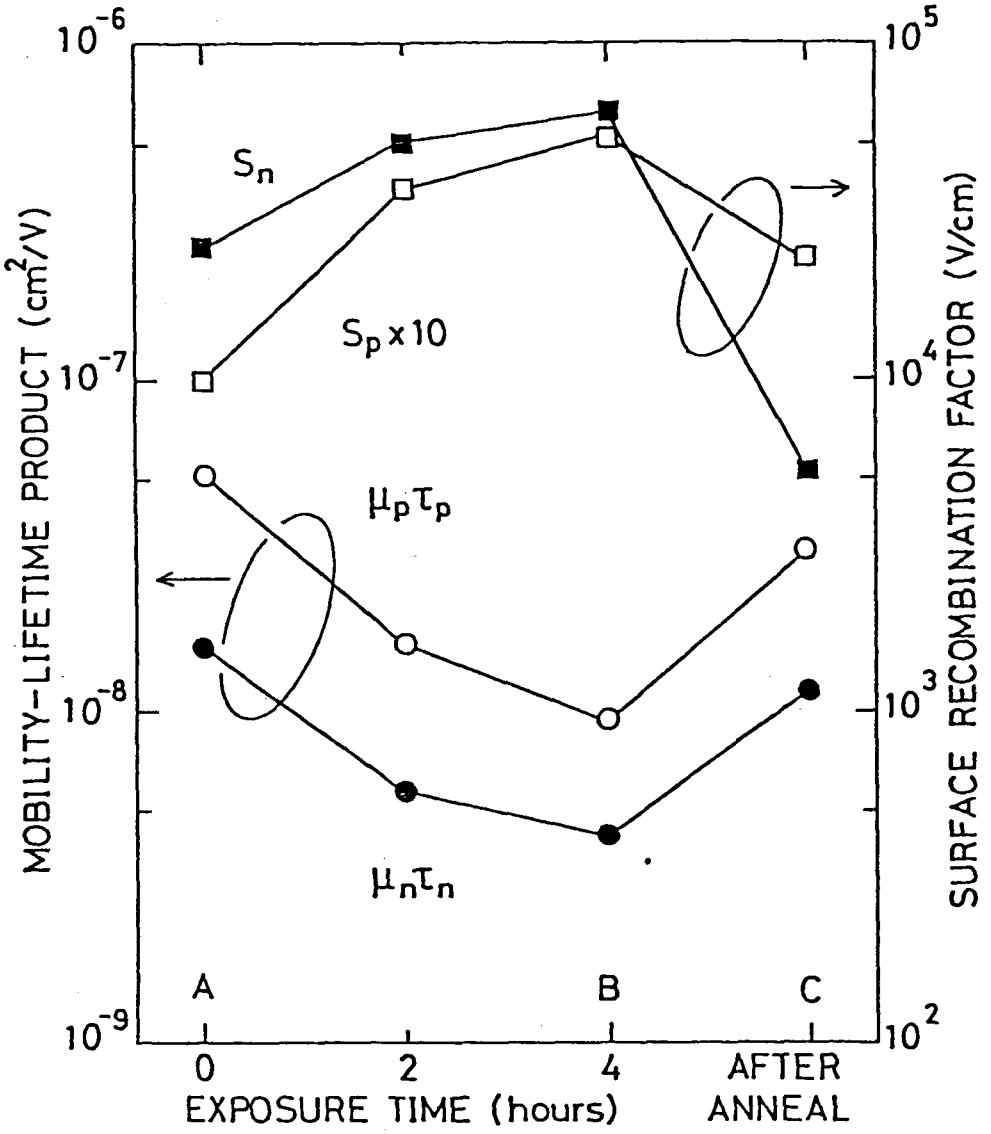

Fig. 5-13 Effects of light exposure and subsequent annealing heat treatment on the mobility-lifetime products and effective surface recombination factors measured at 20°C on a SnO_2/p-i a-Si:H/n μc-Si/Al solar cell. The conditions of light exposure and annealing heat treatment are described in the text.

reported that photoinduced change in the photoconductivity can occur even in moderately doped a-Si:H [32]. Hence, the increase of S_n and S_p might be attributed to a decrease of the mobility-lifetime products in the doped layers with light exposure. While, as seen in Fig.5-13, the S_n is improved from its original value with annealing heat treatment. Accordingly, it would be allowed to speculate that not only $(\mu_n\tau_n)_p$ but also S_{no} are responsible for this improvements of S_n.

The above consideration leads us to a conclusion that the reversible photoinduced change in the photovoltaic performance is mainly caused by that of the mobility-lifetime products, most likely carrier lifetimes, in both the i-layer and doped layers. Furthermore, the interface property at the transparent electrode/doped layer can be improved by a proper annealing heat treatment after the cell fabrication process [16].

5-6. Summary

The normalized carrier collection efficiency spectra were utilized for examining the mobility-lifetime products ($\mu\tau$) and interface property in actual a-Si:H p-i-n junction solar cells. The maximum $\mu\tau$ products were observed when a-Si:H was doped with a small amount of boron atoms. Through the temperature dependence of $\mu\tau$ products, the carrier lifetime dominating photoconductivity was identified to be the hole lifetime in undoped and phosphorus doped a-Si:H and the electron lifetime in boron doped a-Si:H. The effective surface recombination factor was related to the film quality of doped layer and the surface recombination factor at the electrode/doped layer interface. In most cases, the effective surface recombination factor is dominated by $\mu\tau$ products in doped layers. Moreover, the photoinduced change in $\mu\tau$ products and effective surface

recombination factor is dominated by $\mu\tau$ products in doped layers. Moreover, the photoinduced change in $\mu\tau$ products and effective surface recombination factor were clearly confirmed. It was concluded that these photoinduced change are essentially based upon the same physical process as that in the Staebler-Wronski effect. The characterization method and obtained results described in this paper may be useful to optimize the material, structure, and fabrication processes for achieving higher photovoltaic performance together with sufficient reproducibility and stability in a-Si:H p-i-n junction solar cells.

References

[1] R, Crandall, Appl. Phys. Lett. 36 (1980) 607.

[2] T. Yamaguchi, H. Okamoto, S. Nonomura and Y. Hamakawa, Jpn. J. Appl. Phys. 20 (1981) Suppl.20-2, 195.

[3] I. Shimizu, T. Komatsu, K. Saito and E. Inoue, J. Non-cryst. Solids 35&36 (1980) 773.

[4] H. Okamoto, T. Yamaguchi, S. Nonomura and Y. Hamakawa, J. Phys. 42 (1981) C4-507.

[5] S. Nonomura, H. Okamoto, H. Kida and Y. Hamakawa, Jpn. J. Appl. Phys. 22 (1983) Suppl.22-1, 257.

[6] H. Okamoto, H. Kida, S. Nonomura and Y. Hamakawa, Solar Cells 8 (183) 317.

[7] S. Nonomura, H. Okamoto, H. Kida, K. Fukumoto and Y. Hamakawa, Jpn. J. Appl. Phys. 22 (1983) 275.

[8] H. Okamoto, H. Kida, S. Nonomura, K. Fukumoto and Y. Hamakawa, J. Appl. Phys. 54 (1983) 3236.

[9] D.L. Steabler, J. Non-cryst. Solids 35&36 (1980) 387.

[10] Y. Hamakawa, in Y. Hamakawa (ed.), *Amorphous Semiconductors-Technologies and Devices*, Ohm-Sha, Tokyo and North-Holland, Amsterdam, 1982, p.134.

[11] Y. Kuwano, M. Ohnishi, S. Tsuda, Y. Nakashima and N. Nakamura, Jpn. J. Appl. Phys. 21 (1982) 413.

[12] W.E. Spear and P.G. LeComber, Phil. Mag. 33 (1976) 935.

[13] W. Schockley and W.R. Read, Phys. Rev. 87 (1952) 835.

[14] H. Haruki, Y. Uchida, H. Sakai, M. Nishiura and M. Kamiyama, Jpn. J. Appl. Phys. 21 (1982) Suppl.21-1, 283.

[15] M. Konagai, H. Taniguchi, K.S. Lim, P. Sichanugrist and K. Takahashi, Jpn. J. Appl. Phys. 22 (1983) Suppl.22-1, 211.

[16] Y. Tawada, K. Nishimura, S. Nonomura, H. Okamoto and Y. Hamakawa, Proceedings of the Work Shop on Light Induced Changes in a-Si:H and Its Effect on Solar Cell Stability, San Diego, 1982.

[17] J. Dresner, Appl. Phys. Lett. 37 (1980) 742.

[18] J. Dresner, J. Non-cryst. Solids (to be published).

[19] D.A. Anderson and W.E. Spear, Phil. Mag. 36 (1977) 695.

[20] W. Ream, R. Fischer, J. Stuke and H. Wagner, Phys. Status Solidi, B79 (1977) 539.

[21] S. Oda, Y. Saito, I. Shimizu and E. Inoue, Phil. Mag. B43 (1981) 1079.

[22] H. Okamoto, Y. Nitta, T. Yamaguchi and Y. Hamakawa, Solar Energy Mat. 2 (L980) 313.

[23] J. Mort, I. Chen, A. Troup, M. Morgan, J. Knights and R. Lujan, Phys. Rev. Lett. 45 (1980) 1348.

[24] N. Fukada, T. Imura, A. Hiraki, Y. Tawada, K. Tsuge, H. Okamoto and Y. Hamakawa, Jpn. J. Appl. Phys. 22 (1983) Suppl.22-1, 251.

[25] Y. Tawada, M. Kondo, H. Okamoto and Y. Hamakawa, Solar Energy Mat. 6 (1982) 299.

[26] Y. Tawada, K. Tsuge, M. Kondo, H. Okamoto and Y. Hamakawa, Jpn. J. Appl. Phys. 53 (1982) 5273.

[27] Y. Uchida, T. Ichimura, M. Ueno and M. Ohsawa, J. Phys. 42 (1981) C4-265.

[28] Y. Hamakawa, Y. Tawada, K. Nishimura, K. Tsuge, M. Kondo, K. Fujimoto, S. Nonomura and Y. Hamakawa, Proceedings of the 16th IEEE Photovoltaic Specialists Conf., San Diego, (1982).

[29] D.L. Steabler, E.S. Crandall and R. Williams, Appl. Phys. Lett. 39 (1981) 733.

[30] see for example, Proceedings of the Workshop on Light Induced changes in a-Si:H and Its Effect on Solar Cell Stability, San Diego, (1982).

[31] D.L. Steabler and C.R. Wrinski, Appl. Phys. Lett. 31 (1977) 292.

[32] D.L. Steabler and C.R. Wronski, J. Appl. Phys. 51 (1980) 3263.

VI. ANALYSIS OF HIGH EFFICIENCY a-Si:H SOLAR CELLS

6-1. Introduction

Prime conditions required for high photovoltaic performance in a-Si solar cells are an efficient absorption of incident light yielding photocarriers and their efficient collection. The former has been partially satisfied by combining undoped a-Si:H with wide band gap materials such as p-type a-SiC:H [1] and n type μc-Si:H [2] to construct a p-i-n heterojunction. Use of a-Si alloys having narrow band gaps [3] also improves the utilization of incident light. On the other hand, the photocarrier collection process is dominated by several macroscopic transport parameters [4,5]; the built-in potential, mobility-lifetime product and effective surface recombination velocity. These parameters might be significantly influenced by various cell fabrication conditions, that is, substrate materials, deposition conditions of p-, i- and n-layers and other cell fabrication processes including deposition of metals or transparent electrode layers. Therefore, in order to attain higher efficiencies with sufficient reproducibility, it is of great importance to clarify the correlation between these cell fabrication conditions and macroscopic transport parameters.

The auther has conducted a systematic characterization of the built-in potential, mobility-lifetime products and effective surface recombination velocities on a-Si solar cells fabricated under various conditions. In this section, results of characterization are presented and discussed in relation to resulting photovoltaic performances. Moreover, based upon these considerations, it is suggested how to fabricate a-Si solar cells to attain higher photovoltaic performance.

6-2. Fabrication of a-Si:H Solar Cells

In this thesis work, a-Si p-i-n junction cells were fabricated by the plasma deposition technique. Cells were formed by successive growth of p-, i- and n-layers by either single chamber or separate three chamber systems[6]. Figure 6-1 shows a schematic illustration of three chamber system. Each chamber is isolated by gate valve. The p, i and n type a-Si films are deposited with a merit of very little influence of residual impurity atoms. The substrate is set on the heater provided at the cart. The cart can be transfered from a chamber to another. To prevent the open air from invading into the reaction chambers, additional inlet and outlet chamber equipped.

The deposition condition such as pressure and substrate temperature in all the a-Si solar cells are same as described in chapter III. The p-type amorphous silicon carbide (a-SiC:H) [1] and n-type microcrystalline silicon (μc-Si) [2] were employed for p- and n-layer of a-Si solar cells, respectively. As for the p-type a-SiC:H, the gas ratio of $CH_4/(SiH_4+CH_4)$ and $B_2H_6/(SiH_4+CH_4)$ were fixed at 70 vol.% and 0.3 vol.%, respectively. While, in the n-type μc-Si, the gas ratio, PH_3/SiH_4, was chosen at 1.0 vol.%. These values are optimized in a series study of gas fraction . The gas fraction, activation energy and optical gap energy of materials utilized in this section are summalized in Table 3-1.

6-3. Physical Parameters in Various Types of a-Si:H Solar Cells

Table 5-2 summalizes photovoltaic performances and physical parameters evaluated with methods presented in chapter V for various kinds of a-Si p-i-n basis solar cells possessing different structures and preset impurity levels in the i-layer. Cells used in the present work were

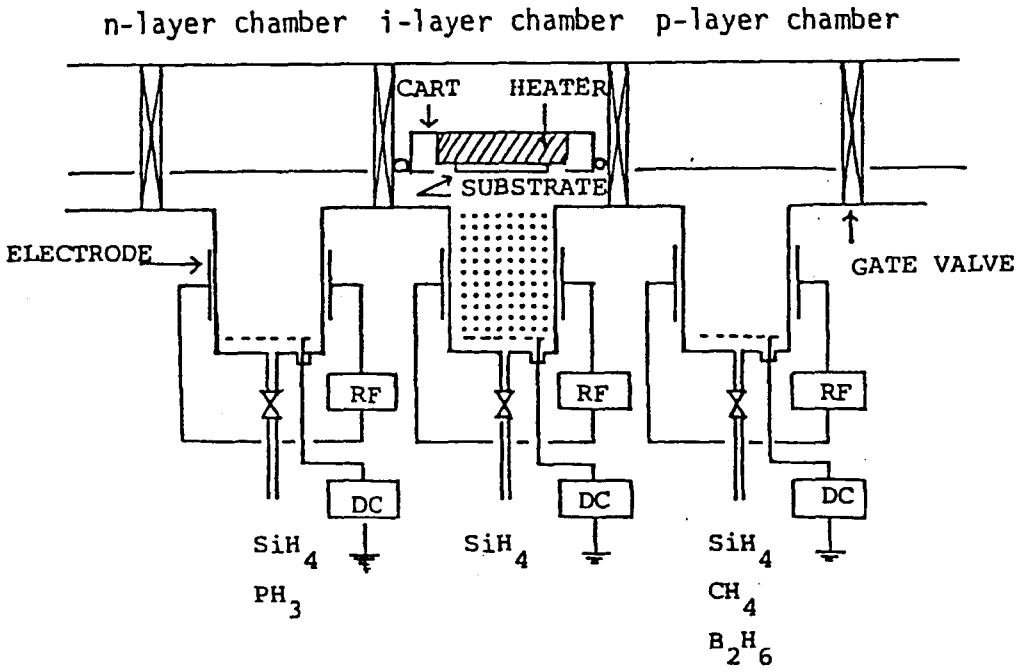

Fig. 6-1 Schematic illustration of separated three chamber deposition system. Respective chamber are divided by gate valve. The heater maintaining the substrate temperature is set up in the cart.

fabricated on glass coated with SnO_2 film under the optimized conditions for each cell structure.

As regards the built-in potential V_b, it is enhanced by ∿0.05V and ∿0.08V with introducing n-type μc-Si and p-type a-SiC:H instead of n and p a-Si:H layers as demonstrated in chapter IV. The effective surface recombination parameters found in the p a-Si:H/i a-Si:H and i a-Si:H/ n a-Si:H interfaces are on the order of 10^4 and 10^2 V/cm, respectively. When applying a-SiC:H or μc-Si doped layer, the effective surface recombination parameter at the corresponding interface increase by one or two order of magnitude from those of the a-Si:H p/i or i/n interfaces as shown in chapter V. As for the mobility-lifetime products, the summation $\mu_n\tau_n+\mu_p\tau_p$ range on the order of 10^{-8} to 10^{-7} cm^2/V, which correspond to the carrier diffusion length of about 1500∿5000Å. The latter part of Table 6-1 shows the results of inclusion of impurity atoms in the i-layer. It is very ture that even a small amount of impurity atoms doped in the i-layer degrades cell performance. Comparison of $\mu_n\tau_n$ and $\mu_p\tau_p$ in three different p/i a-Si:H/n μc-Si solar cells leads us to a conjecture that in truly undoped a-Si $\mu_p\tau_p$ is somewhat larger than $\mu_n\tau_n$.

It is of an essential significance to clear a correlation between physical parameters and cell performances under AM 1 illumination. However, because cell performances are dominated by all the physical parameters and also by optical transparency of the front doped layer in a complicated manner, it might be rather fair to give only a qualitative discussion on the fill factor and conversion efficiency. As can be seen in Table 6-1, the fill factor perfectly corresponds to the magnitudes of $\mu_n\tau_n+\mu_p\tau_p$ and S_n, that is, the larger $\mu_n\tau_n+\mu_p\tau_p$ and the smaller S_n result in the larger fill factor. A demerit of larger S_n in a

Cell Structure	V_b (volts)	$\mu_n\tau_n$ (cm^2/V)	$\mu_p\tau_p$ (cm^2/V)	$S_{n(p/i)}$ (V/cm)	$S_{p(i/n)}$ (V/cm)	η (%)	F.F. (%)	J_{sc} (mA)	V_{oc} (volts)
p-i-n a-Si	0.85	8.1×10^{-9}	8.5×10^{-9}	2.0×10^{4}	1.0×10^{2}	5.2	59.3	10.9	0.805
p-i a-Si/n μc-Si	0.90	2.6×10^{-8}	3.4×10^{-8}	1.5×10^{4}	1.0×10^{3}	6.5	65.7	12.1	0.819
p a-SiC/i a-Si/n μc-Si	0.98	6.3×10^{-9}	1.7×10^{-7}	$10.\times10^{5}$	1.0×10^{3}	8.1	67.1	13.9	0.867
p-i(P) a-Si/n μc-Si	0.85	9.1×10^{-10}	1.8×10^{-9}	1.0×10^{2}	1.0×10^{4}	4.0	57.2	8.9	0.791
p-i(B) a-Si/n μc-Si	0.85	2.5×10^{-8}	1.5×10^{-8}	5.0×10^{4}	1.0×10^{4}	5.0	62.4	10.2	0.791

Table 6-1 Physical parameters and cell performances in various types of a-Si solar cells.

p a-SiC:H/i a-Si:H/n μc-Si type solar cell is sufficiently covered by a larger built-in potential, which leads to a high efficiency in cooperation with a good optical transparency of a-SiC:H layer.

6-4. High Efficiency a-Si:H Solar Cells

6-4-1. p-i-n and inverted p-i-n heterojunction solar cells

Figure 6-2(a) shows the dependence of the built-in potential V_b on the thickness of the front doped layers in two types of a-Si solar cells, ITO/n(μc-Si)-i(a-Si:H)-p(a-SiC:H)/Stainless Steel and SnO_2/p(a-SiC:H)-i(a-Si:H)-n(μc-Si)/Al (or Ag), fabricated by the single chamber deposition method. It is found that V_b of the inverted p-i-n a-Si solar cells are larger by about 0.2V than that of p-i-n type a-Si solar cells. This discrepancy may be accounted for by considering that deoxidization of the transparent electrode causes degradation of film quality of the p-layer [7].

The surface recombination factors evaluated in the above samples are shown in Fig. 6-2(b). The surface recombination factor S_p of the inverted p-i-n type solar cells decreases with increasing n-layer thickness. In the case of the inverted p-i-n type solar cells, the front side transparent electrode (ITO) is deposited by the electron beam evaporation technique after forming the a-Si junction. Through a theoretical study of the effective surface recombination factor S [8] as shown in chapter V, the thinner doped layer region S is dominated by the interface recombination velocity at the conductive electrode/doped layer interface, and that in the thicker doped layer region S is controlled by the film quality of the doped layer and by the recombination velocity at the doped layer/undoped layer interface. Therefore, the present

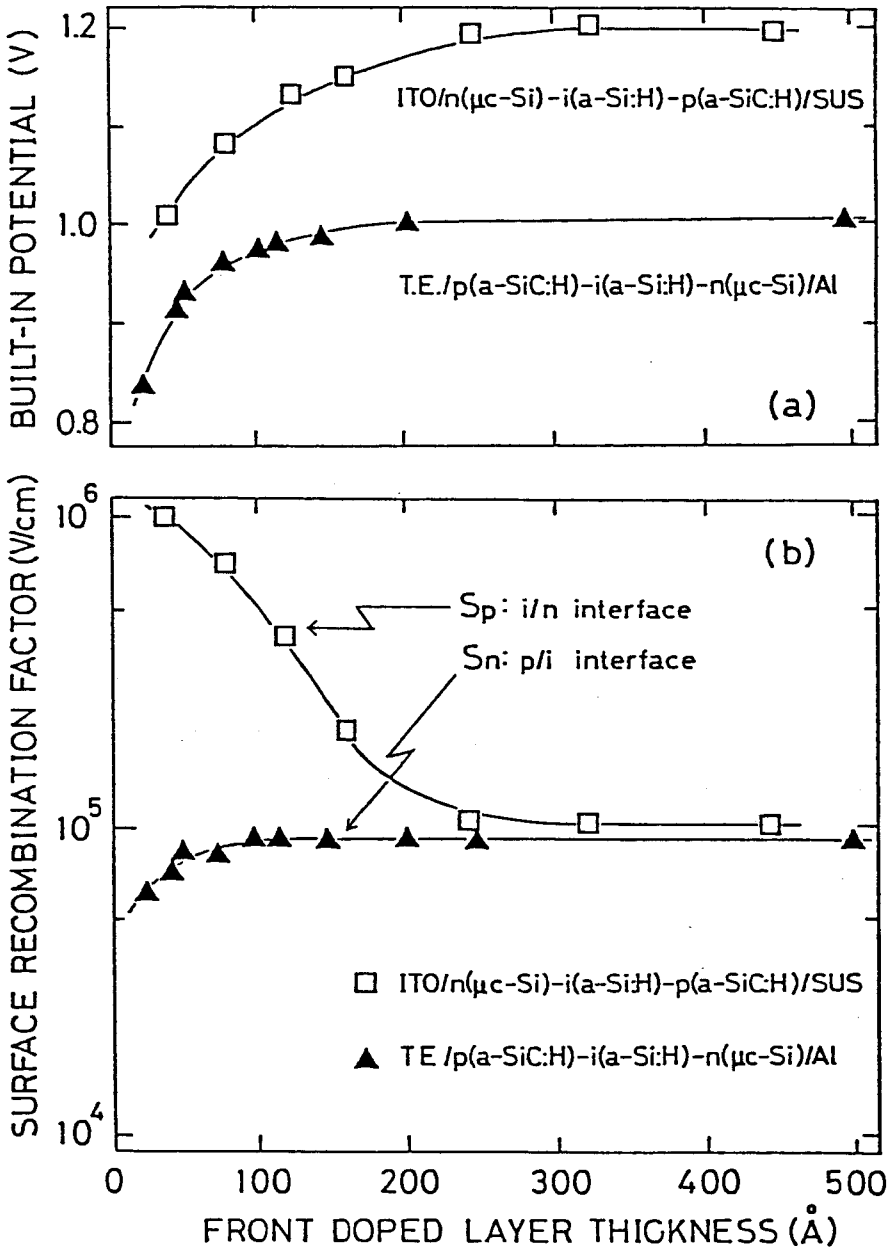

Fig. 6-2 Front doped layer thickness dependence on built-in potential V_b (a) and effective surface recombination factors S (b) of the typical two types in a-Si:H solar cells.

experimental results imply that the electron beam evaporation process degrades the electrical properties of a-Si in the vicinity of the ITO/n-layer interface. The surface recombination factors in the case of p-i-n type solar cells are instead dominated by the film quality of the doped layer and the interface recombination velocity at the doped layer undoped layer interface.

6-4-2. Comparison between single and separated chamber deposition method

Next, the auther will provide an experimental verification of the essential difference between a-Si solar cells fabricated by the single chamber deposition system and those fabricated by the separated chamber system. Here, the focus is placed on the a-SiC:H/a-Si:H heterojunction solar cells made on a transparent electrode. Figure 6-3 shows the p-layer thickness dependence of conversion efficiencies in a-Si solar cells fabricated by the single and separated chamber deposition systems as shown in section 6-2. Here, the author denotes cells fabricated by the former system as A and those by the latter system as B. The thickness of i- and n-layers were fixed at 6000Å and 250Å, respectively. As previously reported, in the case of type A cells the maximum conversion efficiency is obtained around a p-layer thickness of 100Å [1]. For the type B cells, it is found that the p-layer thickness giving the maximum conversion efficiency is around 180Å. Furthermore, an 8% level of conversion efficiency is obtained in the region of p-layer thickness from 150Å to 300Å.

Figure 6-4(a) shows the p-layer thickness dependence of the built-in potential evaluated from the back-surface-reflected-electroabsorption method. The built-in potential becomes gradually larger with thickness of the p-layer and saturates to about 1.0V [11]. There is no significant

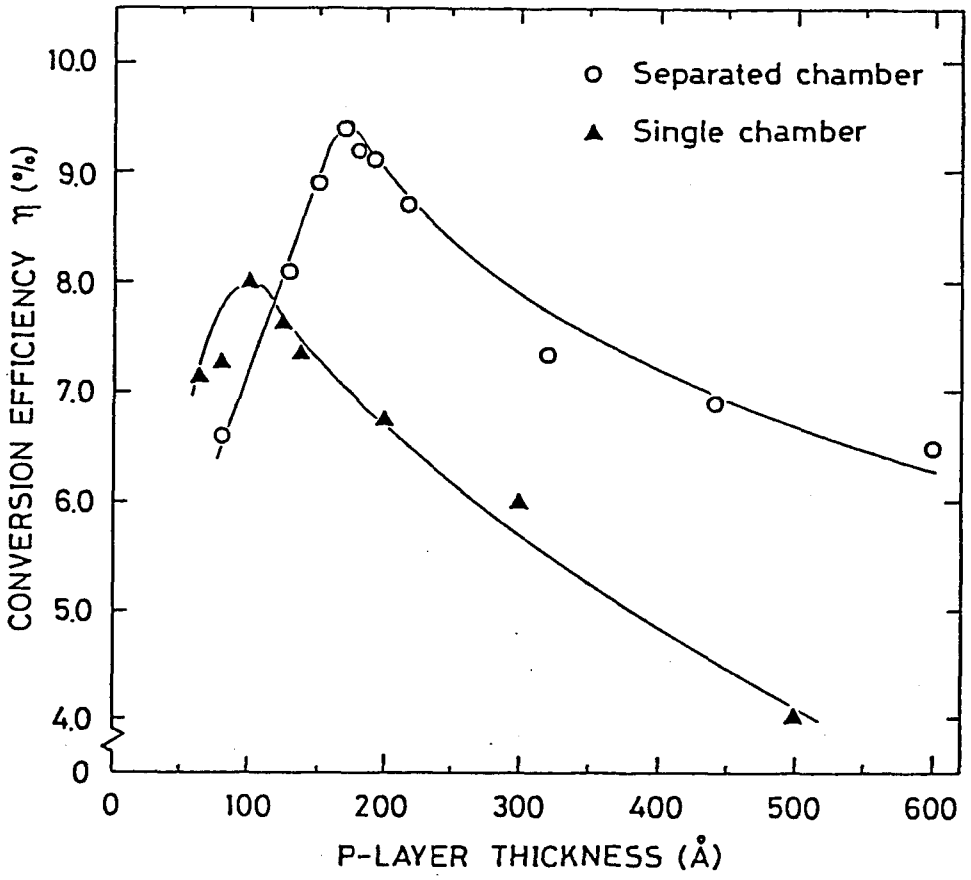

Fig. 6-3 p-layer thickness dependence on conversion efficiency η of a-Si solar cells fabricated by single and separated chamber deposition systems.

difference in the built-in potentials of a-Si solar cells A and B. on the contrary, a clear difference is seen in the mobility-lifetime products $\mu\tau$ in the i-layer, as evaluated by the analysis of collection efficiency spectra shown in Fig. 6-4(b). In the case of cells A, the p-layer thichkness giving the maximum $\mu\tau$ products is 70 Å. The $\mu\tau$ product rapidly decreases with increasing p-layer thickness. As compared with this behavior, the $\mu\tau$ product in cells B, fabricated by the single chamber deposition method, varies only moderately with the p-layer thickness and appears to be generally larger.

This remarkable difference in the $\mu\tau$ product is thought to come from the difference in the amount of boron and carbon atoms incorporated into i-layer during the deposition of the i-layer. It is suggested that an incorporation of boron and carbon atoms into the i-layer is quantitatively proportional to the thickness of the p-layer deposited prior to the i-layer. The p-type a-SiC:H adhered to the chamber wall and substrate holder work as the sources of boron and carbon atoms. Therefore, the amount of boron atoms in i-layer becomes larger with increasing p-layer thickness and this results in a variation of the $\mu\tau$ product. Such effect appears to be important in the single chamber technique, while being substantially eliminated in the case of the separate chamber system. As a matter of facts, the variation of the $\mu\tau$ product shown in Fig. 6-4(b) is qualitatively consistent with that observed for an intentional doping of i-layer [8] with boron atoms. In the case of the single chamber deposition method, the maximum conversion efficiency was obtained at the p-layer thickness of 100Å and the maximum $\mu\tau$ product appears at 70Å. This discrepancy is understood by taking into account the increase of V_b in the p-layer thickness ranging from 0Å to 200Å as shown in Fig. 6-4(a). Namely, the larger built-in

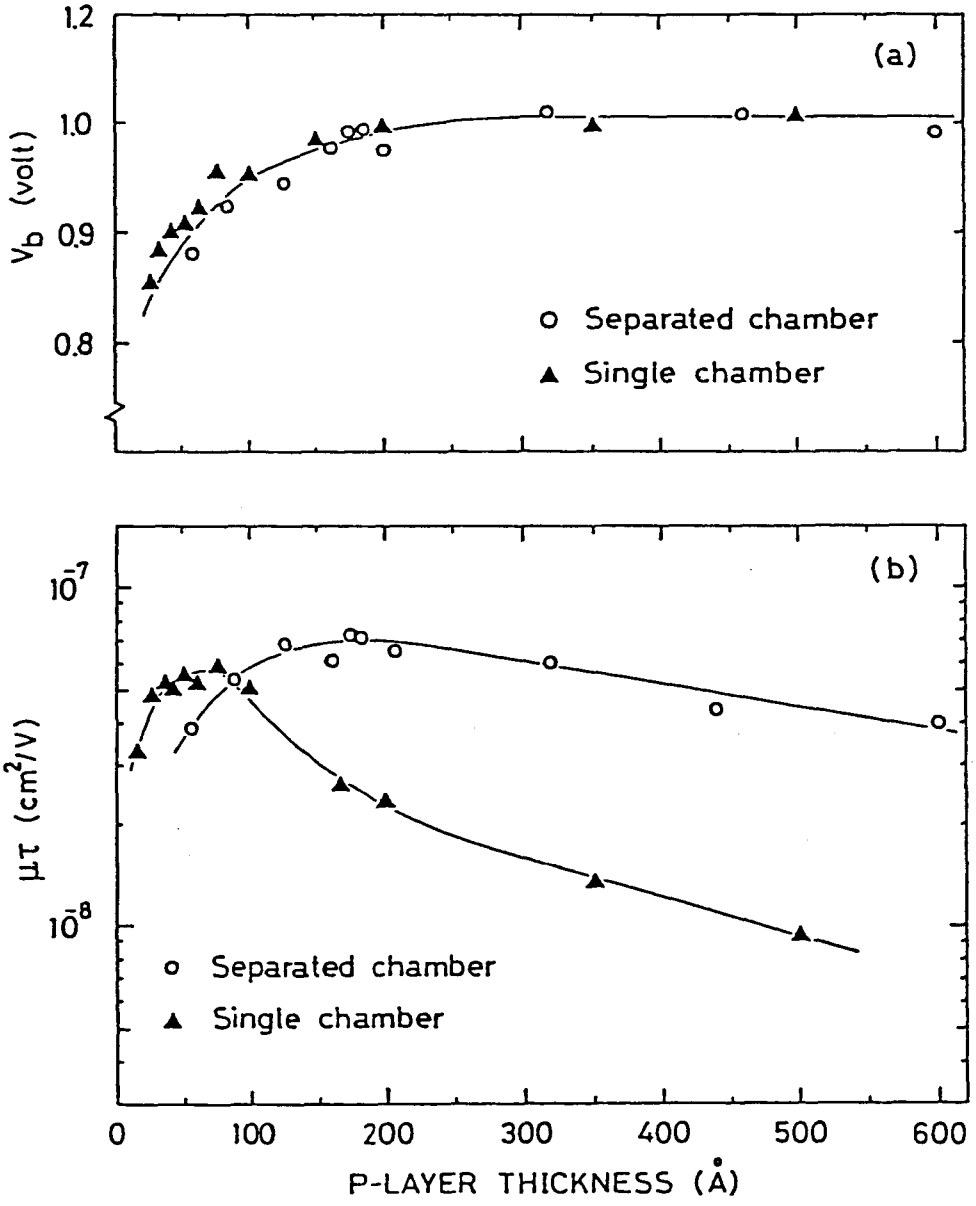

Fig. 6-4 p-layer thickness dependence on built-in potential V_b (a) and mobility-lifetime products μτ (b) of a-Si solar cells fabricated by single and separated chamber deposition systems.

potential recover the decrease of $\mu\tau$ product and shift the p-layer thickness for the maximum conversion efficiency to the thicker region. While, in the case of separated chamber deposition method, the p-layer thickness for the maximum $\mu\tau$ product is coincident with that for the maximum conversion efficiency, because the V_b almost saturates in this thickness range of the p-layer as shown in Fig. 6-4(a). The effective surface recombination factor at the p/i interface are also evaluated from the analysis of collection efficiency spectra. The effective surface recombination factors are around 9×10^4V/cm and 1×10^4V/cm in a-Si solar cells A and B, respectively. These correspond to the surface recombination velocities around 9×10^3cm/s and 1×10^3cm/s if the electron mobility is assumed at $0.1cm^2/Vs$. It can be speculated that the effective surface recombination velocity is enhanced by the presence of Boron and/or Carbon atoms in the vicinity of p/i interface. This may be reason for the significant difference of the effective surface velocities observed in cells A and B. The spectral dependence of the fill factor also gives a qualitative insight of the carrier recombination in the vicinity of the front side interface.

Figure 6-5 shows the spectral dependence of the fill factor measured under the monochromatic light illumination (about 10^4photons/cm^2). The fill factors of cells A and B vary similarly in the range of longer light wavelength (longer than 5500Å). While, it is found that the fill factor rapidly decrease in the range of the shorter light wavelength in the case of cell A. However, for cells B, more than 65% of the fill factor is maintained even at the light wavelength of 4000Å. The penetration depth for this light wavelength is about 200Å in the i-layer employed for this work. Hence this result also proves an improvement

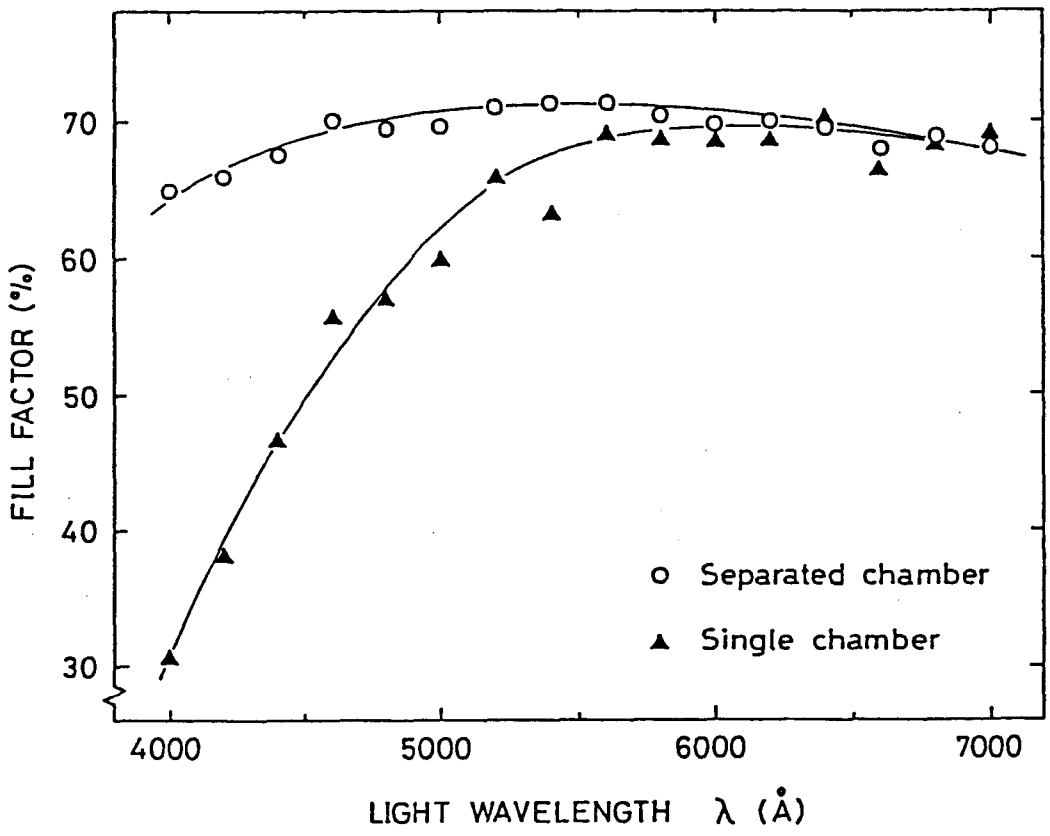

Fig. 6-5 Variation of the fill factor determined from J-V characteristics of a-Si solar cells by single and separated chamber deposition systems illuminated by the monochromatic light wavelength from 4000Å to 7000Å.

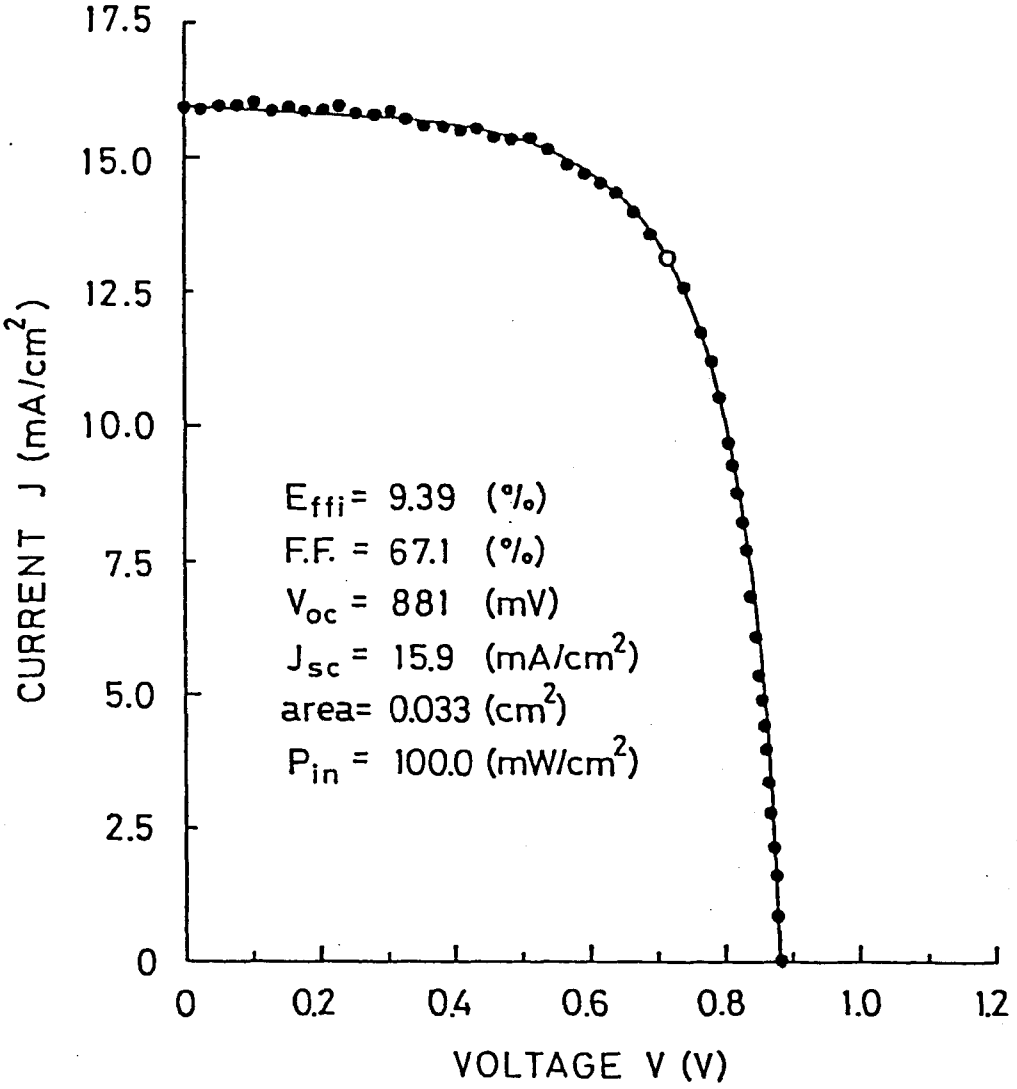

Fig. 6-6 Typical optimized data on the cell performance in a-SiC:H/a-Si:H/μc-Si heterojunction solar cells fabricated by separated chamber deposition system.

of the interface properties of the front side junction (p/i) in the cells B which are fabricated in the separated chamber system.

As a results of the optimization using the separated chamber deposition system, we have obtained a conversion efficiency of 9.39% as shown in Fig. 6-6. The open circuit voltage V_{oc}, fill factor FF and short circuit current J_{sc} are 881 mV, 67.1 % and 15.9 mA/cm^2, respectively.

6-5. Summary

It is worth stressing that such conditions are met in cells that exhibit, as mentioned above, large built-in potential, high mobility-lifetime product and small surface recombination velocity. As for large built-in potential, it is important to improve the film quality of the doped layer. Moreover, a high mobility-lifetime product and small surface recombination velocity are strongly influenced by the quantity and distribution of impurity atoms as well as by the quality of i-layer. These are the key points in order to attain a high photovoltaic performance with good reproducibility.

References

[1] Y. Tawada, M. Kondo, H. Okamoto and Y. Hamakawa, Solar Energy Mat. 6 (1982) 299.

[2] Y. Uchida, T. Ichimura, M, Ueno and M. Ohsawa, J. Phys. 42 (1981) C4-265.

[3] G. Nakamura, K. Sata and Y. Yukimoto, Jpn. J. Appl. Phys. 21 (1982) Suppl.21-2, 197.

[4] H. Okamoto, H. Kida, S. Nonomura and Y. Hamakawa, Solar Cells 8 (1983) 317.

[5] S. Nonomura, H. Okamoto, H. Kida and Y. Hamakawa, Jpn. J. Appl. Phys. 21 (1982) Suppl.21-1, 279.

[6] Y. Kuwano, M. Ohnishi, S. Nakano, T. Fukatsu, H. Nishiwaki and S. Tsuda, 4th EC photovoltaic Solar Energy Conf., Stresa (1982) 704.

[7] S. Nonomura, H. Okamoto and Y. Hamakawa, Appl. Phys. A 32 (1983) 31.

[8] H. Okamoto, H. Kida, S. Nonomura, K. Fukumoto and Y. Hamakawa, J. Appl. Phys. 54 (1983) 3236.

VII. CONCLUSIONS

A systematic study was carried out on the photovoltaic process of hydrogenated amorphous silicon solar cells. The photovoltaic properties of hydrogenated amorphous silicon solar cells were analyzed by a new model considering carrier transport processes. In this model, the characteristic photovoltaic features of a-Si solar cells were fairly well interpreted by some fundamental parameters; built-in potential, mobility-lifetime products of i-layer and surface recombination factors at the p/i and n/i interfaces. On the other hand, from the experimental side, new characterization methods for evaluating these five fundamental parameters was developed. The built-in potential was determined by a back-surface-reflected-electroabsorption method utilizing effects of a field induced change in absorption coefficient. The mobility-lifetime products and the surface recombination factors were obtained from a comparison between calculated collection efficiency spectra under the application of electric field and that obtained from experiments. Utilizing these characterization methods, it was cleared that the fundamental physical parameters responsible for the photovoltaic performance are much influenced by the cell fabrication processes and conditions. Moreover, Glass/SnO_2/p a-SiC:H, i a-Si:H, n μc-Si/Ag heterostructure cells were fabricated under the optimized conditions. The main results obtained in this thesis work are enumerated as follows;

1) The concept of carrier transport in a-Si:H p-i-n junction solar cells was developed, where the operative i-layer is divided into

two regions by variable boundary. In one region, electrons are assumed to behave just like minority carriers, and in the other region holes are regarded as the minority carriers. Based on this model, the carrier collection efficiency spectra and J-V characteristics were obtained.

2) The characteristic carrier collection efficiency spectra and J-V curves under the dark and illuminated conditions were examined for various sets of values of the mobility-lifetime products for electrons ($\mu_n\tau_n$) and holes ($\mu_p\tau_p$), the effective surface recombination factors S_n and S_p, conductivities σ_p and σ_n at the p/i and i/n interfaces, and the built-in potential V_b. The conditions required for better photovoltaic performances were made clear as follows: i) a large built-in potential V_b, ii) large $\mu_n\tau_n+\mu_p\tau_p$ products, iii) $\mu_p\tau_p>\mu_n\tau_n$ ($\mu_n\tau_n>\mu_p\tau_p$) for light absorption on the p- (n-) layer, iv) small S_n and S_p, especially at the front side interface, v) $\sigma_n>\sigma_p$ ($\sigma_p>\sigma_n$) for light incident on the p- (n-) layer.

3) Clear signals of electric field modulated reflectance were observed in hydrogenated amorphous silicon possessing various film qualities. The presence of microcrystallites in the film was confirmed from the continuous variation of line shape with increasing the rf power. It was shown from the dependence of substrate temperature that the half width of electroreflectance signal is corresponding to the film quality, that is, the sharpness of density of states near the optical gap edge, and there is strong correlation between the peak energy of electroreflectance and the optical gap defined from $\sqrt{\alpha\hbar\omega}$ vursus $\hbar\omega$ plotts.

4) The amplitude of electroreflectance signal of the film prepared with various rf power has a quadratic dependence on externally applied modulation voltage. This characteristic feature corresponds to the weak field case in the case of crystalline semiconductors. This quadratic dependence gives a strong evidence that detected signals are real electro-optical signal.
5) The electroreflectance signal was studied in the film with the structure of amorphous silicon solar cells. It was cleared up from the analyses of the signals that detected signal are induced essentially in the light which is reflected at the back surface, that is, electroabsorption signal.
6) It was cleared up that the built-in potential can be evaluated from dc bias dependence of signal amplitude. In the practical a-Si:H solar cells, the internal electric field distribution is fairly uniform. Moreover, the increase of V_b by 50∿130 mV was found in heterojunction solar cells constructed with p-type amorphous silicon carbide and/or n-type microcrystalline silicon as compared with homojunction solar cells.
7) A method for evaluating the mobility-lifetime products of electrons and holes, surface recombination parameters of p/i and n/i interfaces was developed from the analyses of normalized collection efficiency. The experimentally obtained i-layer thickness dependence of collection efficiency and J-V characteristics were well interpreted by utilizing these parameters evaluated from this method.
8) The mobility-lifetime products were strongly influenced by impurity inclusion into the i-layer. The maximum mobility-lifetime products were obtained in the i-layer being slightly p-type.

As for the surface recombination factors, it was pointed out that recombination of the photogenerated carriers at the doped layer or doped layer/i-layer interface was the main origins of the surface recombination.

9) The characteristic features of various types of a-Si:H solar cells were cleared up. In Glass/SnO_2/p a-SiC:H, i a-Si:H, n μc-Si/Ag type solar cells, the considerable improvement of the conversion efficiency η of a-Si:H solar cells fabricated by a separated chamber system is attributable to the higher mobility-lifetime products and the reduction of surface recombination. Consequently, a conversion efficiency of 9.39 % was obtained under AM 1 (100mW/cm^2) illumination.

Appendix A

The internal electric field is calculated in order to derive the Eq.(4-19). It is assumed that the density of localized states in the gap is constant near the Fermi level. Then the potentials ϕ_i, ϕ_p and ϕ_n in the i-, p- and n-layers are given by,

$$-q\phi_i(x) = A\cdot\sinh[\frac{x-x_o}{\Delta_i}], \tag{A-1}$$

$$-q\phi_p(x) = \upsilon + \Delta\mu_p - B\cdot\exp(x/\Delta_p) + C\cdot\exp(-x/\Delta_p), \tag{A-2}$$

$$-q\phi_n(x) = -\upsilon - \Delta\mu_n - D\cdot\exp[(x-L)/\Delta_n] + F\cdot\exp[-(x-L)/\Delta_n]. \tag{A-3}$$

where, arbitrary constants A, B, C, D, F and x_o are to be fixed as a function of the applied bias voltage υ ($= -\frac{q}{2}V_a$). Utilizing the electric field in p-, i-, and n-layer are given from Eq.(A-1), (A-2) and (A-3) by,

$$E_i(x) = -\frac{A}{q\Delta_i}\cosh[\frac{x-x_o}{\Delta_i}], \tag{A-4}$$

$$E_p(x) = -\frac{B}{q_{\Delta p}}\exp(x/\Delta_p) - \frac{C}{q\Delta_p}\exp(-x/\Delta_p), \tag{A-5}$$

$$E_n(x) = -\frac{D}{q\Delta_n}\exp[(x-L)/\Delta_n] - \frac{F}{q\Delta_n}\exp[-(x-L)/\Delta_n]. \tag{A-6}$$

As the boundary condition at p-layer/electrode (n-layer/electrode) interface, $\Delta\psi_p$ ($\Delta\psi_n$) are introduced as shown in Fig.A-1, and described as

$$\Delta\psi_p = \varepsilon_g - \mu_p - \psi_p, \tag{A-7}$$

$$\Delta\psi_n = \varepsilon_g - \mu_n - \psi_n. \tag{A-8}$$

ε_g is the optical gap energy. ψ_p (ψ_n) is the energy difference between ε_{F0} and the conduction band (valence band) in the p-(n-)layer. μ_p (μ_n) is the Fermi level position of p-layer measured from the valence band edge (conduction band edge). Because $\Delta\psi_p$ ($\Delta\psi_n$) results from the energy difference of work functions between p-layer (n-layer) and the

electrode material, $\Delta\psi_p$ ($\Delta\psi_n$) can be regarded as a constant regardless of the p-layer thickness. The constants A, B, C, D, F and x_o are uniquely determined by utilizing Eq.(A-7), (A-8) and the continuity conditions, that is, $E_p(0)=E_i(0)$, $\phi_p(0)=\phi_i(0)$, $E_i(L)=E_n(L)$ and $\phi_i(L)=\phi_n(L)$. Once these constants are determined, the relation of Eq.(4-16) and (4-18) are obtained by inserting the derived internal electric field into Eq.(4-14). In the course of this calculation, the auther assumed $\Delta_i \gg \Delta_n$, Δ_p and $L \gg d_p$, d_n.

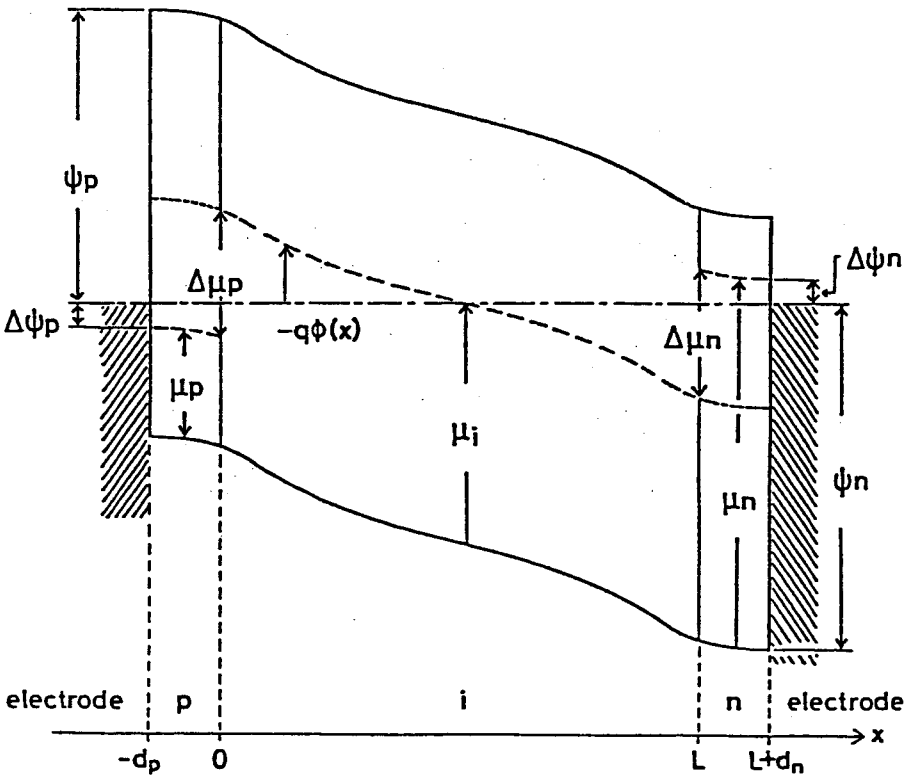

Fig. A-1. Schematic illustration of the band diagram of a-Si:H solar cell.

Appendix B

Consider a situation where electrons are generated by photo-excitation in the i-layer (spreading in the negative direction of the x-axis) and flow towards the p-layer (lying in the range $0 \leqq x \leqq d_p$) in a geometry of i-n/SnO_2. When the internal electric field in the p-layer is negligible, the concentration of excess electrons $\delta n_p(x)$ in the p-layer is expressed by

$$\delta n_p(x) = A \cdot \exp[x/L_{np}] + B \cdot \exp[-x/L_{np}], \qquad (B\text{-}1)$$

where A and B are arbitrary constants to be determined and L_{np} denotes the electron diffusion length in the p-layer, which is defined by $(D_n \tau_{np})^{1/2}$ using the diffusion coefficient D_n and lifetime τ_{np} of electrons in the p-layer. $\delta n_p(x)$ is represented as a function of the electron concentration $\delta n_i(0)$ at the i-layer side of the p/i interface by following boundary conditions;

$$\delta n_p(0) = \exp[-\Delta\varepsilon/k_B T]\delta n_i(0), \qquad (B\text{-}2)$$

and $$S_{no}\delta n_p(d_p) = -D_n \frac{d}{dx} \delta n_p(d_p), \qquad (B\text{-}3)$$

where $\Delta\varepsilon$ is the energy barrier for electrons at the p/i interface. S_{no} is the surface recombination velocity at the SnO_2/p interface divided by the electron mobility. Then the surface recombination factor S_n at the p/i interface can be defined by

$$S_n \delta p_i(0) = S_r \delta p_i(0) + \int_0^{d_p} \delta n_p(x)/\mu_n \tau_{np} dx + S_{no}\delta n_p(d_p), \qquad (B\text{-}4)$$

here S_r is the real surface recombination velocity at the p/i interface divided by the electron mobility. Combination of eqn.(B-1)~(B-4) yields eq.(5-1), where $\mu_n \tau_{np}$ is denoted as $(\mu_n \tau_n)_p$.

VITA

Shuichi Nonomura was born in Hashima, Gifu, Japan in March 9, 1955. He graduated from Gifukita Senior High School, Gifu in March 1973 and entered Gifu University, Gifu in April 1973. He graduated from Gifu University in March 1977 and entered the Graduate School in April of that year. While at Gifu University, he became a member of the Japan Society of Applied Physics. He recieved his Master of Engineering degree in Electrical Engineering in March 1979 from Gifu University. In April 1980, he entered the Graduate School of Osaka University, Toyonaka, Osaka.